A METHOD FOR MODELLING RADIO FREQUENCY DEPOSITION OR ETCH PLASMA CHAMBERS USING AN EQUIVALENT ELECTRONIC COMPONENT CIRCUIT

by

Brian Cregan, B.A.I., B.A.

A thesis submitted in partial fulfilment
of the requirements for the degree of

MEng.

School of Electronic Engineering

Dublin City University

September 2004

Academic Supervisor: Professor David C. Cameron

DECLARATION

I hereby certify that this material, which I now submit for assessment on the programme of study leading to the award of Master of Engineering is entirely my own work and has not been taken from the work of others save and to the extent that such work has been cited and acknowledged within the text of the work.

Signed : Brian Cregan Date: 17/1/05

Brian Cregan

ACKNOWLEDGEMENTS

I would like to thank Professor David Cameron, my Academic Supervisor, for his guidance through this entire project. It was a pleasure and privilege to work with such a dedicated and enthusiastic supervisor. I have benefited greatly from the positive learning environment that has been provided by David and wish him every success in the future.

I would like to thank Stephen Daniels, my manager while I worked at Scientific Systems Ltd., for his invaluable advice on balancing work life and educational life. His belief in further education and the opportunities it brings is both refreshing and encouraging.

Much of this work was carried out while I was working with Scientific Systems Ltd. I am grateful for the financial support and expertise that was provided to me from the staff at Scientific Systems Ltd. I would especially like to thank Mike Hopkins, Francisco Martinez, Jean Pierre Pererienha, Jean Marc Ouvard, Kieron Dobbyn, Donal O'Sullivan, Conor Hilliard, Brian Heil, Predrag Stankovic and Conor Mullaney.

I would like to thank my friends who have endured the fascinating world of radio frequency theory and plasma physics in the recent past. Their support through tough times is greatly appreciated.

Finally, I would like to thank my parents, Donal and Máire, and my sister Claire. They have provided the opportunities for me that have lead to me producing this work. They have been the one constant over the years and have given me the confidence and self belief to keep on educating and improving myself.

CONTENTS

Abstract

Extensive work continues to be carried out on correlating the electric characteristics of parallel-plate discharges with an equivalent model. Theoretical models have been developed for capacitive radio frequency driven plasmas. Voltage, current and phase measurements of radio frequency discharges have been used to gain empirical data of a wide range of discharge parameters. It has been found that parasitic impedances within a plasma chamber have a substantial effect on impedance measurements of plasmas. This means that simple a priori models are inadequate for understanding plasmas. Complicated experimental setups have been used to better understand the propagation of radio frequency electromagnetic radiation through plasmas/plasma chambers. These however can not be transferred to a manufacturing environment due to non uniformity issues across a given wafer. The effect of the plasma chamber setup on plasma characteristics has been demonstrated.

Although plasma processes are widely used in industry, the general understanding of these processes is poor and process control is difficult. The ability to etch fine lines and the control of anisotropy, etching rate, uniformity, selectivity and end point detection are obtained by experimental trial and error.

This thesis describes a method of characterising the condition of a radio or microwave frequency excited plasma etching or deposition system as would be used in the semiconductor industry. This process can be used for:

(i) monitoring the state of a system as it ages to detect when cleaning or repair is required

(ii) checking that the characteristics of the system are as expected after manufacture, rebuild or modification.

The location of any defects may be detected by simulating the frequency response of the altered system to see which electrical component values have changed. These can then be related to the physical components of the system. This characterisation can be integrated into the normal process flow; when the plasma is not powered up e.g., during pump down or loading for example, the network analyser can be switched in and the measurements made. In this way, the system can be characterised on a "real-time" basis.

Chapter 1 Introduction

1.1 Introduction

The ever shrinking dimensions of microelectronic devices have necessitated the use of plasma processing in integrated circuit (IC) factories worldwide. Revenues in the plasma processing industry now exceed $3 billion per annum, well in excess of predictions made only a few years ago [1]. Besides the use of plasmas in etching and depositing thin films, other processes include the removal of photoresist remnants after development (descumming), stripping developed photoresist after pattern transfer (ashing), and passivating defects in polycrystalline material [2]. Plasma based surfaces are also critical for the aerospace, automotive, steel, biomedical and toxic waste management industries. Materials and surface structures can be fabricated that are not attainable by any other commercial method, and the surface properties of materials can be modified in unique ways.

The semiconductor industry has advanced from revolutionary development to evolutionary advances with a focus on manufacturing. While product and process advances are still very much industry issues, greater emphasis is being placed on the business factors, and while high yields are a must, new processes and equipment are being measured by overall productivity. Strategies to increase the bottom line include maximising cost of ownership, automation, cost control, computer-automated manufacturing, computer-integrated manufacturing and statistical process control.

A number of factors contribute to the cost of producing a functioning dice (figure1.1). They are generally divided into fixed and variable categories. Fixed costs are those that exist whether or not any die are being made or shipped. Variable costs are those that go up or down with the volume of product being produced.

Fixed Costs	Variables Costs
Overhead-administration and facilities Equipment	Materials-direct and indirect Labour Yield

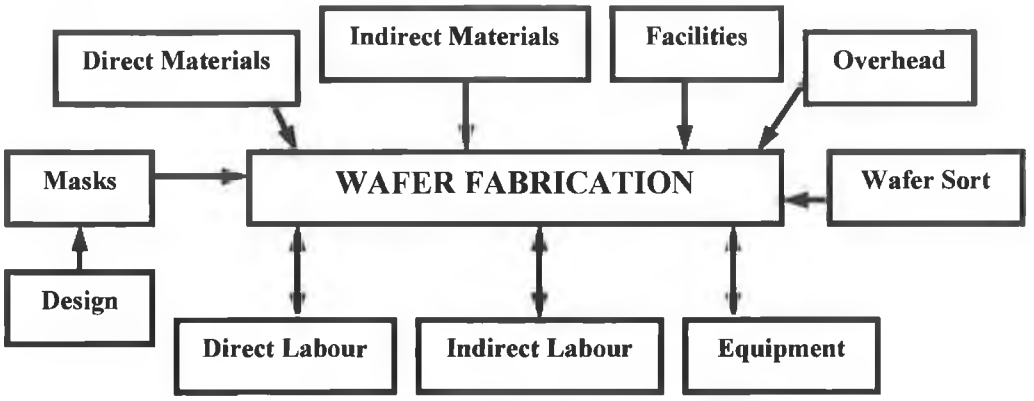

Figure 1.1 Fabrication Cost Factors.

Equipment as a cost factor is of particular interest for this thesis. Over the years semiconductor processing has changed from a laboratory activity to full manufacturing using sophisticated and dedicated equipment. The development of semiconductor specific equipment has allowed the advances into the ultra large scale integration (ULSI) era and the spread of the technology throughout the world.

IBM coined the term *tool*, for semiconductor process machines and it has become part of the industry vocabulary. As the tools have become more sophisticated, the prices have risen to the point where they are a major expense in any new facility. A number of considerations go into the selection of a particular process tool. They can be roughly divided into two broad categories: performance and economic. Performance factors relate to the ability of the tool to produce the required results. Economic factors relate to price, costs and support factors. Figure 1.2 shows how these four factors have varied as the industry has moved into the manufacturing era.

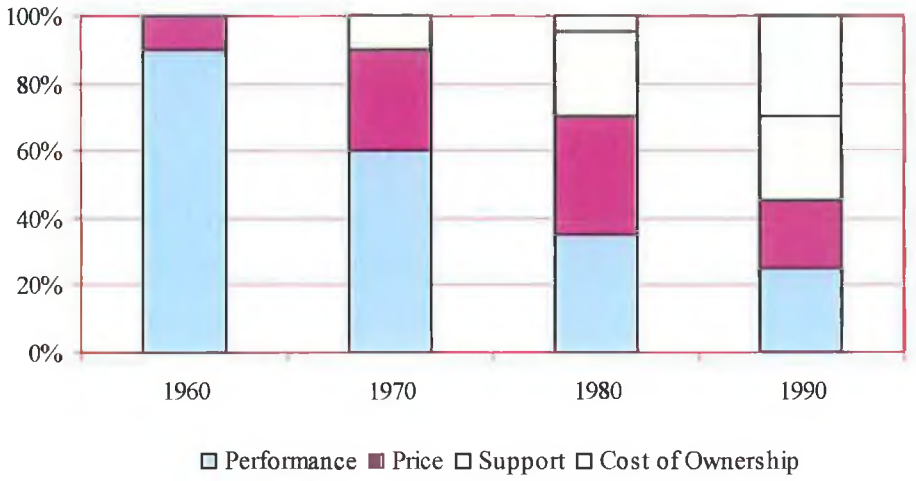

Figure 1.2 Changes in equipment purchase factors (Source: Semiconductor International, May 1993, p. 58).

While performance has fallen as a selection criterion, any tool must have the basic capability to meet the process requirements. If the machine cannot routinely produce the right product, it is of no use. Other performance factors are repeatability, flexibility, upgradeability, ease of operation, set-up and reliability/downtime factors.

- Repeatability is the ability to produce the same result every time and over long periods of time.
- Flexibility relates to the ease with which a machine can be switched to run a variety of products and processes.
- Upgradeability is the ability of the machine to handle future process requirements, such as increasing wafer diameters.
- Ease of operation and set-up factors address the issue of minimising operator mistakes by good design and user friendly controls.
- Set-up issues relate to the amount of time required to bring the tool on-line (tests, calibrations etc.) and the related loss of production time.

Most companies run their equipment two or three shifts per day, sometimes six to seven days a week. Scheduled maintenance and unscheduled breakdowns stall product flow and run up the expenses. The factors are: *scheduled maintenance frequency and time*, *mean time to failure* and *mean time to repair*. Given the expense of most machines, having back-ups is a costly luxury. It falls on the vendor to provide a machine that runs for long periods of

time, can be repaired quickly when failure occurs and does not need frequent and lengthy routine maintenance. Cost also includes the price of materials needed for the machine process. Machines that waste materials also waste money.

Vendor support has emerged as a critical factor. The advancement of process technology and equipment sophistication has forced close cooperation and alliances between the chip manufacturers and their suppliers. The cost of machine development requires input from the using-process engineers and the detailed nature of the machines requires on-time back-up from vendors.

1.2 Review of Plasma Chamber Modelling

Extensive work continues to be carried out on correlating the electric characteristics of parallel-plate discharges with an equivalent model. Theoretical models have been developed for capacitive radio frequency driven plasmas [3]. Voltage, current and phase measurements of radio frequency discharges have been used to gain empirical data for a wide range of discharge parameters [4]. It has been found that parasitic impedances within a plasma chamber have a substantial effect on impedance measurements of plasmas [5]. This means that simple a priori models are inadequate for understanding plasmas. Complicated experimental setups have been used to better understand the propagation of radio frequency electromagnetic radiation through plasmas/plasma chambers [6]. These however can not be transferred to a manufacturing environment due to non uniformity issues across a given wafer. The effect of the plasma chamber setup on plasma characteristics has been demonstrated [7].

1.3 Research Objectives and Summary

Although plasma processes are widely used in industry, the general understanding of these processes is poor and process control is difficult. The ability to etch fine lines, the control of anisotropy, etching rate, uniformity, selectivity and end point detection are obtained by experimental trial and error.

This thesis describes a method of characterising the condition of a radio or microwave frequency excited plasma etching or deposition system as would be used in the semiconductor industry. The method involves measuring the electrical impedance of the chamber over a wide frequency range (e.g. 1-200MHz for a

system normally operating at 13.56MHz) by using an impedance analyser. The frequency response may then be simulated by an electrical network of components based on the physical arrangement of the system components. Any changes in the system due to electrical connections can be detected by observing changes in impedance without access to the interior of the system. This process can be used for:

(iii) monitoring the state of a system as it ages to detect when cleaning or repair is required

(iv) checking that the characteristics of the system are as expected after manufacture, rebuild or modification.

The location of any defects may be detected by simulating the frequency response of the altered system to see which electrical component values have changed. These can then be related to the physical components of the system. This characterisation can be integrated into the normal process flow; when the plasma is not powered up e.g., during pump down or loading for example, the network analyser can be switched in and the measurements made. In this way, the system can be characterised on a "real-time" basis.

1.4 Organisation of the Thesis

This thesis is organised into five chapters, references and one appendix.

- A review of plasma chamber modelling, the research objectives and summary of this thesis have been described in Chapter 1.
- The required theoretical background for this thesis is given in Chapter 2. Three areas are covered viz. radio frequency theory, plasma theory and mesh current network analysis.
- The equipment used and the experimental set-up is described in Chapter 3.
- The experimental method and results are recorded in Chapter 4.
- The conclusions of this work and suggestions for future research are given in Chapter 5.
- References.
- Appendix A contains the Scilab program files.

Chapter 2 Theory

2.1 Introduction

There are various fields of expertise that are used to design and build industrial and research plasma chambers. There are three main areas referred to in this thesis. The first is Radio Frequency Theory. Many industrial plasmas are driven by radio frequency power sources. A strong knowledge of how radio frequency electromagnetic radiation propagates through a plasma chamber system is therefore essential. References [8], [9] and [10] are used to present the fundamental concepts of radio frequency theory and how these concepts relate to plasmas and plasma chamber systems.

The second field of expertise is Plasma Theory. The plasma is the central component of the plasma chamber. Everything within a plasma chamber system is designed around producing plasma that will complement a given process. The basic properties of plasmas, their parameters and how they exist in different systems must be understood. References [11] and [12] are used to present the fundamental concepts of capacitively coupled discharges.

In this thesis the plasma chamber is modelled using algorithms that are based on matrices. A basic theory of matrices has been included in this chapter, with specific reference to Cramer's rule. A description of the Simplex Method for curve fitting is also given. Large amounts of data are needed to generate the models for the chamber. Storing this data in matrix form allows the use of matrices functions, providing strong processing power. References [13] and [14] are used to present the matrices theory required for the derivation of the algorithms in this thesis.

2.2 *Radio Frequency Theory*

2.2.1 *The Electromagnetic Spectrum*

Radio Frequency signals belong to a family of waves called the Electromagnetic Spectrum. All electromagnetic waves share the following fundamental properties:

- An electromagnetic wave consists of electric and magnetic field intensities that oscillate at the same frequency ***f***.
- The phase velocity of an electromagnetic wave propagating is a universal constant given by the velocity of light ***c***, defined as

$$c = \frac{1}{\sqrt{\mu_0 \varepsilon_0}}$$

  where μ_0 is the magnetic permeability of free space and ε_0 is the permeability of free space.
- In vacuum, the wavelength λ of an electromagnetic wave is related to its oscillation frequency *f* by

$$\lambda = \frac{c}{f}$$

Whereas all electromagnetic waves share these properties, each is distinguished by its own wavelength λ, or equivalently by its own oscillation frequency *f*.

Figure 2.1 shows the electromagnetic spectrum. The visible part of the

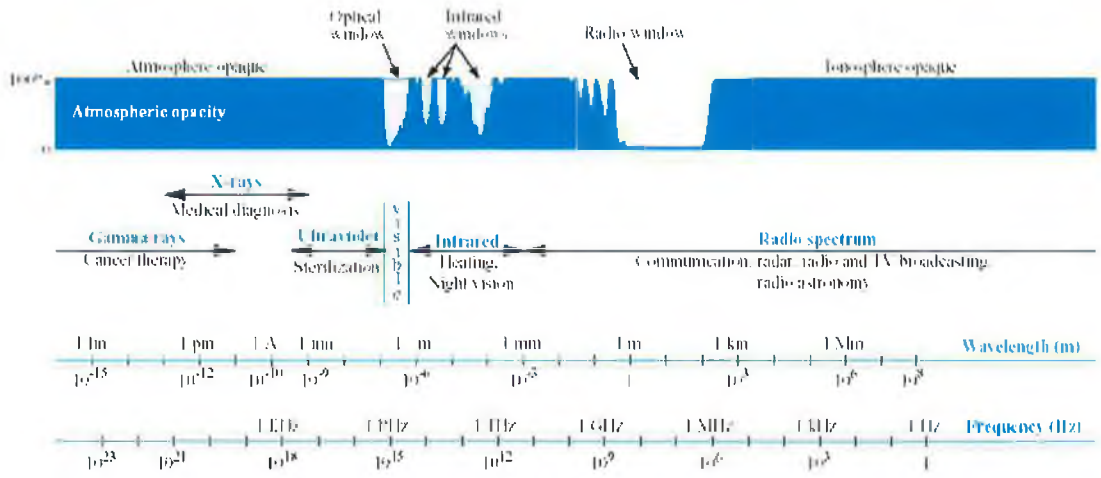

Figure 2.1 The Electromagnetic Spectrum

electromagnetic spectrum covers a very narrow wavelength range extending between λ = 0.4μm (violet) and λ = 0.7μm (red). As we move progressively

toward shorter wavelengths, we encounter the ultraviolet, x-ray and gamma-ray bands, each so named because of historical reasons associated with the discovery of waves with those wavelengths. On the other side of the visible spectrum lie the infrared band and then the radio region. Because of the link between λ and f given above, each of these spectral ranges may be specified in terms of its wavelength range or alternatively in terms of its frequency range. In practice however, a wave is specified in terms of its wavelength if $\lambda < 1$mm, which encompasses all parts of the electromagnetic spectrum except for the radio region, and the wave is specified in terms of its frequency f if $\lambda > 1$mm (i.e. in the radio region). A wavelength of 1mm corresponds to a frequency of 3×10^{11} Hz = 300 GHz in free space.

The radio spectrum consists of several individual bands. Each band covers one decade of the radio spectrum and has a letter designation based on a nomenclature defined by the International Telecommunication Union. Different frequencies have different applications because they are excited by different mechanisms, and the properties of an electromagnetic wave propagating in a material may vary considerably from one band to another. The extremely low frequency (ELF) band from 3 to 30 Hz is used primarily for the detection of buried metal objects. Lower frequencies down to 0.1 Hz are used in magnetotelluric sensing of the structure of the earth, and frequencies in the range from 1 Hz to 1kHz sometimes are used for communications with submerged submarines and for certain kinds of sensing of Earth's ionosphere. The very low frequency (VLF) region from 3 to 30kHz is used both for submarine communications and for position location by the Omega navigation system. The low-frequency (LF) band, from 30 to 300 kHz, is used for some forms of communication and for the Loran C position-location system. Some radio beacons and weather broadcast stations used in air navigation operate at frequencies in the higher end of the LF band. The medium-frequency (MF) region from 300 kHz to 3 MHz contains the standard AM broadcast band from 0.5 to 1.5 MHz.

Long-distance communications and short-wave broadcasting over long distances use frequencies in the high-frequency (HF) band from 30 MHz because waves in this band are strongly affected by reflections by the ionosphere and least

affected by absorptions in the ionosphere. The next frequency region, the very high frequency (VHF) band from 30 to 300 MHz, is used for aircraft and other vehicles. Some early radio-astronomy research was also conducted in this range. The ultrahigh frequency (UHF) region from 300 MHz to 3 GHz is extensively populated with radars, although part of this band also is used for television broadcasting and mobile communications with aircraft and surface vehicles. The radars in this region of the spectrum are normally used for aircraft detection and tracking. Some parts of this region have been reserved for radio astronomical observation.

Many point-to-point radio communication systems and various kinds of ground-based radars and ship radars operate at frequencies in the super high frequency (SHF) range from 3 to 30 GHz. Some aircraft navigation systems operate in this range as well. Most of the extremely high frequency (EHF) band from 30 to 300 GHz is used less extensively, primarily because the technology is not as well developed and because of excessive absorption by the atmosphere in some parts of this band. Some advanced communication systems are being developed for operation at frequencies in the "atmospheric windows", where atmospheric absorption is not a serious problem, as are automobile collision-avoidance radars and some military imaging radar systems. These atmospheric windows include the ranges from 30 to 35 GHz, 70 to 75 GHz, 90 to 95 GHz, and 135 to 145 GHz.

The radio frequencies generally used in capacitively coupled plasma discharge chambers are 2 MHz, 13.56 MHz and 27 MHz. The system developed for this thesis uses a 13.56 MHz power source. The corresponding wavelength is $\lambda \approx 22.1$ metres. There is no particular reason for the use of the HF band of radio frequencies. It has simply been allocated by the International Telecommunications Union for use in plasma chamber systems. The power levels of the signal can range from 0 to 3000 Watts. A range of 0 to 150 Watts is used in the system developed for this thesis. It is clear that, even in the small window of the electromagnetic spectrum and power settings, there is a wide range of conditions that can be used to generate plasmas.

2.2.2 Radio Frequency versus DC or Low AC Signals

There are several major differences between signals at higher radio frequency and there counterparts at low AC frequency or DC. These differences, which greatly influence electronic circuits and their operation, become increasingly important as the frequency is raised. The following four effects provide a brief summary of the effects of radio frequency signals in a circuit that are not present at DC or low AC signals:

a). ***Presence of stray capacitances.*** This is the capacitance that exists:

- Between conductors of the circuit
- Between conductors or components and ground
- Between components

b). ***Presence of stray inductances.*** This is the inductance that exists due to:

- The inductance of the conductors that connect components
- The parasitic inductance of the components themselves

These stray parameters are not usually important at DC and low AC frequencies, but as frequency increases, they become a much larger portion of the total.

c). ***Skin effect.*** This is due to the fact that AC signals penetrate a metal partially and flow in a narrow band near the outside surface of each conductor. This effect is in contrast to DC signals that flow through the whole cross-section of the conductor, as shown in figures 2.1 and 2.2.

Figure 2.1 DC case of skin effect in a wire.

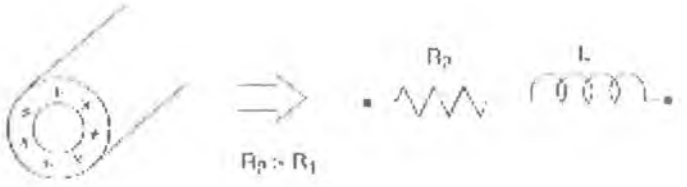

Figure 2.2 AC case of skin effect in a wire.

For AC signals, the current density falls off exponentially from the surface of the conductor toward the centre. At a critical depth δ, called the skin depth or depth

of penetration, signal amplitude is $1/e$ or 36.8% of its surface amplitude. The skin depth is given by:

$$\delta = \sqrt{\frac{1}{\pi f \mu \sigma}}$$

where μ is the permeability and σ is the conductivity of the conductor. It is observed that as frequency increases, skin effect produces a smaller zone of conduction and a correspondingly higher value of AC resistance compared with DC resistance.

d). ***Radiation*** This is caused by leakage or escape of signals into the air. This, in essence, means that the signals bypass the conducting medium, and not all of the source energy reaches the load. Radiation can occur outside or within the circuit and can cause coupling effects such as:

- Coupling between elements of the circuit
- Coupling between the circuit and its environment
- Coupling from the environment to the circuit

"Electromagnetic Interference" (EMI), also called "radio frequency interference" (RFI) or "RF-noise", is due to radiation of signals at RF/MW frequencies and is considered to be negligible in most low frequency AC circuits and absent in DC circuits.

2.2.3 Component Basics

a). ***Wire*** A wire is the simplest element to study having negligible resistance, which makes it appear as a short circuit at DC and low AC frequencies. Yet at radio frequencies it becomes a very complex element. Wire in a circuit can take on many forms such as

- Wire wound resistors
- Wire wound inductors
- Leaded capacitors
- Element-to-element interconnect applications

The behaviour of a wire in the radio frequency range depends to a large extent on the wire's diameter and length. A system for different wire sizes is the American Wire Gauge (AWG) system. In this system, the diameter of a wire will roughly double for every six gauges.

Problems associated with a wire can be traced to two areas: skin effect and straight-wire inductance. As frequency increases, the electrical signals propagate less and less in the inside of the conductor. The current density increases near the outside perimeter of the wire and causes a higher impedance to be seen by the signal. This is because resistance of the wire is given by:

$$R = \frac{\rho l}{A}$$

and if the effective area, A, decreases, this leads to an increase in resistance, R.

In the medium surrounding any current carrying conductor, there exists a magnetic field. If the current I is AC, this magnetic field is alternately expanding and contracting (and even reversing direction if there is no DC bias present). This produces an induced voltage (as specified by Faraday's law) in the wire that opposes any change in the current flow. This opposition to change is called "self-inductance". The concept of inductance is important because at radio frequency, any and all conductors including hook up wires, capacitor leads, bonding wires, and all interconnects tend to become inductors and exhibit the property of inductance as shown in figure 2.3.

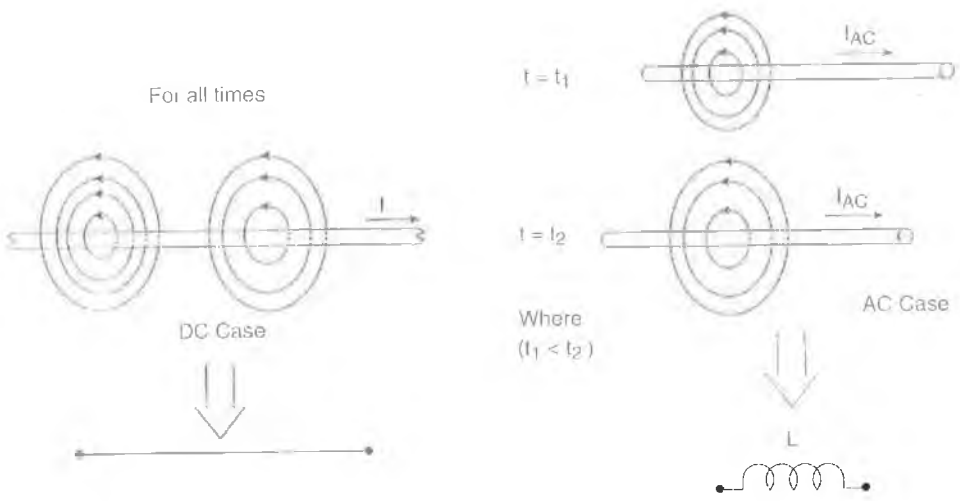

(a) *(b)*

Figure 2.3 Interactive properties of a wire: (a) DC case, self-inductance not present; (b) AC case, self-inductance present.

b). ***Resistors*** These are elements specialising in the resistance property of a material. The resistance of a material is a property whose value determines, when an electric current passes through it, the rate at which electrical energy is converted into thermal energy. Figure 2.4 shows a simple resistor at DC.

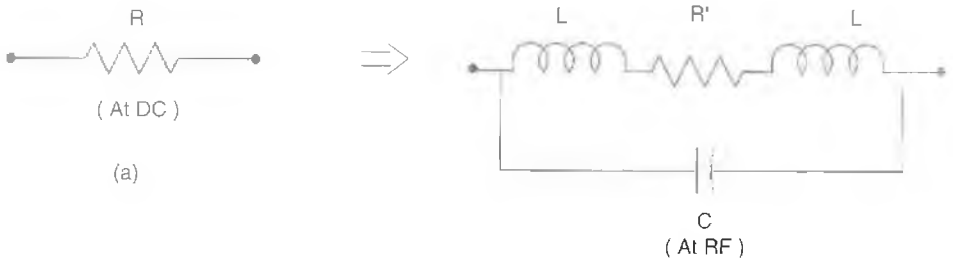

Figure 2.4 A simple resistor at (a) DC, (b) high RF frequency.

As frequency increases, the lead wire inductance (L), increased resistor value ($R'>R$) due to skin effect and parasitic capacitances becomes prominent. The net effect of all these parasitic elements, on the average, is a decrease in the resistor value as for carbon-composition and metal resistors. Therefore, at radio frequency, a resistor appears as a combination of several elements.

c). ***Capacitors*** These are devices that consist of two conducting surfaces separated by an insulating material or dielectric. Figure 2.5 shows a simple parallel plate capacitor.

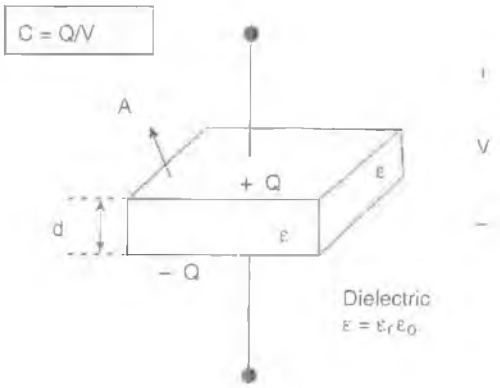

Figure 2.5 A parallel plate capacitor.

The dielectric is usually ceramic, air or Teflon. The capacitance is the property that permits the storage of charge when a potential difference between the conductors exists. It is measured in Farads.

The performance of a capacitor is primarily dependent on the characteristics of its dielectric. The dielectric determines the voltage and temperature range in which the capacitor is operational. Any losses or imperfections in the dielectric have an enormous effect on the circuit's operation. A practical capacitor has several parasitic elements that become important at higher frequencies as shown in figure 2.6.

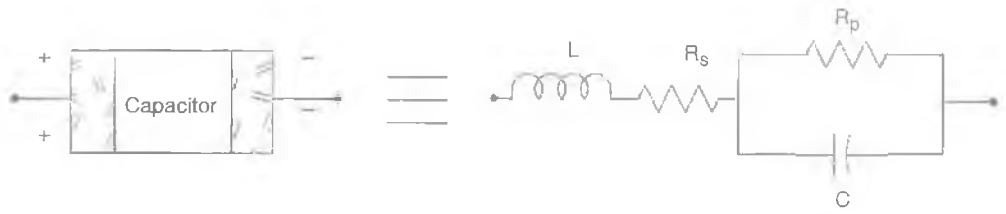

Figure 2.6 Parasitic elements in a capacitor.

C is the actual capacitance, L is the lead inductance, R_S is the series resistance, and R_P is the insulation resistance. Both resistances create heat and loss. The existence of parasitic elements brings the concept of real-world capacitors to the fore front, which needs further explanation.

In a perfect capacitor the current will lead the applied voltage in phase by 90 degrees. In phasor notation the can be written as

$$I = j\omega CV = \omega CVe^{j90^\circ}$$

In a real-world capacitor, the phase angle (φ) will be less than 90 degrees (i.e., $\varphi < 90°$). The reason $\varphi < 90°$ is the existence of R_S and R_P (parasitic resistances shown in figure 2.6), which combine into one equivalent resistor R_{EQ}, as shown in the figure 2.7.

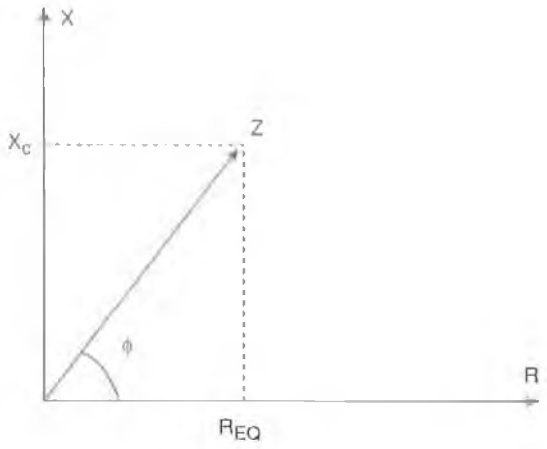

Figure 2.7 Equivalent Resistance

In a practical capacitor $cos(\varphi)$, called the power factor, can be written as

$$\cos(\varphi) = \frac{R_{EQ}}{\sqrt{X_C{}^2 + R_{EQ}{}^2}}$$

Usually $R_{EQ} << X_C$ where $X_C = 1/\omega C$. Therefore we can write:

$$\cos(\varphi) = \frac{R_{EQ}}{X_C}$$

An important factor in practical capacitors or in general any imperfect element is the Quality Factor (Q). It is the measure of the ability of an element (or circuit with periodic behaviour) to store energy, equal to 2π times the average energy stored divided by the energy dissipated per cycle. Q is a figure of merit for a reactive element and can be shown to be the ratio of the elements reactance to its effective series resistance. For a capacitor, Q is given by:

$$Q = \frac{X_C}{R_{EQ}} = \frac{1}{\omega C R_{EQ}} \approx \frac{1}{\cos(\varphi)}$$

From this equation we can observe that for a practical capacitor, as the effective series resistance (R_{EQ}) decreases, Q will increase until $R_{EQ} = 0$, which corresponds to a perfect capacitor having $Q = \infty$, i.e.,

$$R_{EQ} = 0 \Rightarrow \cos(\varphi) = 0$$

The effect of these imperfections in a capacitor is shown in the figure 2.8.

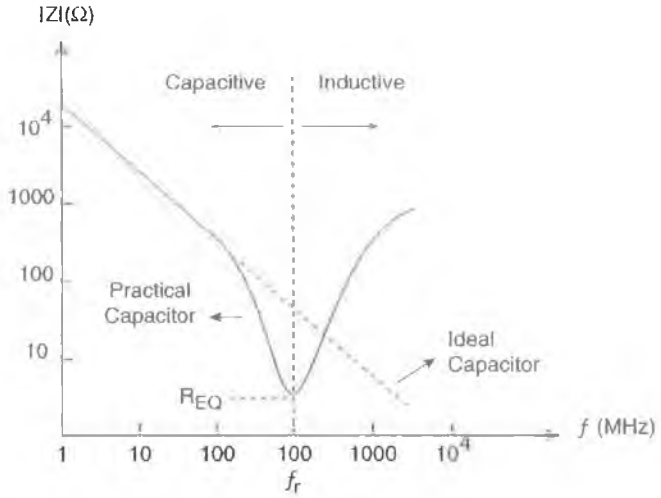

Figure 2.8 The behaviour of a capacitor verus frequency.

Two distinct regions in the frequency response plot of a capacitor can be identified. These two regions straddle the resonance frequency (f_r) as follows:

- $f < f_r$. In this region as frequency increases, the lead inductance's reactance goes up gradually, cancelling the capacitor's reactance and thus causing resonance (f_r).
- $f > f_r$. In this region the capacitor acts like an inductor and is no longer performing its intended function.

c). ***Inductors*** An inductor is wire that is wound (or coiled) in such a manner as to increase the magnetic flux linkage between the turns of the coil. The

increased flux linkage increases the wire's self-inductance, as shown in figure 2.9.

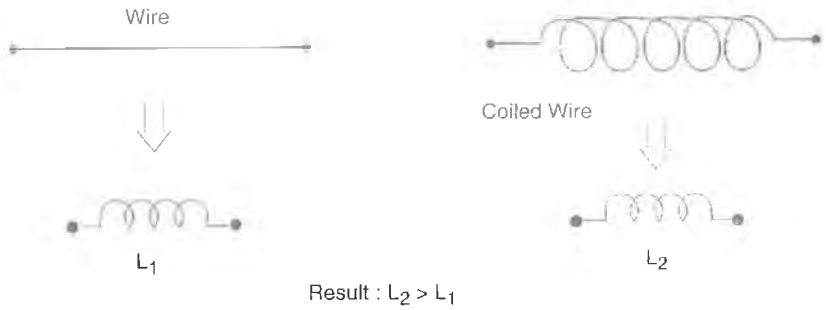

Figure 2.9 A wire's self inductance.

Inductors have a variety of applications in radio frequency circuits such as in resonance circuits, filters, phase shifters, delay networks, and radio frequency chokes.

There is no such thing as a perfect component. Among all components, inductors are most prone to very drastic changes over frequency. This is due to the fact that the distributed capacitance (C_d) and series resistance (R) in an inductor at radio frequency play a major role in the performance of an inductor, as shown in figure 2.10.

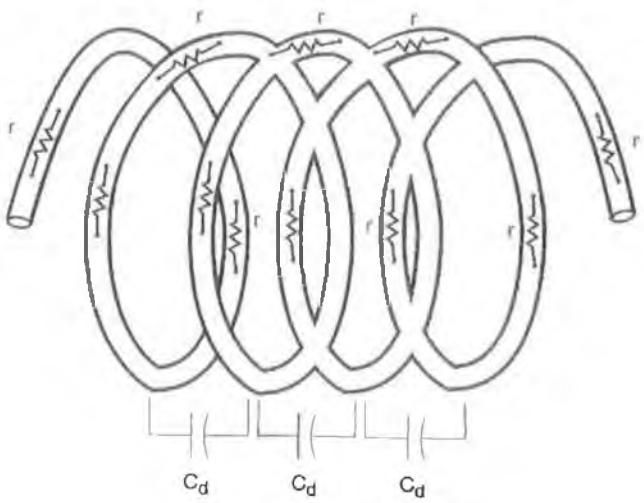

Figure 2.10 The distributed parasitic elements of an inductor

We can see from figure 2.10 that C_d exists due to a voltage drop in the coil caused by internal resistance. The voltage drop causes a voltage difference between two turns of the coil separated from each other (with air as the dielectric). The aggregate of all small C_d's and R's provides the equivalent circuit shown in figure 2.11.

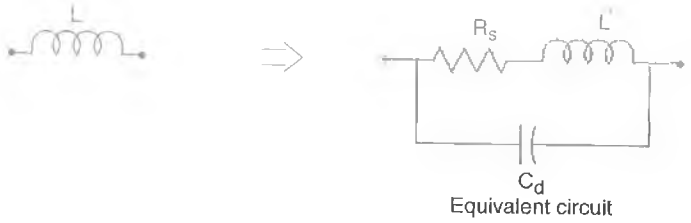

Figure 2.11The equivalent circuit of an inductor at RF frequencies

The effect of C_d on an inductor's frequency response is shown in figure 2.12. Again, just like a capacitor, there are two regions that straddle the resonant

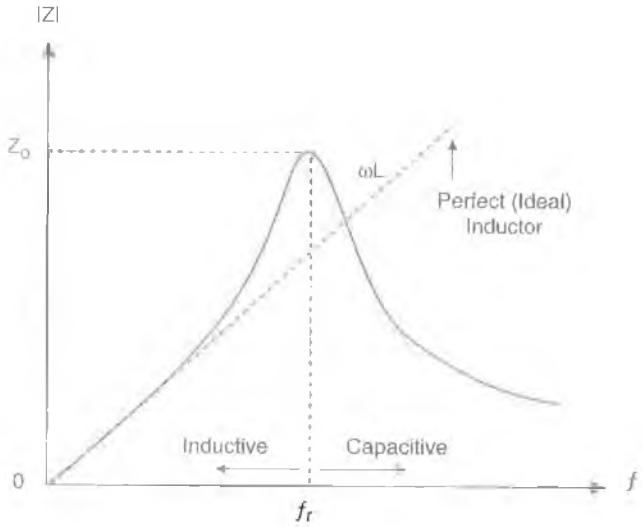

Figure 2.12 Effect of a parasitic C_d on an inductor's reactance.

circuit. These regions can be identified as follows:

- $f < f_r$. In this region, the inductor's reactance ($X_L=\omega L$) increases as frequency is increased.
- $f > f_r$. In this region the inductor behaves like a capacitor, and as frequency is increased the reactance decreases.

At $f = f_r$ resonance takes place in an inductor (inductor's reactance is cancelled by parasitic distributed capacitor), and theoretically the inductor's reactance is infinity; however, in practice, the total impedance of the element is finite due to a nonzero series resistance.

The quality factor (Q) of an inductor is defined to be:

$$Q = \frac{X_L}{R_S} = \frac{\omega L}{R_S}$$

For a perfect inductor the series resistance is zero; thus we have:

$$R_S = 0 \Rightarrow Q = \infty$$

At low frequencies, Q is very large because R_S is very small; however, as frequency increases the skin effect and winding distributed capacitor (Cd) begin to degrade the Q of an inductor as shown in figure 2.13.

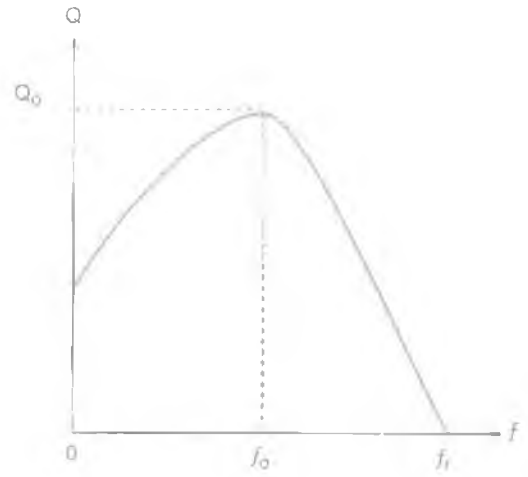

Figure 2.13 Degradation of Q of an inductor

It can be seen that as frequency increases, Q will increase up to Q_O, which is at $f = f_O$. For frequencies $f_O < f < f_r$, R_s and C_d combine to decrease the Q of the inductor toward zero. At resonance ($f = f_r$), where the total reactance of the elements is zero, the inductor is no longer useful.

To extend the frequency range of an inductor (by increasing its Q), we can use one of the following solutions:

- Use a larger diameter for the wire, which effectively reduces the resistance value.
- Spread the winding apart, which reduces the distributed capacitance (C_d) between the windings.
- Increase the inductance (L) by increasing the permeability of the flux linkage path by using a magnetic-core material.

2.2.4 Radio Frequency Impedance Matching

A resonant circuit's (or filter's) function is to pass selectively a certain frequency or frequency range from the source to the load, while attenuating all other frequencies outside of this passband. As there is no perfect component, a perfect circuit does not exist and cannot be built. Therefore, knowing the mechanics of resonant circuits, we can tailor an imperfect resonant circuit to suit our needs.

Impedance matching is necessary in the design of radio frequency plasma chamber systems to provide the maximum possible transfer of power between the radio frequency power source and its load, i.e. the plasma chamber. To understand this, consider a discharge modelled as a load having impedance

$$Z_D = R_D + jX_D$$

where R_D is the discharge resistance and X_D is the discharge reactance. The power source connected to Z_D is modelled by its Thevenin equivalent circuit, consisting of a voltage source with complex amplitude V_T in series with a source resistance R_T. The time average power flowing into the discharge is

$$P = \frac{1}{2}\mathrm{Re}(V_{rf} I_{rf}^*)$$

where V_{rf} is the complex voltage across Z_D. Solving for I_{rf} and V_{rf} for these series elements, we obtain

$$\overline{P} = \frac{1}{2}|V_T|^2 \frac{R_D}{(R_T + R_D)^2 + X_D^2}$$

For fixed source parameters V_T and R_T (typically 50-ohms) maximum power transfer is obtained by setting $\partial\overline{P}/\partial X_D = 0$ and $\partial\overline{P}/\partial R_D = 0$, which gives $X_D = 0$ and $R_D = R_T$. The maximum power supplied by the source to the load is then

$$\overline{P}_{\max} = \frac{1}{4}\frac{|V_T|^2}{R_T}$$

If maximum power transfer is obtained, then we say that the source and load are matched.

Since X_D is not zero, and typically $R_D << R_T$, the power P is generally much less than $P_{\max}$. To increase P to $P_{\max}$, thus matching the source to the load, a lossless *matching network* can be placed between the source and load. As R_D and X_D are two independent components of Z_D, the simplest matching network consists of two independent components. The most common configuration, called an "L-network", is inserted between the source and the load as in figure 2.14.

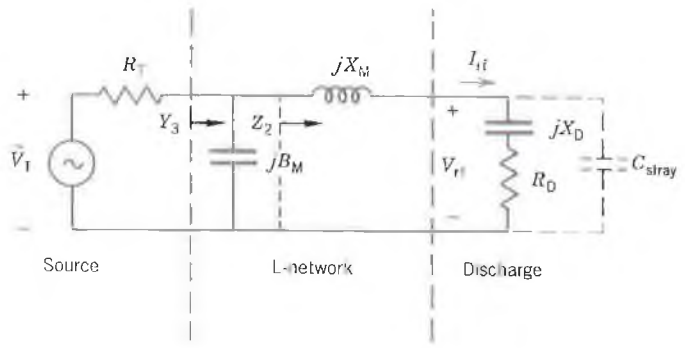

Figure 2.14 Equivalent circuit for matching the radio frequency power source to the discharge using an L-network.

It consists of a shunt capacitor having susceptance $B_M = \omega C_M$ and a series inductor having a reactance of $X_M = \omega L_M$. The end goal is for the source to see an impedance of 50-ohms. The combination of the matching unit impedance and the plasma chamber impedance will give 50-ohms and facilitate maximum power transfer. Smith Chart analysis is used to develop the matching network and is discussed in § 2.2.6. An overview is given of transmission lines first to lead into Smith Chart analysis.

2.2.5 Transmission Lines

Fundamentally, a transmission line is a two-port network with each port consisting of two terminals, as illustrated in figure 2.15.

Figure 2.15 A transmission line is a two-port network connecting a generator circuit at the sending end to a load at the receiving end.

One of the ports is the sending end and the other is the receiving end. The source connected to its sending end may be any circuit with an output voltage, such as a radio frequency generator. From circuit theory, any such source can be represented by a Thevenin equivalent *generator circuit* as discussed in § *2.2.4*. In the case of AC signals, the generator circuit is represented by a voltage phasor $\boldsymbol{V_g}$ and impedance $\boldsymbol{Z_g}$. The circuit connected to the receiving end of the transmission

line is called the *load circuit*, or simply the *load*. This will be the capacitively coupled plasma chamber and is represented by an equivalent load resistance R_L or a load impedance Z_L in the AC case.

In low-frequency electrical circuits, we usually use wires to connect the elements of the circuit in the desired configuration. In the circuit shown in figure 2.16, for example, the generator is connected to a simple *RC* load via a pair of

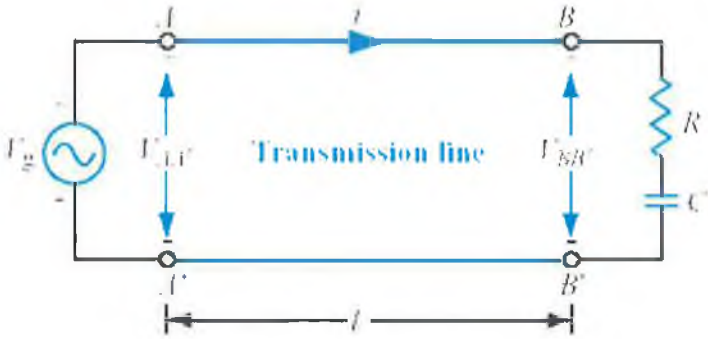

Figure 2.16 Generator connected to an RC circuit through a transmission line of length l.

wires. In view of the definition in the preceding paragraphs of what constitutes a transmission line, the following questions are posed: Is the pair of wires between terminals *AA'* and terminals *BB'* a transmission line? If so, why is it important? After all, the current in the circuit and the voltage across its elements is usually solved without regard for the wires connecting the elements. The answer to this question is yes, but the impact of the line on the current and voltages in the circuit depends on the length of the line l and the frequency f of the signal provided by the generator. (As we will see later, the determining factor is the ratio of the length l to the wavelength λ of the wave propagating on the transmission line between *AA'* and *BB'*.) If the generator voltage is cosinusoidal in time, then the voltage across the input terminals *AA'* is

$$V_{AA'} = V_g(t) = V_0 \cos \omega t \text{ Volts}$$

where $\omega = 2\pi f$ is the angular frequency, and if we assume that the current flowing through the wires travels at the speed of light, $c = 3 \times 10^8$ m/s, then the voltage across the output terminals *BB'* will have to be delayed in time relative to that across *AA'* by the travel delay time l/c. Thus, assuming no significant ohmic losses in the transmission line,

$$V_{BB'}(t) = V_{AA'}(t - l/c) = V_0 \cos[\omega(t - t - l/c)] \text{ Volts}$$

Let us compare $V_{BB'}$ to $V_{AA'}$ at $t = 0$ for an ultralow-frequency electronic circuit operating at a frequency $f = 1$ kHz. For a typical wire length $l = 5$cm, the above equations give $V_{AA'} = V_0$ and $V_{AA'} = V_0 \cos(2\pi fl/c) = 0.999999999998\ V_0$. Thus, for all practical purposes, the length of the transmission line may be ignored and terminal *AA'* may be treated as identical to *BB'*. On the other hand, had the line been 20km long telephone cable carrying a 1 kHz voice signal, then the same calculation would have led to $V_{BB'} = 0.91V_0$. The determining factor is the magnitude of $\omega l/c$. The velocity of propagation u_p of a travelling wave is related to the oscillation frequency f and the wavelength λ by

$$u_p = f\lambda \text{ m/s}$$

In the present case, $u_p = c$. Hence, the phase factor

$$\frac{\omega l}{c} = \frac{2\pi fl}{c} = 2\pi \frac{l}{\lambda} \text{ radians}$$

When l/λ is very small, transmission-line effects may be ignored, but when $l/\lambda >$ 0.01, it may be necessary to account not only for the phase shift associated with the time delay, but also for the presence of *reflected* signals that may have been bounced back by the load toward the generator. *Power loss* on the line and *dispersive* effects may need to be considered as well. A dispersive transmission line is one on which the wave velocity is not constant as a function of the frequency f. This means that the shape of a rectangular pulse, which through Fourier analysis is composed of many waves of different frequencies, will be distorted as it travels down the line because its different frequency components will not propagate at the same velocity. The relevance of these factors to the design of plasma chambers may be important when the distance between the power generator and plasma chamber is large, for example if the power generator is in the "sub-fab" area of a semiconductor fabrication factory.

2.2.5.2 Propagation Modes

Transmission lines may be classified into two basic types:

Transverse electromagnetic (TEM) transmission lines: Waves propagating along these lines are characterised by electric and magnetic fields that are entirely *transverse* to the direction of propagation. This is called a TEM mode. A good example is the coaxial load shown in figure 2.17; the electric field lines are in the

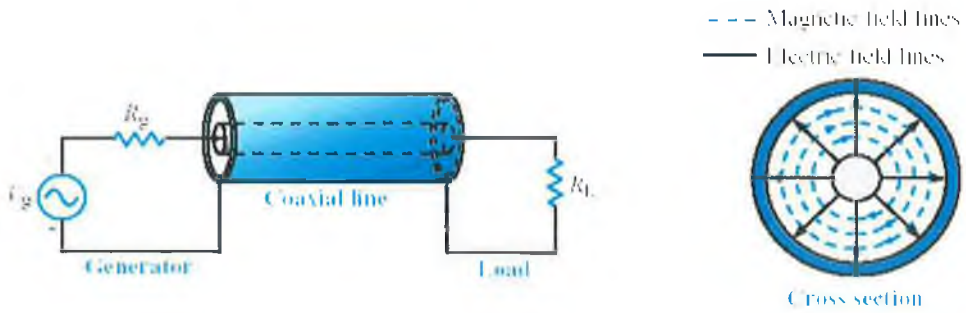

Figure 2.17 Coaxial transmission line.

radial direction between the inner and outer conductors, the magnetic field forms circles around the inner conductor, and hence neither has any components along the length of the line (the direction of wave propagation).

Higher-order transmission lines: Waves propagating along these lines have at least one significant field component in the direction of propagation. Hollow conducting waveguides, dielectric rods and optical fibres belong to this class of lines. TEM mode transmission lines are only ones of interest for this thesis.

Firstly, the transmission line will be represented in terms of a lumped-element circuit model. The model leads to the *telegrapher's equations*. By combining these equations, wave equations for the voltage and current can be obtained for any point on the line. Solutions of the wave equations for the sinusoidal steady-state case lead to a set of formulas that can be used to solve a wide range of practical problems. In § 2.2.6 we will use the graphical technique known as the *Smith chart*, which facilitates the solution of many transmission-line problems without having to perform laborious calculations involving complex numbers.

2.2.5.3 Lumped-Element Model

A transmission line can be represented by a parallel-wire configuration, regardless of the specific shape of the TEM line under consideration. The functionality of the transmission line can be represented by an equivalent circuit. The line is orientated along the z-direction, subdivided into differential sections each of length Δz as shown in figure 2.18. An equivalent circuit represents each

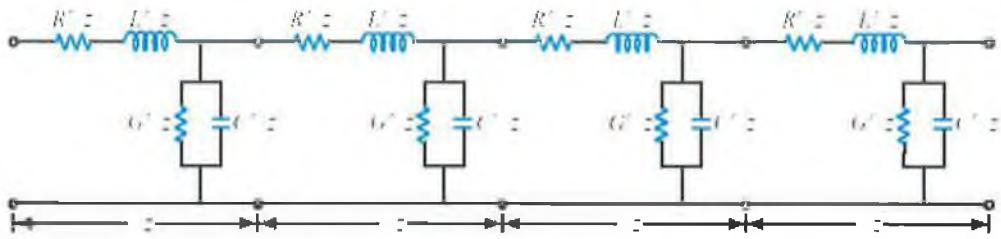

Figure 2.18 Equivalent circuit of a TEM transmission line.

section and is called the *lumped-element circuit* model, consisting of four basic elements which are called the *transmission line parameters*. These are:

R': the combined resistance of both conductors per unit length, in ohms/m,

L': the combined inductance of both conductors per unit length, in H/m

G': the conductance of the insulation medium per unit length, in S/m

C': the capacitance of the two conductors per unit length, F/m

Whereas the four line parameters have different expressions for different types and dimensions of transmission lines, the equivalent model represented by figure 2.18 is equally applicable to all transmission lines characterised by TEM-mode wave propagation.

Expressions for the line parameters *R'*, *L'*, *G'*, and *C'* are given in Table 2.1 below for three types of TEM transmission lines.

Parameter	***Coaxial***	***Two wire***	***Parallel Plate***	***Unit***
R'	$\frac{Rs}{2\pi}\left(\frac{1}{a}+\frac{1}{b}\right)$	$\frac{Rs}{\pi a}$	$\frac{2Rs}{w}$	Ω/m
L'	$\frac{\mu}{2\pi}\ln\left(\frac{b}{a}\right)$	$\frac{\mu}{\pi}\ln\left[\left(\frac{d}{a}\right)+\sqrt{\left(\frac{d}{2a}\right)^2-1}\right]$	$\frac{\mu d}{w}$	H/m
G'	$\frac{2\pi\sigma}{\ln\left(\frac{b}{a}\right)}$	$\frac{\pi\sigma}{\ln\left[\left(\frac{d}{a}\right)+\sqrt{\left(\frac{d}{2a}\right)^2-1}\right]}$	$\frac{\sigma w}{d}$	S/m
C'	$\frac{2\pi\varepsilon}{\ln\left(\frac{b}{a}\right)}$	$\frac{\pi\varepsilon}{\ln\left[\left(\frac{d}{a}\right)+\sqrt{\left(\frac{d}{2a}\right)^2-1}\right]}$	$\frac{\varepsilon w}{d}$	F/m

Table 2.1 Transmission-line parameters for three types of lines.

The expressions are functions of two sets of parameters: (1) geometric parameters defining the cross-sectional dimensions of the given line and (2) electromagnetic constitutive parameters characteristic of the materials of which the conductors and the insulating material between them are made. The pertinent geometric parameters are as follows:

Coaxial line

- a = outer radius of inner conductor
- b = inner radius of outer conductor

Two-wire line

- a = radius of each wire
- d = spacing between wire's centres

Parallel-plate line

- w = width of each plate
- d = thickness of insulation between plates

The constitutive parameters apply to all three lines and consist of two groups: μ_c and σ_c are the magnetic permeability and electrical conductivity of the conductors, and ε, μ and σ are the electrical permittivity, magnetic permeability, and electrical conductivity of the insulation material separating the conductors.

The lumped-element model represents the physical processes associated with the currents and voltages on any TEM transmission line. The model (shown in figure 2.18 above) leads to a set of equations called the *telegrapher's equations*. It consists of two series elements, R' and L', and two shunt elements, G' and C'. By way of providing a physical explanation for the lumped-element model, consider a small section of a coaxial line shown in figure 2.19.

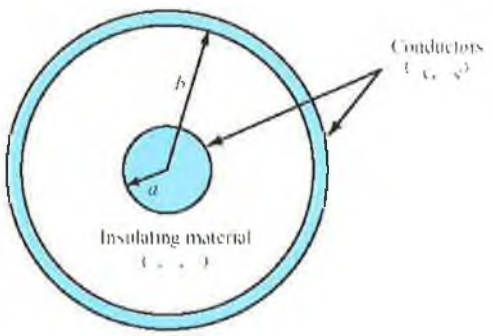

Figure 2.19 Cross section of a coaxial line.

The line consists of an inner conductor of radius a separated from an outer conducting cylinder of radius b by a material with permittivity ε, permeability μ, and conductivity σ. The two metal conductors are made of a material with conductivity σ_c and permeability μ_c. When a voltage source is connected across the two conductors at the sending end of the line, currents will flow through the conductors, primarily along the outer surface of the inner conductors and the inner surface of the outer conductor. The line resistance R' accounts for the combined resistance per unit length of the inner and outer conductors. The expression for R' is given by

$$R' = \frac{R_s}{2\pi}\left(\frac{1}{a}+\frac{1}{b}\right) \text{ (Ω/m)}$$

where R_s, which represents the surface resistance of the conductors, is called the *intrinsic resistance* and is given as

$$R_s = \sqrt{\frac{\pi f \mu_c}{\sigma_c}} \text{ (Ω)}$$

The intrinsic resistance depends not only on the material of the conductors (σ_c and μ_c), but on the frequency f of the wave travelling on the line as well. For a *perfect conductor* with $\sigma_c = \infty$ or a high-conductivity material such that $(f\mu_c/\sigma_c) << 1$, R_s approaches zero and so does R'.

The inductance per unit length of a coaxial line is given by

$$L' = \frac{\mu}{2\pi}\ln\left(\frac{b}{a}\right) \text{ (H/m)}$$

The shunt conductance per unit length G' accounts for current flow between the outer and inner conductors, made possible by the material conductivity σ of the insulator. It is precisely because the current flow is from one conductor to the other that G' is a shunt element in the lumped-element model. Its expression is given by

$$G' = \frac{2\pi\sigma}{\ln\left(\frac{b}{a}\right)} \text{ (S/m)}$$

If the material separating the inner and outer conductors is a *perfect dielectric* with $\sigma = 0$, then $G' = 0$.

The last line parameter on our list is the capacitance per unit length C'. When equal and opposite charges are placed on any two non contacting

conductors, a voltage difference will be induced between them. Capacitance is defined as the ratio of charge to voltage difference. For the coaxial line, C' is given by

$$C' = \frac{2\pi\varepsilon}{\ln\left(\frac{b}{a}\right)} \text{ (F/m)}$$

All TEM transmission lines share the following useful relations:

$$L'C' = \mu\varepsilon$$

and

$$\frac{G'}{C'} = \frac{\sigma}{\varepsilon}.$$

2.2.5.4 Transmission Line Equations

A transmission line usually connects a source on one end to a load on the other end. Equations have been developed that describe the voltage across the transmission line and the current carried by the line as a function of time t and spatial position z. These equations are known as the telegrapher's equations:

$$\text{Equation 1:} \quad -\frac{d\tilde{V}(z)}{dz} = (R' + j\omega L')\tilde{I}(z)$$

$$\text{Equation 2:} \quad -\frac{d\tilde{I}(z)}{dz} = (G' + j\omega C')\tilde{V}(z)$$

Equation 1 and equation 2 are first-order coupled equations and can be combined to give two second-order uncoupled wave equations, one for $\tilde{V}(z)$ and one for $\tilde{I}(z)$.

$$\text{Equation 3:} \quad \frac{d^2\tilde{V}(z)}{dz^2} - \gamma^2\tilde{V}(z) = 0$$

$$\text{Equation 4:} \quad \frac{d^2\tilde{I}(z)}{dz^2} - \gamma^2\tilde{I}(z) = 0$$

where

$$\gamma = \sqrt{(R' + j\omega L')(G' + j\omega C')}$$

Equations 3 and 4 are called *wave equations* for $\tilde{V}(z)$ and $\tilde{I}(z)$, and γ is called the *complex propagation constant* of the transmission line. γ consists of a real part α, called the *attenuation constant* of the line with the units of Np/m, and an

imaginary part β, called the *phase constant* of the line with units of the line with units of rad/m. Therefore,

$$\gamma = \alpha + \beta$$

with

$$\alpha = \mathrm{Re}(\gamma) = \mathrm{Re}\left(\sqrt{(R'+j\omega L')(G'+j\omega C')}\right)$$

$$\beta = \mathrm{Im}(\gamma) = \mathrm{Im}\left(\sqrt{(R'+j\omega L')(G'+j\omega C')}\right)$$

Equations 3 and 4, the wave equations, have travelling wave solutions of the following form:

Equation 5: $\tilde{V}(z) = V_0^+ e^{-\gamma z} + V_0^- e^{\gamma z}$ Volts

Equation 6: $\tilde{I}(z) = I_0^+ e^{-\gamma z} + I_0^- e^{\gamma z}$ Amps

where the $e^{-\gamma z}$ term represents wave propagation in the + z-direction and the $e^{\gamma z}$ term represents wave propagation in the – z-direction. There are four unknowns in these solutions, V_o^+ and I_o^+ propagating in the + z-direction, V_o^- and I_o^- propagating in the - z-direction. The current wave amplitudes I_o^+ and I_o^- can be related to the voltage wave amplitudes V_o^+ and V_o^- by using equation 5 in equation 1 and then solving for the current $\tilde{I}(z)$ to get the result

$$\tilde{I}(z) = \frac{\gamma}{R'+j\omega L'}\left[V_0^+ e^{-\gamma z} - V_0^- e^{\gamma z}\right]$$

Comparison of each term with the corresponding term in the expression given by equation 6 leads to the conclusion that

$$\frac{V_0^+}{I_0^+} = Z_0 = \frac{-V_0^-}{I_0^-}$$

where

$$Z_0 = \frac{R'+j\omega L'}{\gamma} = \sqrt{\frac{R'+j\omega L'}{G'+j\omega C'}}\ \Omega$$

is defined as the *characteristic impedance* of the line. It should be noted that Z_0 is equal to the ratio of the voltage amplitude to the current amplitude for each of the travelling waves individually (with an additional minus sign in the case of the –z propagating wave), but it is not equal to the ratio of the total voltage $\tilde{V}(z)$ to

the total current $\tilde{I}(z)$, unless one of the two waves is absent. The equation for $\tilde{I}(z)$ can be rewritten as

Equation 7: $$\tilde{I}(z) = \frac{V_0^+}{Z} e^{-\gamma z} - \frac{V_0^-}{Z} e^{\gamma z}$$

Expressions for the wave amplitudes V_o^+ and V_o^- can be found by applying boundary conditions to the load and sending end of the transmission line. In general, each will be a complex quantity composed of a magnitude and a phase angle. Thus

$$V_o^+ = |V_0^+| e^{j\phi^+}$$

$$V_o^- = |V_0^-| e^{j\phi^-}$$

Upon substituting these definitions into Equation 5 and replacing γ with $\gamma = \alpha + \beta$, we can convert back to the time domain to obtain an expression for $v(z,t)$, the instantaneous voltage on the line:

Equation 8: $$v(z,t) = |V_o^+| e^{-\alpha z} \cos(\omega t - \beta z + \phi^+) + |V_o^-| e^{\alpha z} \cos(\omega t + \beta z + \phi^+)$$

The first term in the above equation is a wave travelling in the + z-direction (as the coefficients of *t* and *z* have opposite signs) and the second term as a wave travelling in the – z-direction (the coefficients of *t* and *z* are both positive), both propagating with a phase velocity u_p given by

$$u_p = f\lambda = \frac{\omega}{\beta}$$

The factor $e^{-\alpha z}$ accounts for the attenuation of the +z propagating wave and the $e^{+\alpha z}$ accounts for the attenuation of the –z propagating wave. The presence of two waves on the line propagating in opposite directions produces a *standing wave*. To gain a physical understanding of what this means an examination of the *lossless line* $(\alpha = 0)$ is required. The results of this examination can be extended to the *lossy transmission line* $(\alpha \neq 0)$.

2.2.5.5 The Lossless Transmission Line

As has been shown, a transmission line is characterised by two fundamental properties, its propagation constant γ and its characteristic impedance Z_0, both

of which are specified by the angular frequency ω and the line parameters R', L', G' and C'. In many practical situations the transmission line can be designed to minimise ohmic losses by selecting conductors with very high conductivities and dielectric materials (separating the conductors) with negligible conductivities. As a result R' and G' assume very small values such that $R' << \omega L'$ and $G' << \omega C'$. These lossless-line conditions allow $R' = G' = 0$, resulting in

$$\gamma = \alpha + j\beta = j\omega\sqrt{L'C'}$$

which means that

$$\alpha = 0 \quad \text{(lossless line)}$$

$$\beta = \omega\sqrt{L'C'} \quad \text{(lossless line).}$$

Application of the lossless-line conditions gives the characteristic impedance

$$Z_0 = \sqrt{\frac{L'}{C'}} \quad \text{(lossless-line)}$$

which is now a real number. Using the lossless expression for β, the following relations for the wavelength λ and the phase u_p are obtained:

$$\lambda = \frac{2\pi}{\beta} = \frac{2\pi}{\omega\sqrt{L'C'}},$$

$$u_p = \frac{\omega}{\beta} = \frac{1}{\sqrt{L'C'}}.$$

Applying these relationships to $L'C' = \mu\varepsilon$ results in

$$\beta = \omega\sqrt{\mu\varepsilon}$$

$$u_p = \frac{1}{\sqrt{\mu\varepsilon}}$$

where μ and ε are the magnetic permeability and electrical permittivity of the insulating material separating the conductors. Materials used for this purpose are usually characterised by the permeability $\mu = \mu_0$, where $\mu_0 = 4\pi \times 10^{-7}$ H/m is the permeability of free space, and the permittivity is usually specified in terms of the relative permittivity ε_r

$$\varepsilon_r = \frac{\varepsilon}{\varepsilon_0},$$

where $\varepsilon_0 = 8.854 \times 10^{-12}$ F/m is the permittivity of free space. Hence

$$u_p = \frac{1}{\sqrt{\mu_0 \varepsilon_r \varepsilon_0}} = \frac{1}{\sqrt{\mu_0 \varepsilon_0}} \cdot \frac{1}{\sqrt{\varepsilon_r}} = \frac{c}{\sqrt{\varepsilon_r}},$$

where $c = 1/\sqrt{\mu_0 \varepsilon_0} = 3 \times 10^8 m/s$ is the velocity of light in a vacuum. If the insulating material between the conductors is air, then $\varepsilon_r = 1$ and $u_p = c$. Therefore, given the relationship between λ and u_p

$$\lambda = \frac{u_p}{f} = \frac{c}{f} \cdot \frac{1}{\sqrt{\varepsilon_r}} = \frac{\lambda_0}{\sqrt{\varepsilon_r}},$$

where $\lambda_0 = c/f$ is the wavelength in air corresponding to a frequency f. It should be noted that, because both u_p and λ depend on ε_r, the choice of the type of insulating material used in a transmission line is dictated not only by its mechanical properties, but by its electrical properties as well.

When the phase velocity of a medium is independent of frequency, the medium is called *nondispersive*, which clearly is the case for a lossless TEM transmission line. This is an important feature for the transmission of digital data in the form of pulses. A rectangular pulse or a series of pulses is composed of many Fourier components with different frequencies. If the phase velocity is the same for all frequency components (or at least for the dominant ones), the pulse shape will remain the same as the pulse propagating in a dispersive medium gets progressively distorted, and the pulse length increases (stretches out) as a function of distance in the medium, thereby imposing a limitation on the maximum data rate (which is related to the length of the individual pulses and the spacing between adjacent pulses) that can be transmitted through the medium without loss of information.

Table 2.2 provides a list of expressions for γ, Z_0 and u_p for the general case of a lossy line and for several types of lossless lines.

	Propagation Constant $\gamma = \alpha + j\beta$	***Phase Velocity*** u_p	***Characteristic Impedance*** Z_0
General Case	$\gamma = \sqrt{(R'+j\omega L')(G'+j\omega C')}$	$u_p = \omega/\beta$	$Z_0 = \sqrt{\frac{(R'+j\omega L')}{(G'+j\omega C')}}$
Lossless $(R'=G'=0)$	$\alpha = 0,\ \beta = \omega\frac{\sqrt{\varepsilon_r}}{c}$	$u_p = \frac{c}{\sqrt{\varepsilon_r}}$	$Z_0 = \sqrt{\frac{L'}{C'}}$
Lossless Coaxial	$\alpha = 0,\ \beta = \omega\frac{\sqrt{\varepsilon_r}}{c}$	$u_p = \frac{c}{\sqrt{\varepsilon_r}}$	$Z_0 = \left(\frac{60}{\sqrt{\varepsilon_r}}\right)\ln\left(\frac{b}{a}\right)$
Lossless Parallel Plate	$\alpha = 0,\ \beta = \omega\frac{\sqrt{\varepsilon_r}}{c}$	$u_p = \frac{c}{\sqrt{\varepsilon_r}}$	$Z_0 = \left(\frac{120\pi}{\sqrt{\varepsilon_r}}\right)\left(\frac{d}{w}\right)$

Table 2.2 Characteristic parameters of transmission lines.

2.2.5.6 Voltage Reflection Coefficient

With $\gamma = j\beta$ for the lossless line, the expressions given by Equation 5 and Equation 7 for the total voltage and current on the line become

Equation 9: $$\tilde{V}(z) = V_0^{+}e^{-j\beta z} + V_0^{-}e^{j\beta\gamma z}$$

Equation 10: $$\tilde{I}(z) = \frac{V_0^{+}}{Z}e^{-j\beta z} - \frac{V_0^{-}}{Z}e^{j\beta z}$$

These expressions contain two unknowns V_0^{+} and V_0^{-}, the voltage amplitudes of the incident and reflected waves, respectively. To determine V_0^{+} and V_0^{-}, we need to consider the lossless transmission line in the context of the complete circuit, including a generator circuit at its input terminals and a load at its output terminals, as shown in figure 2.20.The line, of length *l*, is terminated in an arbitrary *load impedance* Z_L. For convenience, the reference of the spatial coordinate z is chosen such that $z = 0$ corresponds to the location of the load. At the sending end at $z = -l$, the line is connected to a sinusoidal voltage source with phasor $\tilde{V}_g$ and internal impedance Z_g. At the load, the phasor voltage across it, $\tilde{V}_L$, and the phasor current through it, $\tilde{I}_L$, are related by the load

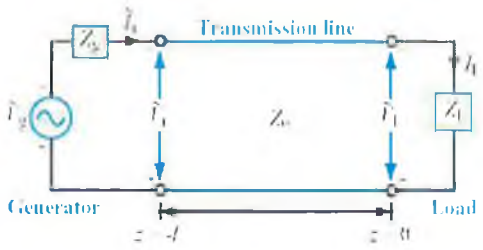

Figure 2.20 Transmission line of length l connected on one end to a generator circuits and on the other end to a load Z_L.

impedance Z_L as follows:

$$Z_L = \frac{\tilde{V}_L}{\tilde{I}_L}.$$

The voltage $\tilde{V}_L$ is equal to the voltage on the line $\tilde{V}(z)$ given by Equation 9, and $\tilde{I}_L$ is equal to $\tilde{I}(z)$ given by Equation 10, both evaluated at $z = 0$:

$$\tilde{V}_L = \tilde{V}(z=0) = V_0^+ + V_0^-,$$

$$\tilde{I}_L = \tilde{I}(z=0) = \frac{V_o^+}{Z_0} - \frac{V_o^-}{Z_0}.$$

These expressions used in the load impedance expression give the result:

$$Z_L = \left(\frac{V_0^+ + V_0^-}{V_0^+ - V_0^-}\right) Z_0.$$

Solving for V_0^- gives

$$V_0^- = \left(\frac{Z_L - Z_0}{Z_L + Z_0}\right) V_0^+.$$

The ratio of the amplitude of the reflected voltage wave to the amplitude of the incident voltage wave at the load is known as the *voltage reflection coefficient* Γ:

$$\Gamma = \frac{V_0^-}{V_0^+} = \frac{Z_L - Z_0}{Z_L + Z_0} = \frac{Z_L/Z_0 - 1}{Z_L/Z_0 + 1}.$$

It is noted that

$$\frac{I_0^-}{I_0^+} = -\frac{V_0^-}{V_0 +} = -\Gamma$$

Γ is governed by a single parameter, the load impedance Z_L, normalised to the characteristic impedance of the line, Z_0, a real number. However Z_L is in

general a complex quantity, as in the case of a series RL circuit, for example, for which $Z_L = R + j\omega L$. Hence in general Γ may be complex also:

$$\Gamma = |\Gamma| e^{j\theta_r}$$

where $|\Gamma|$ is the magnitude of Γ and θ_r is its phase angle. Note that $|\Gamma| \leq 1$.

A load is said to be matched to the line if $Z_L = Z_0$ because then there will be no reflection by the load ($\Gamma = 0$ and $V_0^- = 0$). On the other hand, when the load is an open circuit ($Z_L = \infty$), $\Gamma = 1$ and $V_0^- = V_0^+$, and when it is a short circuit ($Z_L = 0$), $\Gamma = -1$ and $V_0^- = -V_0^+$.

2.2.5.7 Standing Waves

Using the relation $V_0^- = \Gamma V_0^+$ in Equation 9 and Equation 10 gives the expressions

$$\text{Equation 11:} \quad \tilde{V}(z) = V_0^+ \left(e^{-j\beta z} + \Gamma e^{j\beta\gamma z}\right)$$

$$\text{Equation 12:} \quad \tilde{I}(z) = \frac{V_0^+}{Z_0}\left(e^{-j\beta z} - \Gamma e^{j\beta\gamma z}\right)$$

which now contain only one, yet to be determined unknown, V_0^+. Before solving for this unknown, it is important to examine the physical meaning represented by these expressions. Firstly an expression for $|\tilde{V}(z)|$, the magnitude of $\tilde{V}(z)$, is derived. Using $\Gamma = |\Gamma| e^{j\theta_r}$ in Equation 11 and applying the relation $|\tilde{V}(z)| = \left[\tilde{V}(z)\tilde{V}^*(z)\right]$, where $\tilde{V}^*(z)$ is the complex conjugate of $\tilde{V}(z)$ gives:

$$|\tilde{V}(z)| = \left\{\left[V_0^+\left(e^{-j\beta z} + |\Gamma| e^{j\theta_r} e^{j\beta z}\right)\right]\left[\left(V_0^+\right)^*\left(e^{j\beta z} + |\Gamma| e^{-j\theta_r} e^{-j\beta z}\right)\right]\right\}^{1/2}$$

$$= \left|V_0^+\right|\left[1 + |\Gamma|^2 + |\Gamma|\left(e^{j(2\beta z + \theta_r)} + e^{-j(2\beta z + \theta_r)}\right)\right]^{1/2}$$

$$= \left|V_0^+\right|\left[1 + |\Gamma|^2 + 2|\Gamma|\cos(2\beta z + \theta_r)\right]^{1/2}$$

where we have the identity

$$e^{jx} + e^{-jx} = 2\cos x$$

for any real quantity x. By applying the same steps to Equation 12, a similar expression can be derived for $|\tilde{I}(z)|$, the magnitude of the current $\tilde{I}(z)$.

The variations of $|\tilde{V}(z)|$ and $|\tilde{I}(z)|$ as a function of z, the position on the line relative to the load at $z = 0$ are illustrated in figure 2.21 for a line with

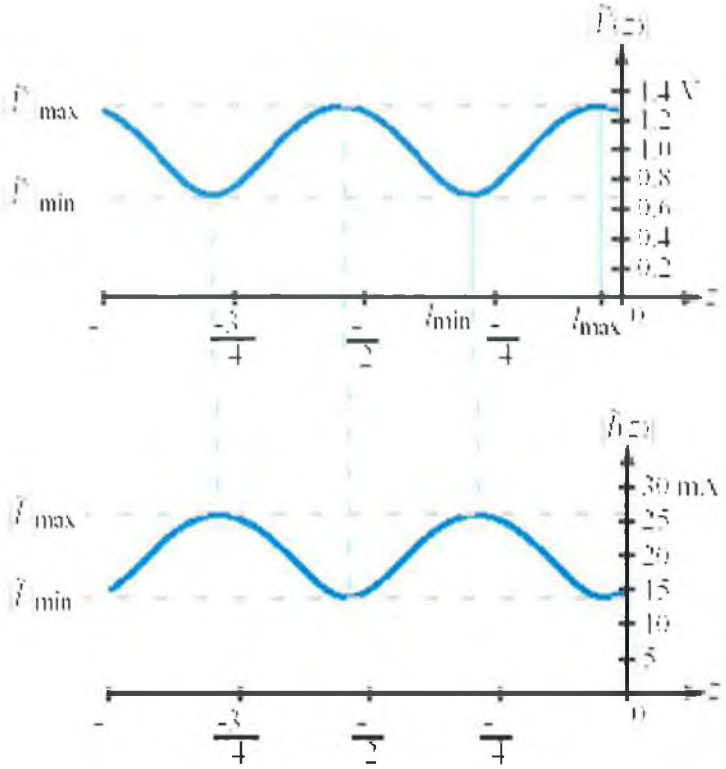

Figure 2.21 Standing-wave pattern for a lossless transmission line of characteristic impedance Z_0=50Ω, terminated in a load with reflection coefficient $\Gamma = 0.3e^{j30°}$.

$|V_0^+| = 1$ volt, $|\Gamma| = 0.3$, $\theta_r = 30°$ and $Z_0 = 50(\Omega)$. The sinusoidal pattern is called a *standing wave* and it is caused by the interference of the two waves. The standing wave will have maximum voltages, $|\tilde{V}|_{max}$, and minimum voltages, $|\tilde{V}|_{min}$, along the line. The ratio of $|\tilde{V}|_{max}$ and $|\tilde{V}|_{min}$ is called the *voltage standing-wave ratio* S and is given by

$$S = \frac{|\tilde{V}|_{min}}{|\tilde{V}|_{max}} = \frac{1+|\Gamma|}{1-|\Gamma|}.$$

This quantity, often referred to by its acronym VSWR provides a measure of the mismatch between the load and the transmission line; for a matched load with $\Gamma = 0$, we get $S = 0$, and for a line with $|\Gamma| = 1$, $S = \infty$. Figure 2.22 shows the voltage standing-wave patterns for a matched load, a short-circuited line and an open line.

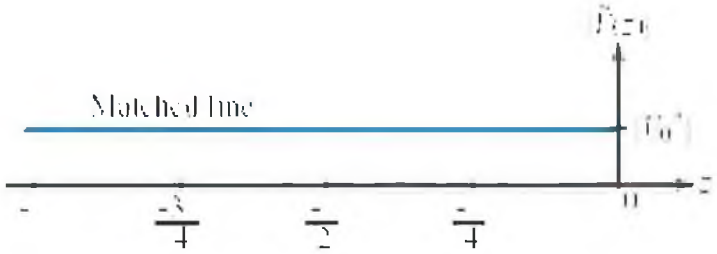

Figure 2.22 a)Z_L=Z_0, matched line.

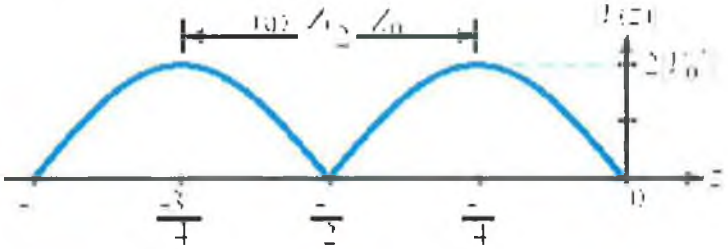

Figure 2.22 b) Z_L=0, short circuit.

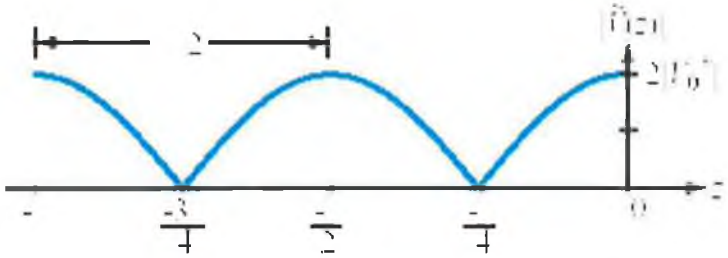

Figure 2.22 c) Z_L=∞, open circuit.

2.2.5.8 Input Impedance of the lossless Line

The standing-wave patterns indicate that for a mismatched line the voltage and current magnitudes are oscillatory with position on the line and in phase opposition with each other. Hence, the voltage to current ratio, called the *input impedance* Z_{in}, must also vary with position. Using Equation 11 and Equation 12, Z_{in} is given by

$$Z_{in}(z)=\frac{\tilde{V}(z)}{\tilde{I}(z)}=\frac{V_0^+\left[e^{-j\beta z}+\Gamma e^{j\beta z}\right]}{V_0^+\left[e^{-j\beta z}-\Gamma e^{j\beta z}\right]}Z_0=Z_0\left[\frac{1+\Gamma e^{j2\beta z}}{1-\Gamma e^{j2\beta z}}\right](\Omega)$$

Note that $Z_{in}(z)$ is the ratio of the total voltage (incident-wave and reflected-wave voltages) to the total current at any point z on the line, in contrast with the characteristic impedance of the line Z_0, which relates the voltage and current of each of the two waves individually $\left(Z_0=V_0^+/I_0^+=-V_0^-/I_0^-\right)$.

Of particular interest in many transmission-line problems is the input impedance at the input of the line at $z=-l$, which is given by

Equation 13: $$Z_{in}(-l) = Z_0\left[\frac{e^{j\beta l} + \Gamma e^{-j\beta l}}{e^{j\beta l} - \Gamma e^{-j\beta l}}\right] = Z_0\left[\frac{1 + \Gamma e^{-j2\beta l}}{1 - \Gamma e^{-j2\beta l}}\right].$$

Using $\Gamma = Z_L/Z_0 - 1/Z_L/Z_0 + 1$ and the relations

$$e^{j\beta} = \cos\beta l + j\sin\beta l\,, e^{-j\beta} = \cos\beta l - j\sin\beta l$$

Equation 13 can be written in terms of Z_L as

$$Z_{in}(-l) = Z_0\left(\frac{Z_L\cos\beta l + jZ_0\sin\beta l}{Z_0\cos\beta l + jZ_L\sin\beta l}\right) = Z_0\left(\frac{Z_L + jZ_0\tan\beta l}{Z_0 + jZ_L\tan\beta l}\right).$$

From the standpoint of the generator circuit, the transmission line can be replaced with an impedance Z_{in}, as shown in the figure 2.23.

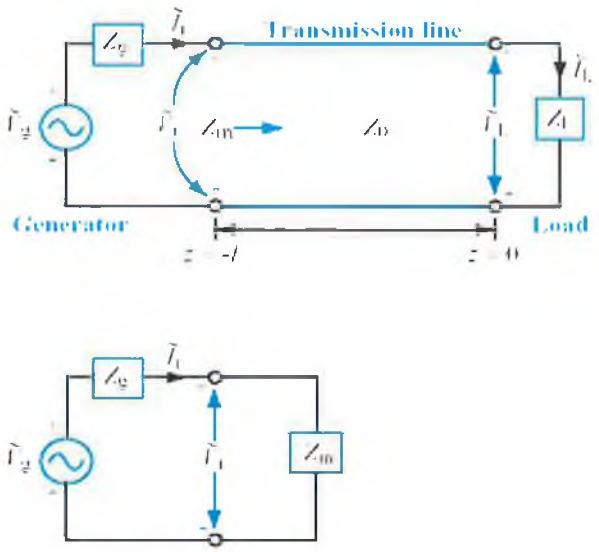

Figure 2.23 At the generator end, the terminated transmission line can be replaced with the input impedance of the line Z_{in}.

The phasor voltage across Z_{in} is given by

Equation 14: $$\tilde{V}_i = \tilde{I}_i Z_{in} = \frac{\tilde{V}_g Z_{in}}{Z_g + Z_{in}}$$

but from the standpoint of the transmission line, the voltage across it at the input of the line given by Equation 11 with $z = -l$:

Equation 15: $$\tilde{V}_i = \tilde{V}(-l) = V_0^+\left[e^{j\beta l} + \Gamma e^{-j\beta l}\right]$$

Equating Equation 14 and Equation 15 and then solving for V_0^+ leads to the result

$$V_0^+ = \left(\frac{\tilde{V}_g Z_{in}}{Z_g + Z_{in}}\right)\left(\frac{1}{e^{j\beta l} + \Gamma e^{-j\beta l}}\right)$$

This completes the solution of the transmission-line wave equations, given by Equation 3 and Equation 4 for the special case of a lossless transmission line.

Finally, some important relationships are noted. A network analyser is a radio-frequency instrument capable of measuring the impedance of any load connected to its input terminal. When used to measure Z_{in}^{sc}, the input impedance of a lossless line terminated in a short circuit, and again Z_{in}^{oc}, the input impedance of the line when terminated in an open circuit, the combination of the two measurements can be used to determine the characteristic impedance of the line Z_0 and its phase constant β. It can be shown that

$$Z_0 = \sqrt{Z_{in}^{sc} Z_{in}^{oc}}.$$

A matched lossless transmission line with $Z_L = Z_0$, has input impedance $Z_{in} = Z_0$ for all locations on the line. $\Gamma = 0$ and all the incident power is delivered to the load regardless of the line length l.

2.2.6 The Smith Chart

One of the most valuable and pervasive graphical tools in all radio frequency engineering is the Smith Chart, originally developed in 1939 by P. Smith. It is used for analysing and designing transmission-line circuits. The chart is the reflection coefficient-to-impedance/admittance converter or vice versa. It avoids tedious manipulations of complex numbers and allows an engineer to design impedance-matching circuits with relative ease. A picture of the Smith chart is shown in figure 2.24. A derivation of the Smith chart will not be given in this thesis. Further information on the Smith Chart can be obtained from references [10] and [11]. However, some of the applications of the Smith Chart relative to the design of plasma chambers will be discussed viz. impedance matching.

A transmission line usually connects a generator circuit at one end to a load at the other end. In the case of a plasma chamber system, the plasma chamber is the load and will have complex input impedance Z_L. A radio frequency generator is used to drive the plasma in the plasma chamber. A transmission-line is placed between the generator and load and is said to be matched to the load when its characteristic impedance $Z_0 = Z_L$, in which case no reflection occurs at the load end of the line. Since the primary uses of

transmission lines are to transfer power, a matched load ensures that the power delivered to the load is a maximum.

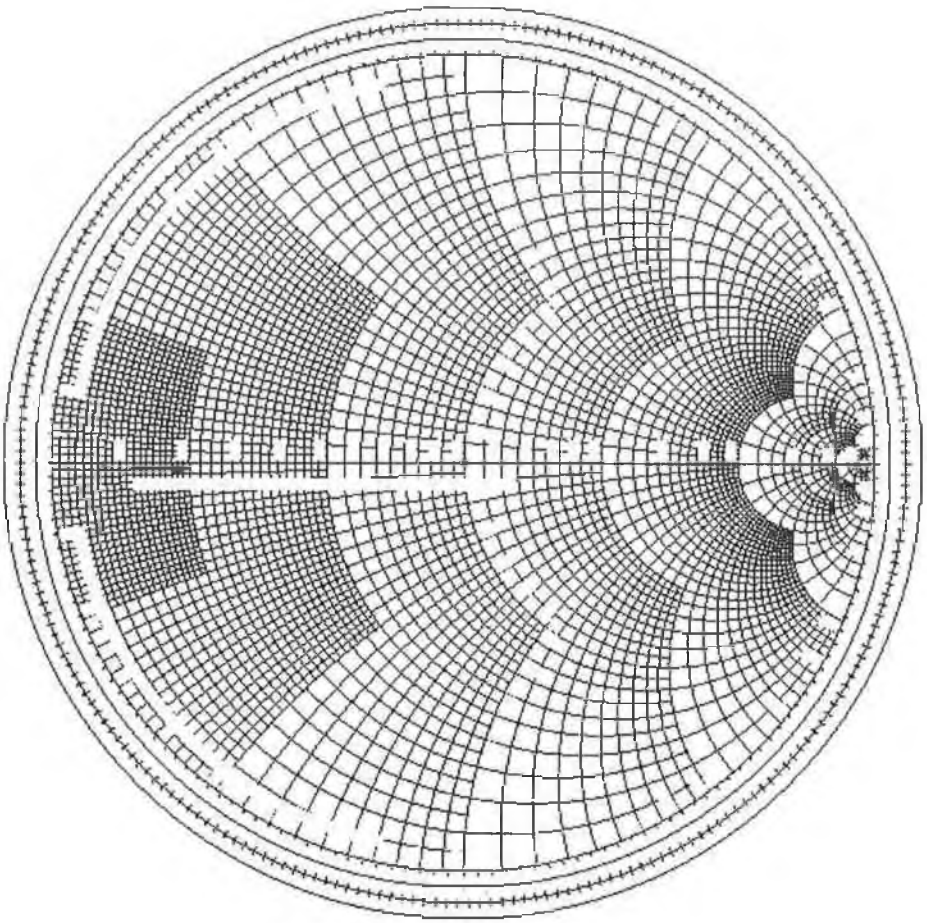

Figure 2.24 The Smith Chart

The simplest solution to matching a load to a transmission line is to design the load circuit such that its impedance $Z_L = Z_0$. Unfortunately, this may not be possible in practice because the load circuit may have to satisfy other requirements such as the geometry to hold a 300mm wafer for example. An alternative solution is to place an *impedance-matching network* between the load and the transmission line as shown in the figure 2.25.

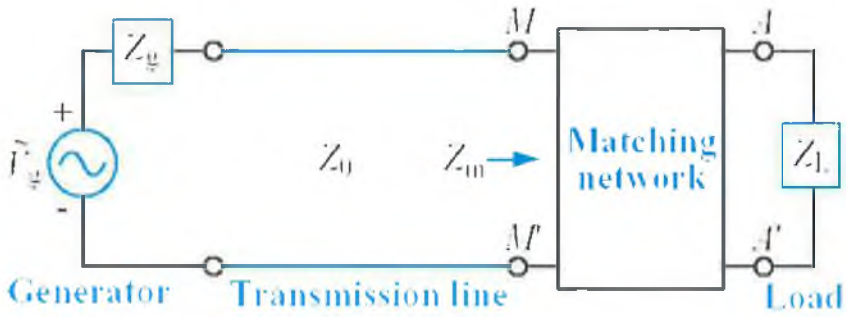

Figure 2.25 The function of a matching network is to transform the load impedance Z_L such that the input impedance Z_{in} looking into the network is equal to Z_0 of the transmission line.

The purpose of the matching network is to eliminate reflections at the juncture *MM'* between the transmission line and the network. This is achieved by designing the matching network to exhibit an impedance equal to Z_0 at *MM'* when looking into the network from the transmission line side. If the network is lossless, then all the power going into it will end up in the load. Matching networks may consist of lumped elements and in order to avoid ohmic losses only capacitors and inductors are used.

The matching network is intended to match a load impedance $Z_L = R_L + jX_L$ to a lossless transmission line with characteristic impedance Z_0. This means that the network has to transform the real part of the load impedance from R_L at the load to Z_0 at *MM'* in figure 2.25 and to transform the reactive part from X_L at the load to zero at *MM'*. The matching network has to have at least two degrees of freedom to achieve these two transformations; i.e. at least two adjustable parameters. There are many different types of matching network that can be used for plasma chambers. The components used in the matching network will depend on the complex impedance of the plasma chamber. When designing matching networks four main criteria should be considered:

- **Simplicity**

  The simplest design is usually highly preferable because simpler matching networks have fewer elements, require less work to manufacture, are cheaper, are less lossy and are more reliable compared to a more complicated and involved design.

- **Bandwidth**

  Any matching network can provide zero reflection at a single frequency; however, if impedance matching over a frequency band is required then more complex designs need to be used. Thus, there is a trade-off between design simplicity and matching bandwidth and eventually the network price.

- **Feasibility of manufacturing**

  The plasma chamber system parameters have to be considered when designing a matching network. Clear specifications for the plasma chamber's impedance range, breakdown voltage and breakdown current must be determined so that the matching network will be able to function within the system and not become a limiting factor to the system.

- **Ease of tunability**

  Variable loads such as plasma chambers require variable tuning. Thus, the matching network design and implementation should take account of this by, for example, employing feedback systems.

2.2.7 Insertion Loss

The *insertion loss* is the attenuation resulting from inserting a circuit between the source (e.g. a radio frequency generator) and the load (e.g. a plasma chamber). The attenuation is expressed in decibels (dB). The unit for power P is watts (W). When considering insertion loss the quantity of interest is the ratio of two power levels, P_1 and P_2, such as the incident and reflected powers on a transmission line. The ratio P_1/P_2 may often vary over several orders of magnitude. The dB scale is logarithmic, thereby providing a convenient representation of the power ratio, particularly when numerical values of P_1/P_2 are plotted against some variable of interest. If

$$G = \frac{P_1}{P_2}$$

then

$$G_{dB} = 10\log G = 10\log\left(\frac{P_1}{P_2}\right) \text{ (dB).}$$

Table 2.3 provides a comparison between some values of G and the

G	G_{dB}
10^x	$10x$ dB
4	6 dB
2	3 dB
1	0 dB
0.5	-3 dB
0.25	-6 dB
0.1	-10 dB
10^{-3}	-30 dB

Table 2.3 Power ratios in natural numbers and in decibels.

corresponding values of G_{dB}. Even though decibels are defined for power ratios, they can sometimes be used to represent other quantities. For example, if $P_1 = V_1^2/R$ is the power dissipated in a resistor R with voltage V_1 across it at time t_1, and $P_2 = V_2^2/R$ is the power dissipated in the same resistor at time t_2, then

$$G_{dB} = 10\log\left(\frac{P_1}{P_2}\right) = 10\log\left(\frac{V_1^2/R}{V_2^2/R}\right)$$

$$= 20\log\left(\frac{V_1}{V_2}\right) = 20\log(g) = g_{dB}$$

where $g = V_1/V_2$ is the voltage ratio. Note that for voltage (or current) ratios the scale factor is 20 rather that 10, which implies that $G_{dB} = g_{dB}$

2.3 Plasma Theory

2.3.1 An overview of Plasma

A plasma is a collection of free, charged particles moving in random directions that are, on the average, electrically neutral. The semiconductor industry generally uses weakly ionised plasma discharges which have the following properties:

- They are driven electrically.
- Charged particle collisions with neutral gas molecules are important.
- There are boundaries at which surface losses are important.
- Ionisation of neutrals sustains the plasma in the steady state.
- The electrons are not in thermal equilibrium with the ions.

A simple discharge is shown schematically in figure 2.26. It consists of a

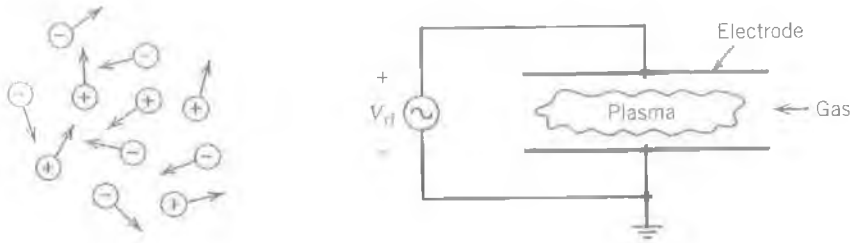

Figure 2.26 Schematic of a simple discharge

voltage source that drives current through a low-pressure gas between two parallel conducting electrodes. The gas "breaks down" to form plasma that is usually weakly ionised, i.e. the plasma density is only a small fraction of the neutral gas density. Plasmas are often called a fourth state of matter. A solid substance in thermal equilibrium generally passes into a liquid state as the temperature is increased at a fixed pressure. The liquid passes into a gas as the temperature is further increased. At sufficiently high temperature, the molecules in the gas decompose to form a gas of atoms that move freely in random directions, except for infrequent collisions between atoms. It the temperature is further increased, then the atoms decompose into freely moving charged particles (electrons and positive ions), and the substance enters the plasma state. This state is characterised by a common charged particle density $n_e \approx n_i \approx n$ particles/m^3 and, in equilibrium, a temperature $T_e = T_i = T$. The temperatures required to form plasmas from pure substances in thermal equilibrium range from roughly 4000 K

for easy-to-ionise elements like cesium to 20000 K for hard-to-ionise elements like helium. The fractional ionisation of a given plasma is

$$x_{iz} = \frac{n_i}{n_g + n_i}$$

where n_g is the neutral gas density. x_{iz} is near unity for fully ionised plasmas, and $x_{iz} << 1$ for weakly ionised plasmas.

Much of the matter in the universe is in the plasma state. This is true because stars, as well as most interstellar matter, are plasmas. Although stars are plasmas in thermal equilibrium, the light and heavy charged particles in low-pressure processing discharges are almost never in thermal equilibrium, either between themselves or with their surroundings. Because these discharges are electrically driven and are weakly ionised, the applied power preferentially heats the mobile electrons, while the heavy ions efficiently exchange energy by collisions with the background gas. Hence, $T_e >> T_i$ for these plasmas.

Figure 2.27 identifies different kinds of plasmas on a log n versus T_e diagram. There is and enormous range of densities and temperatures for both

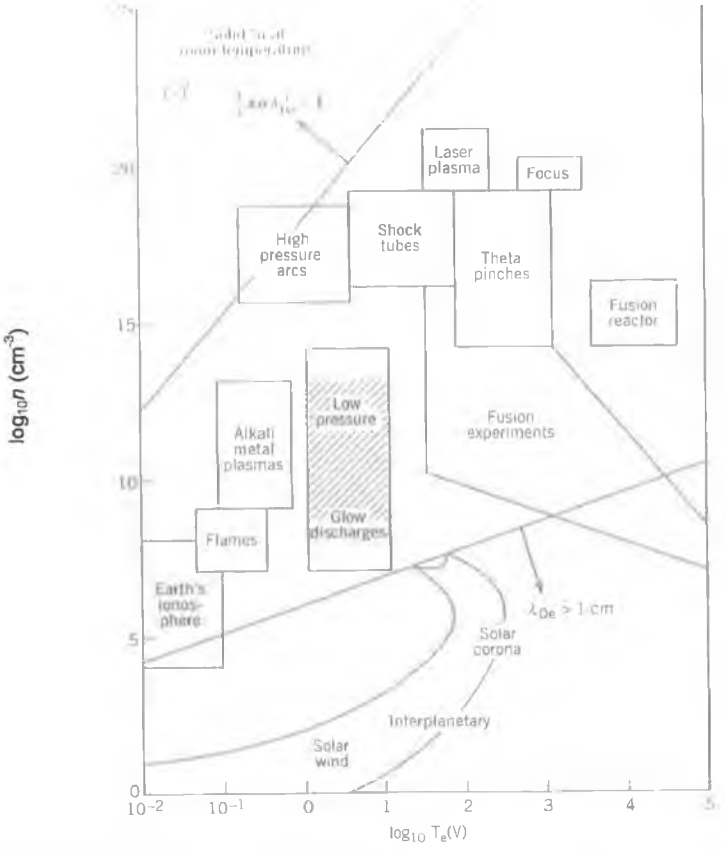

Figure 2.27Space and laboratory plasmas on a log n versus log T_e diagram.

laboratory and space plasmas. Two important types of processing discharges are indicated in figure 2.27. Low-pressure discharges are characterised by $T_e \approx$ 1-10 Volts, $T_i << T_e$, and $n \approx 10^8$-10^{13} cm^{-3}. These discharges are used as miniature chemical factories in which feedstock gases are broken into positive ions and chemically reactive etchants, deposition precursors, etc., which then flow to and physically or chemically react at the substrate surface. While energy is delivered to the substrate also, e.g., in the form of bombarding ions, the energy flux is there to promote the chemistry at the substrate, and not to heat the substrate. The gas pressures for these discharges are low: $p \approx$ 1 mTorr -1 Torr. These plasmas and their use for processing are the principal concern for this thesis.

Figure 2.28 shows the densities and temperatures (or average energies) for

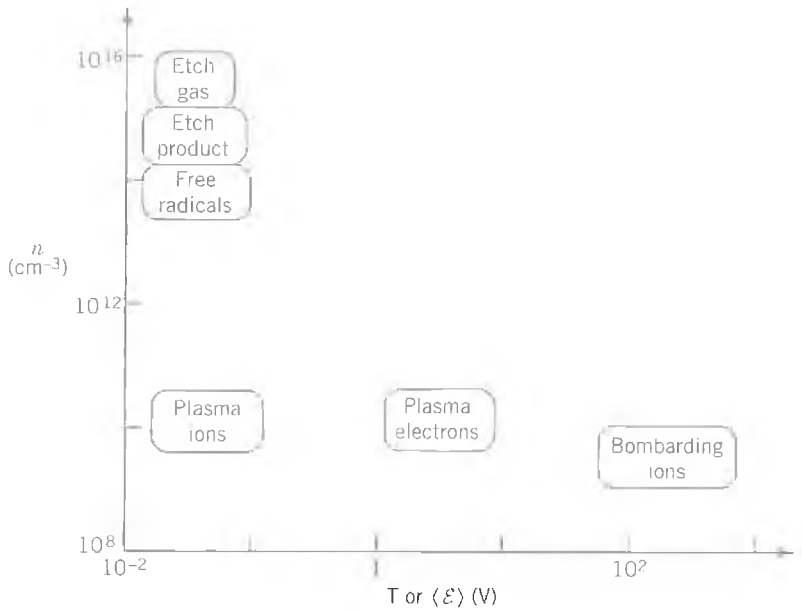

Figure 2.28 Densities and energies for various species in a low-pressure capacitive radio frequency discharge.

various species in a typical rf-driven, capacitively-coupled, low-pressure discharge; e.g. for silicon etching using CF_4. The feedstock gas, etchant atoms, etch-product gas and plasma ions have roughly the same temperature, which does not exceed a few times room temperature (0.026 Volts). The etchant F and product SiF_4 densities are significant fractions of the CF_4 density, but the fractional ionisation is very low: $n_i \sim 10^{-5}\ n_g$. The electro temperature T_e is two orders of magnitude larger than the ion temperature T_i. However, we note that the energy of ions bombarding the substrate can be 100-1000 Volts, much exceeding

T_e. The acceleration of low-temperature ions across a thin sheath region, where the plasma and substrate meet, is central to all processing discharges.

Although n_i, n_e may be five orders of magnitude lower than n_g, the charged particles play central roles in sustaining the discharge in processing. Because $T_e >> T_i$, it is the electrons that dissociate the feedstock gas to create the free radicals, etchant atoms, and deposition precursors, required for the chemistry at the substrate. Electrons also ionise the gas to create the positive ions that subsequently bombard the substrate. Energetic ion bombardment can increase chemical reaction rates at the surface, clear inhibitor films from the surface, and physically sputter materials from or implant ions into the surface.

T_e is generally less than the threshold energies ξ_{diss} or ξ_{iz} for dissociation and ionisation of the feedstock gas molecules of energies. Letting $g_e(\xi)\,\mathbf{d\xi}$ be the number of electrons per unit volume with energies lying between ξ and $\xi+\mathbf{d}\xi$, then the distribution function $g_e(\xi)$ is as is shown in figure 2.29. Electrons giving

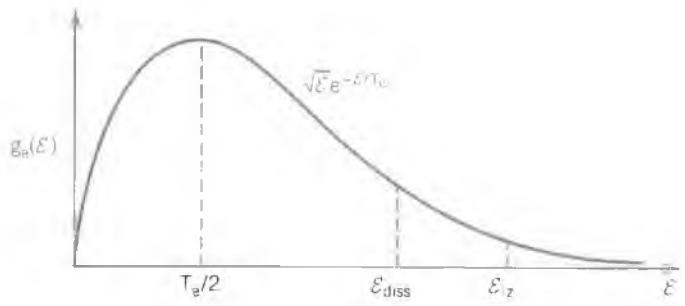

Figure 2.29 Electron distribution function in a weakly ionised discharge.

energies below ξ_{diss} or ξ_{iz} cannot dissociate or ionise the gas. The dissociation and ionisation are produced by the high-energy tail of the distribution. Although the distribution is shown in figure 2.29 as if it were Maxwellian at the bulk electron temperature T_e, this may not be the case. The tail distribution might be depressed below or enhanced above a Maxwellian by electron heating and electron-neutral collision processes. Two temperature distributions are sometimes observed, with T_e for the bulk electrons lower than T_h for the energetic electron tail.

2.3.2 Plasma Sheaths

Plasmas, which are quasineutral ($n_i \approx n_e$), are joined to wall surfaces across thin positively charged layers called sheaths. To see why, first note that the electron thermal velocity $(eT_i/m)^{1/2}$ is at least 100 times the ion thermal $(eT_i/M)^{1/2}$ velocity because $m/M << 1$ and $T_e \geq T_i$. Consider a plasma of width l with $n_e = n_i$ initially

confined between two grounded ($\Phi = 0$) absorbing walls (figure 2.30). Because the net charge density $\rho = e\,(n_i - n_e)$ is zero, the electric potential Φ and the

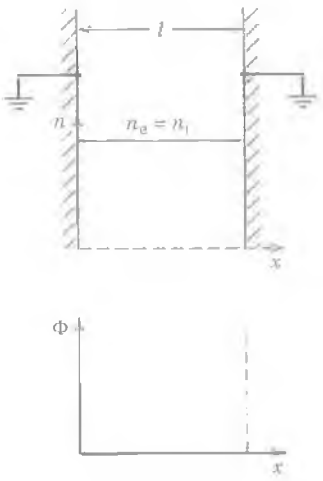

Figure 2.31Initial ion and electron densities and potential.

electric field E_x is zero everywhere. Hence, the fast-moving electrons are not confined and will rapidly be lost to the walls. On a very short timescale, however, some electrons near the walls are lost, leading to the situation shown in figure 2.31. Thin ($s << l$) positive ion sheaths from near each wall in

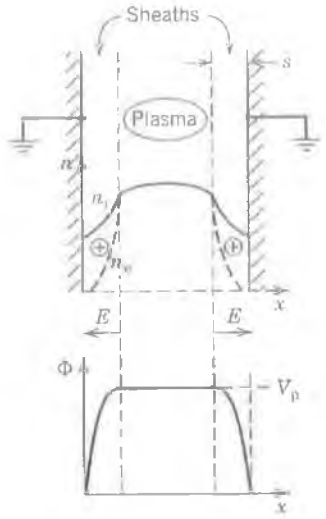

Figure 2.31 Densities, electric field and potential after formation of the sheath.

which $n_i >> n_e$. The net positive charge ρ within the sheath leads to a potential profile $\Phi(x)$ that is positive within the plasma and falls sharply to zero near both walls. This acts as a confining potential "valley" for electrons and a "hill" for ions because the electric fields within the sheaths point from the plasma to the wall. Thus the force $-eE_x$, acting on electrons is directed into the plasma; this reflects electrons travelling toward the walls back into the plasma. Conversely,

ions from the plasma that enter the sheaths are accelerated into the walls. If the plasma potential (with respect to the walls) is V_p, then we expect that $V_p \sim$ a few T_e in order to confine most of the electrons. The energy of the ions bombarding the walls is then $\xi_i \sim$ a few T_e.

2.3.3 RF diodes

Capacitively driven radio frequency discharges - so-called rf diodes – are commonly used in materials processing. An idealised discharge in plane parallel geometry, shown in figure 2.32, consists of a vacuum chamber containing two

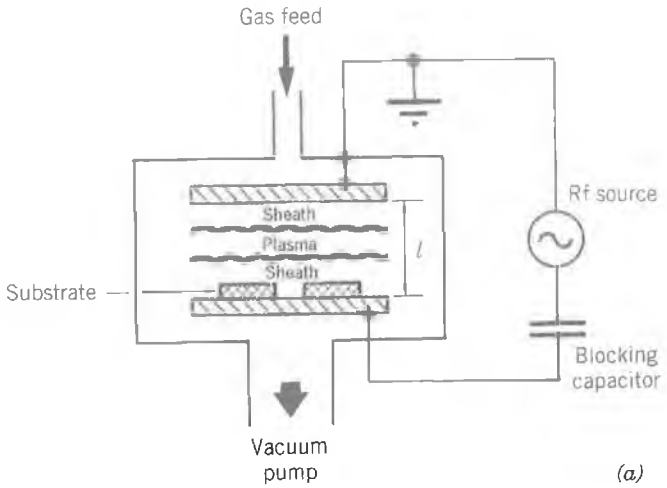

Figure 2.32 Capacitive radio frequency discharge in a plane parallel geometry.

planar electrodes separated by a spacing l and driven by a radio frequency power source. The substrates are placed on one electrode, feedstock gases are admitted to flow through the discharge, and effluent gases are removed by the vacuum pump. Coaxial discharge geometries, such as the "hexode" shown in figure 2.33,

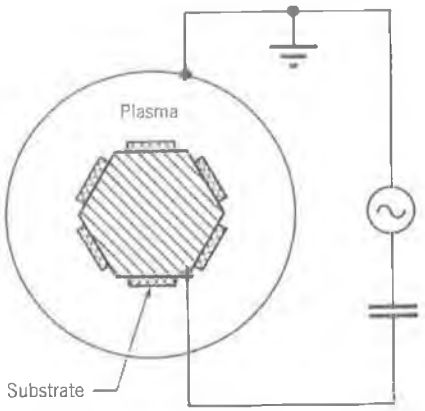

Figure 2.33 Capacitive radio frequency discharge in a coaxial "hexode" geometry.

are also in widespread use. Typical parameters are shown in Table 2.4. The typical radio frequency driving voltage V_{rf} = 100-1000 Volts, and the plate separation is l = 2-10cm. When operated at low pressure, with the wafer mounted on the

Parameter	**RF Diode**	**High Density Source**
Pressure, p (m Torr)	10-1000	0.5-50
Power, P (Watt)	50-2000	100-5000
Frequency, f (MHz)	0.05-13.56	0-2450
Volume, V (L)	1-10	2-50
Cross-sectional Area, A (cm^2)	300-2000	300-500
Magnetic Field B (kG)	0	0-1
Plasma density, n (cm^3)	10^9-10^{11}	10^{10}-10^{12}
Electron temperature, T_e (Volt)	1-5	2-7
Ion acceleration Energy, ξ_i (Volt)	200-1000	20-500
Fractional Ionisation, x_{iz}	10^{-6}-10^{-3}	10^{-4}-10^{-1}

Table 2.4 Range of parameters for radio frequency diode and high-density discharges.

powered electrode and used to remove substrate material, such reactors are commonly called reactive ion etchers (RIEs) - a misnomer since the etching is a chemical process enhanced by energetic ion bombardment of the substrate, rather than a removal due to reactive ions alone.

For anisotropic etching, typically pressures are in the range 10-1000 mTorr, power densities are 0.1-1W/cm^3, the driving frequency is 13.56MHz, and multiple wafer systems are common. Typical plasma densities are relatively low, 10^9-$10^{11}cm^{-3}$, and the electron temperature is of the order of 3 Volts. Ion acceleration energies (sheath voltages) are high, greater than 200 Volts, and

fractional ionisation is low. The degree of dissociation of the molecules into reactive species is seldom measured but can range widely from less than 0.1% to nearly 100% depending on gas composition and plasma conditions. For deposition and isotropic etch applications, pressures tend to be higher, ion bombarding energies are lower, and frequencies can be lower than the commonly used standard of 13.56MHz.

The operation of capacitively driven discharges is reasonably well understood. As shown in figure 2.34, for a symmetrically driven discharge, the

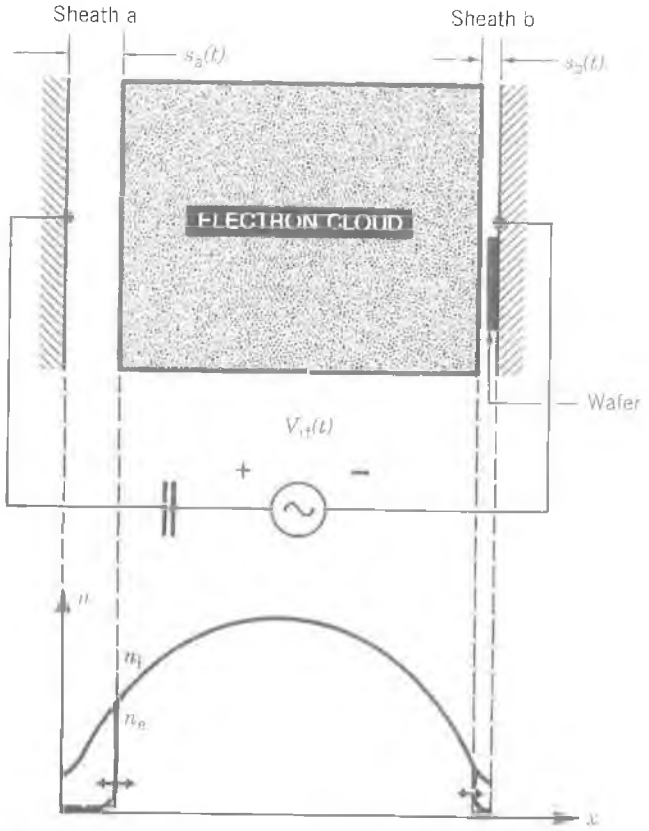

Figure 2.34 The physical model of a radio frequency diode.

mobile plasma electrons, responding to the instantaneous electric fields produced by the radio frequency driving voltage, oscillate back and forth within the positive space charge cloud of the ions. The massive ions respond only to the time-averaged electric fields. Oscillation of the electron cloud creates sheath regions near each electrode that contain net positive charge when averaged over an oscillation period; i.e., the positive charge exceeds the negative charge in the system, with the excess appearing in the sheaths. This excess produces a strong time-averaged electric field within each sheath directed from the plasma to the electrode. Ions flowing out of the bulk plasma near the centre of the discharge

can be accelerated by the sheath fields to high energies as they flow to the substrate, leading to energetic ion enhanced processes. Typical ion bombardment energies ξ_i can be as high as $V_{rf}/2$ for symmetric systems and as high as V_{rf} at the powered electrode for asymmetric systems.

The positive ions continuously bombard the electrode over a radio frequency cycle. In contrast, electrons are lost to the electrode only when the oscillating cloud closely approaches the electrode. During that time, the instantaneous sheath potential collapses near zero allowing sufficient electrons to escape to balance the ion charge delivered to the electrode. Except for such brief moments, the instantaneous potential of the discharge must always be positive with respect to any large electrode and wall surface; otherwise the mobile electrons would quickly leak out. Electron confinement is ensured by the presence of positive space charge sheaths near all surfaces.

A crucial limiting feature of radio frequency diodes is that the ion bombarding flux $\Gamma_i = nu_B$ and bombarding energy ξ_i cannot be varied independently. The situation is analogous to the lack of independent voltage and current control in diode vacuum tubes or semiconductor pn junctions. For a reasonable (but relatively low) ion flux, as well as a reasonable dissociation of the feedstock gas, sheath voltages at the driven electrode are high. For wafers placed on the driven electrode, this can result in undesirable damage, or loss of line width control. Furthermore, the combination of low flux and high ion energy leads to a relatively narrow process window for many applications. The low process rates resulting from the limited ion flux in radio frequency diodes often mandates multiwafer or batch processing, with consequent loss of wafer to wafer reproducibility. Higher ion and neutral fluxes are generally required for single wafer processing in a clustered tool environment, in which a single wafer is moved by a robot through a series of process chambers. Clustered tools are used to control interface quality and are said to have the potential for significant cost savings in fabricating integrated circuits.

Although the need for low pressures, high fluxes, and controllable ion energies has motivated high-density source development, there are many issues that need to be resolved. A critical issue is achieving the required process uniformity over 200mm to 300mm wafer diameters. In contrast to the nearly one

dimensional geometry of typical radio frequency diodes (two closely spaced parallel electrodes), high density cylindrical sources can have length to diameter ratios of order exceeding unity. Plasma formation and transport in such geometries are inherently radially nonuniform. Another critical issue is efficient power transfer (coupling) across dielectric windows over a wide range of plasma parameters. Degradation of any deposition on the window can also lead to irreproducible source behaviour and the need for frequent, costly cleaning cycles. Low-pressure operation leads to severe pumping requirements for high deposition or etching rates and hence to the need for large, expensive vacuum reactor surface conditions, leading to problems of reactor aging and process irreproducibility. Finally, dc magnetic fields are required for some source concepts. These can lead to magnetic field-induced process nonuniformities and damage.

Figure 2.35 illustrates schematically the central problem of discharge

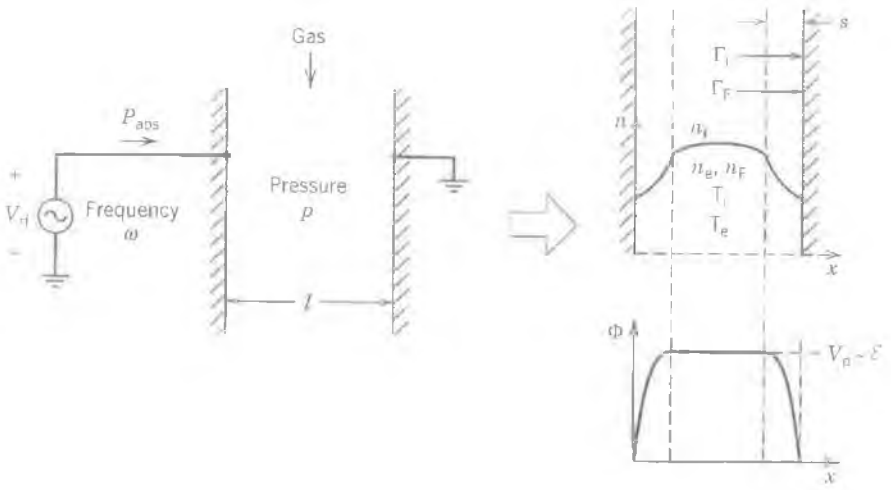

Figure 2.35 The central problem of discharge analysis.

analysis, using the example of a radio frequency diode. Given the control parameters for the power source (frequency f, driving voltage V_b or absorbed power P_{abs}), the feedstock gas (pressure p, flow rate and chemical composition), and the geometry (simplified here to the discharge length l), then find the plasma parameters, including the plasma density n_i, the etchant density n_F, the ion and etchant fluxes Γ_i and Γ_F hitting the substrate, the electron and ion temperatures T_e and T_i, the ion bombarding energy ξ_i and the sheath thickness s. The control parameters are the "knobs" that can be "turned" in order to "tune" the properties of the discharge.

The tuning range of a given discharge is generally limited. Sometimes one type of discharge will not do the job no matter how it is tuned, so another type must be selected. As a result there is a big variety of discharges used for processing. Some are driven by radio frequency, some by direct current and some by microwave discharges. Some use magnetic fields to increase the plasma confinement or the efficiency of power absorption. A capacitively coupled plasma discharge has been used in this thesis. It is a relatively simple plasma chamber. If this chamber can be modelled, as is the ultimate goal of this work, then the modelling techniques can be applied to more complicated systems. A theoretical model of a capacitively coupled discharge is given in the next section.

2.3.4 Theoretical Model of a Capacitively Coupled Plasma Discharge

A complete description of a plasma discharge requires a choice of heating mechanisms and geometric configuration that sustains those mechanisms. One of the most widely used types of low pressure discharges is sustained by radio frequency currents and voltage, introduced through a capacitive sheath. The currents in the main body of the plasma lead to ohmic heating, while the voltage across the sheath leads to stochastic sheath heating. The complete self-consistent model of such a discharge is quite complicated, even in the simplest plane-parallel geometry. This leads to various simplifying assumptions in order to obtain analytic solutions in which the scalings of plasma parameters with control parameters are explicit.

A uniform, symmetric model for a capacitive parallel-plate radio frequency discharge was developed by V.A. Godyak et al [4]. A brief description of its derivation is given. The model is qualitively correct but, because simplifying assumptions are made, cannot be used to predict the quantitive behaviour of "real" discharges. Most discharges are asymmetric because more electrode surfaces are naturally grounded rather than driven. This leads to a DC bias voltage on the driven electrode with respect to ground. A brief description of the asymmetric model is also given.

Figure 2.36 shows the basic homogenous model. A sinusoidal current $I_{rf}(t)$, having complex representation $I_{rf} = \mathrm{Re}\, \boldsymbol{I}_{rf}\, e^{j\omega t}$, flows across discharge plates a and b. $\boldsymbol{I}_{rf}$ is taken to be a real number I_1. The plates are separated by a distance l and each has a cross sectional area A. A gas having neutral density n_g is present

between the plates. In response to current flow, a discharge plasma forms between the plates, accompanied by a voltage $V(t)$ across the plates and a power flow $P(t)$ into the plasma. The plasma has ion density $n_i(\mathbf{r},t)$ and an electron temperature $T_e(\mathbf{r},t)$. Because of quasineutrality, $n_e \sim n_i$ almost everywhere except within the oscillating sheaths near the plates, where $n_e < n_i$. The instantaneous sheath thickness is $s(t)$ and its time-averaged value is $\boldsymbol{s}$, with $\boldsymbol{s} << l$.

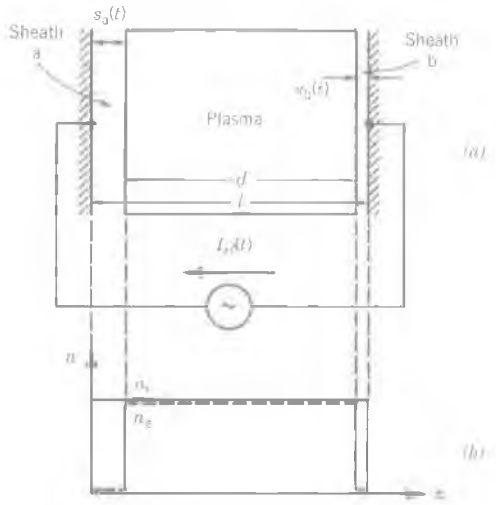

Figure 2.36 The basic radio frequency discharge model: (a) sheath and plasma thicknesses; (b) electron and ion densities.

The state of the discharge is specified once a complete set of control parameters is given. The remaining plasma and circuit parameters are then specified as functions of the control parameters. A convenient choice for the control parameters is $\boldsymbol{I_{rf}}$, $\boldsymbol{\omega}$, n_g and l. Given these, the basic model is developed to determine n_e, T_e, s, $\boldsymbol{s}$, V and $\boldsymbol{P}$. The choice of control parameters is not unique. We choose $\boldsymbol{I}$, rather than V and $\boldsymbol{P}$, for ease of analysis.

In general, the discharge parameters n_e, n_i and T_e are complicated functions of position and time. Assumptions are made to simplify the analysis:

a) The ions respond only to the time-averaged potentials. This is a good approximation provided

$$\omega_{pi}^2 << \omega^2$$

where ω_{pi} is the ion plasma frequency.

b) The electrons respond to the instantaneous potentials and carry the rf discharge current. This is a good approximation provided

$$\omega_{pe}^2 >> \omega^2 (1+ \nu_m^2/\omega^2)^{1/2}$$

c) The electron density is zero within the sheath regions. This is a good approximation provided $\lambda_{De} << s$ where λ_{De} is the electron Debye length. This holds if $T_e << V$, where V is the DC voltage across the sheath.

d) There is no transverse variation (along the plates). This is a good approximation provided $l << \sqrt{A}$. Since the divergence of Maxwell's equation **curl.(H)** = **J** + $\varepsilon_0 \delta \mathbf{E}/\delta t$ is zero, we see that at any instant of time, the sum of the conduction current **J** and the displacement current $\varepsilon_0 \delta \mathbf{E}/\delta t$ within the discharge is then independent of x.

2.3.4.1 Plasma Admittance

The admittance of a bulk plasma slab of thickness d and cross-sectional area A is $Y_p = j\omega\, \varepsilon_p A/d$, where

$$\varepsilon_p = \varepsilon_0 \left(1 - \frac{\omega_{pe}^{\ 2}}{\omega(\omega - j\nu_m)} \right)$$

is the plasma dielectric constant . Within the uniform ion density approximation

$$d = l\text{-}2s = \text{const}$$

independent of time. It is then found that

$$Y_p = j\omega C_0 + \frac{1}{j\omega L_p + R_p}$$

where $C_0 = \varepsilon_0 A/d$ is the vacuum capacitance, $L_p = \omega_{pe}^{-2} C_0^{-1}$ is the plasma inductance, and $R_p = \nu_m L_p$ is the plasma resistance. This form of Y_p represents the series combination of L_p and R_p in parallel with C_0. By assumption b), the displacement current that flows through C_0 is much smaller that the conduction current that flows through L_p and R_p. The sinusoidal current

$$I_{rf}(t) = \text{Re}\, I_{rf} e^{j\omega t}$$

that flows through the plasma bulk produces a voltage across the plasma

$$V_p(t) = \text{Re}\, V_p e^{j\omega t}$$

where $V_p = I_{rf} / Y_p$ is the complex voltage amplitude. We see that the plasma voltage is linear in the applied current and that there is no harmonic generation or DC component of V_p.

2.3.4.2 Sheath Admittance

In contrast to the plasma, the current that flows through the two sheaths is almost entirely displacement current; i.e. it is due to a time-varying electric field. This is

true because the conduction current in a discharge is carried mainly by electrons, and the electron density is approximately zero within the time-varying sheath. We will see that the conduction current carried by the steady flow of ions across the sheath to the plates is much smaller than the displacement current.

a) ***Displacement Current*** The electric field **E** = **x***E* within sheath *a* (see figure 2.36) is given by Poisson's equation

$$\frac{dE}{dx} = \frac{en}{\varepsilon_0} \qquad , x \le \boldsymbol{s}_a(t)$$

which on integration yields

$$E(x,t) = \frac{en}{\varepsilon_0}\left(x - s_a(t)\right)$$

The boundary condition is $E \approx 0$ at $x = \boldsymbol{s}_a$ because E is continuous across the plasma-sheath interface (no surface charge) and the electric field is small in the plasma. The displacement current flowing through sheath *a* into the plasma is

$$I_{ap}(t) = \varepsilon_0 A \frac{\delta E}{\delta t}$$

Substituting the previous two equations we get

$$I_{ap}(t) = -enA\frac{\delta s}{\delta t}$$

We see that the sheath boundary $\boldsymbol{s}_a$ oscillates linearly with the applied current. Setting $I_{ap}(t) = I_{rf}(t)$, where $I_{rf} = I_1 \cos \omega t$, we integrate the above equation to get

$$s_a = s - s_0 \sin \omega t$$

where

$$s_0 = \frac{I_1}{en\omega A}$$

is the sinusoidal oscillation amplitude about the DC value *s*. The voltage across the sheath is given by

$$V_{ap}(t) = \int_0^s E dx = -\frac{en}{\varepsilon_0}\frac{s_a^{\,2}}{2}$$

From this expression the sheath voltage is a nonlinear function of s_a and therefore of the applied current. Substituting the equation for s_a into the above equation we

get

$$V_{ap} = -\frac{en}{2\varepsilon_0}\left(s^2 + \frac{1}{2}s_0^{\,2} - 2ss_0 \sin\omega t - \frac{1}{2}s_0^{\,2}\cos 2\omega t\right)$$

We see the nonlinearity leads to second-harmonic voltage generation and a constant average value.

Similarly for the sheath b we obtain

$$I_{bp}(t) = -enA\frac{\delta s_a}{\delta t}$$

and the voltage across this sheath is

$$V_{bp} = -\frac{en}{\varepsilon_0}\frac{s_b^{\,2}}{2}$$

By continuity of current, $I_{bp} = -I_{ap}$, therefore

$$\frac{d}{dt}(s_a + s_b) = 0$$

Integrating, we obtain

$$s_a + s_b = 2s,$$

a constant so that $d = l - 2\boldsymbol{s}$ = const, as previously stated. For sheath b,

$$s_b = s + s_0 \sin\omega t$$

with the nonlinear voltage response,

$$V_{bp} = -\frac{en}{2\varepsilon_0}\left(s^2 + \frac{1}{2}s_0^{\,2} - 2ss_0 \sin\omega t - \frac{1}{2}s_0^{\,2}\cos 2\omega t\right)$$

Although V_{ap} and V_{bp} are nonlinear, the combined voltage $V_{ab} = V_{ap} - V_{bp}$ across both sheaths is

$$V_{ab} = \frac{ens}{\varepsilon_0}(s_b - s_a)$$

Substituting for $\boldsymbol{s}_b$ and $\boldsymbol{s}_a$ we find

$$V_{ab} = \frac{2enss_0}{\varepsilon_0}\sin\omega t$$

which is a linear voltage response. We obtain the surprising result that although each sheath is nonlinear, the combined effect of both sheaths is linear. This is true only for the simplified model assumptions of a symmetric, homogeneous (constant ion density) discharge. The total voltage V_{rf} across the discharge is the

sum of V_{ab} and V_p. However, for typical discharge conditions, it is usual to have **abs**(V_p)<<**abs**(V_{ab}), and it is often approximated that $V_{rf} = V_{ab}$.

b) ***Conduction Current.*** Although the conduction current in each sheath is small, the average sheath thickness s is determined by the balance between ion and electron conduction currents. By assumption a) in § 2.3.4, there is a steady flow of ions from the plasma through sheath a, carrying a steady current

$$I_i = enu_B A$$

where the loss velocity is taken to be the Bohm velocity u_B.

By symmetry, the time-average conduction current flowing to plate "a" is zero. There is a steady flow of ions to the plate. For the basic model, the electron density is assumed zero in the sheath. The sheath thickness $s_a(t)$ must therefore collapse to zero at some time during the radio frequency cycle in order to transfer electrons from the plasma to the plate. It follows that

$$\bar{s} = s_0 = \frac{I_i}{en\omega A}$$

and that

$$V_{pa} = \frac{en}{2\varepsilon_0} s_0^2 (1 - \sin \omega t)^2$$

Since the sheath voltage collapses to zero at the time that the electrons are transferred to the plate, this acts like an ideal diode across the sheath whose preferred direction of current flow is into the plasma. A similar result holds for sheath "b".

A linear sheath capacitance C_s can be defined because the voltage across both sheaths is sinusoidal. Differentiating the expression for V_{ab} and substituting for I_{rf} we obtain the simple result

$$I_{rf} = C_s \frac{dV_{ab}}{dt}$$

where

$$C_s = \frac{\varepsilon_0 A}{2s_0}$$

is a linear capacitance. Physically, this capacitance is the series combination of the two nonlinear capacitances $C_a = \varepsilon_0 A / s_a(t)$ and $C_b = \varepsilon_0 A / s_b(t)$.

Figure 2.37 shows the nonlinear circuit of the homogenous radio frequency plasma discharge. The dashed lines indicate that the series connection of the nonlinear elements C_a and C_b, and R_b and R_b, yield the corresponding linear elements C_s and R_s, respectively.

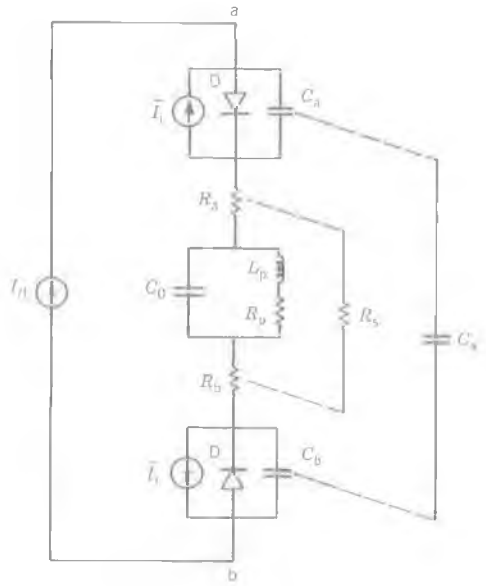

Figure 2.37 Nonlinear circuit model of the homogenous radio frequency discharge. The dashed lines indicate that the series connection of the nonlinear elements C_a and C_b, and R_a and R_b, yield the corresponding linear C_s and R_s, respectively.

2.4 Mesh Current Network Analysis

The voltage sources in an electric circuit or network cause currents in each of the branches and corresponding voltages across the circuit elements. The solution to the network consists of finding the currents in the branches or the voltages across the elements.

2.4.1 Mesh Currents

The mesh current method is applied by selecting closed loops of current called mesh currents as in figure 2.38. Three equations are written in the unknowns $\mathbf{I}_1$, $\mathbf{I}_2$ and $\mathbf{I}_3$ and are solved. The current in any branch is given either directly by one of the mesh currents or by a combination of them. Thus the current in $\mathbf{Z}_\mathbf{A}$ is $\mathbf{I}_1$, and the current in $\mathbf{Z}_\mathbf{B}$, assuming a positive direction downward through the impedance, is $\mathbf{I}_1$- $\mathbf{I}_2$. The current in any branch of the network is obtained in a

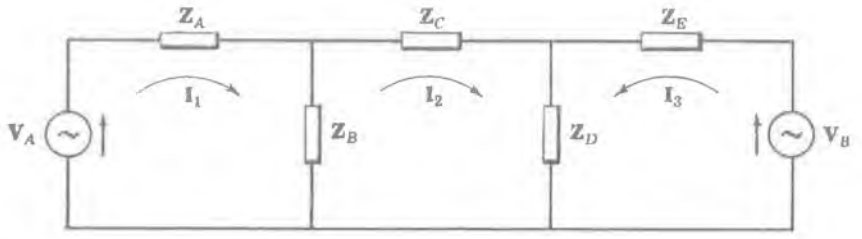

Figure 2.38 Mesh or loop currents in a network.

similar manner. The voltage across any circuit element is then the product of the phasor current in the element and the complex impedance. To obtain the set of three equations, Kirchoff's voltage law is applied to each current loop. The $\mathbf{I_1}$ loop is redrawn in figure 2.39 and the sum of the voltage rises.

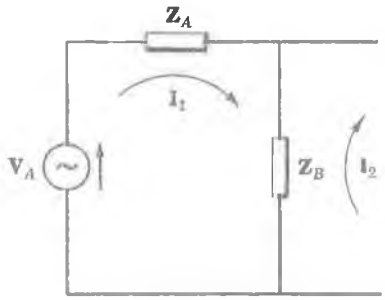

Figure 2.39 I_1 loop.

$$\mathbf{I_1 Z_A + (I_1 - I_2) Z_A = V_A} \qquad (1)$$

The second loop contains no source; therefore the sum of the voltage drops is zero.

$$\mathbf{I_2 Z_C + (I_2 + I_3) Z_D + (I_2 - I_1) Z_B = 0} \quad (2)$$

Applying Kirchoff's voltage law to the third loop,

$$\mathbf{I_3 Z_E + (I_3 + I_2) Z_D = V_B} \qquad (3)$$

Rearranging,

$$(Z_A + Z_B)\ I_1 - I_2 = V_A \quad \textbf{(1')}$$

$$-Z_B\ I_1 + (Z_B + Z_C + Z_D)\ I_2 + Z_D\ I_3 = 0 \quad \textbf{(2')}$$

$$Z_D\ I_2 + (Z_D + Z_E)\ I_3 = V_B \quad \textbf{(3')}$$

The above set of equations can be derived directly. Consider loop one shown in figure 2.39. The direction of the current $\mathbf{I_1}$ is taken clockwise and all voltage drops in loop one caused by $\mathbf{I_1}$ are positive. Mesh current $\mathbf{I_2}$ also flows in $\mathbf{Z_B}$, but in opposite direction to $\mathbf{I_1}$. Then the voltage drop in $\mathbf{Z_B}$ caused by $\mathbf{I_2}$ is –

$\mathbf{Z_B I_2}$. The voltage $\mathbf{V_A}$ is positive because it has the same direction as $\mathbf{I_1}$. Now with these considerations Kirchoff's law is applied to loop one and equation (1') follows. Equations (2') and (3') are derived similarly.

The terms voltage rise and voltage drop are carryovers from basic DC circuits where their meaning is clearer than in sinusoidal circuits where instantaneous currents and voltages have positive and negative intervals. In the sinusoidal steady state, Kirchoff's voltage law applied to a closed loop results in a phasor equality where the phasor sum of the voltages across the loop impedances is equal to the phasor sum of all voltage sources acting in the loop.

2.4.2 Choice of Mesh Currents

In applying the mesh current method, it is possible to simplify the solution of a given problem by the appropriate choice of the loops in the network. In figure 2.38 above it is required to determine only the currents in the branch containing $\mathbf{Z_B}$, then it is convenient to let only one loop pass through $\mathbf{Z_B}$. Thus we need solve only the mesh current $\mathbf{I_1}$. Figure 2.40 shows the new selected loops.

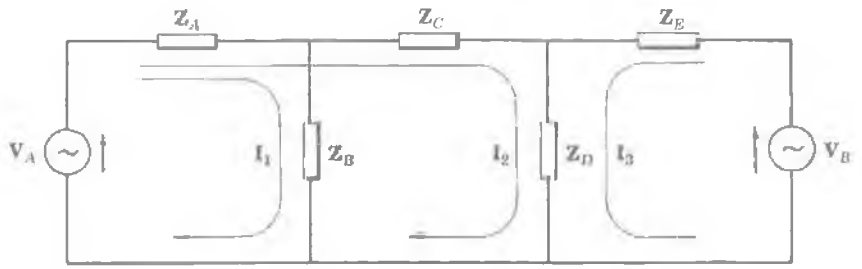

Figure 2.40 Alternate loop selection.

The corresponding set of mesh current equations is

$$(Z_A + Z_B)\ I_1 - Z_A\ I_2 = V_A \quad \textbf{(1')}$$

$$Z_A\ I_1 + (Z_A + Z_C + Z_D)\ I_2 + Z_D\ I_3 = V_A \quad \textbf{(2')}$$

$$Z_D\ I_2 + (Z_D + Z_E)\ I_3 = V_B \quad \textbf{(3')}$$

With any choice of mesh currents for the network, each circuit element must have at least one current and no two branches may be forced to have the same current or the same combination of currents. Rules are given, in the following paragraph, which determine the required number of mesh currents to solve a network; a lesser number of mesh currents can never be a valid set.

2.4.3 Number of Mesh Currents Required

The number of mesh currents required by a simple coplanar network is apparent. More involved networks will require a method which gives the necessary number of equations. One method is to count the branches and junctions in the network. The necessary number of mesh currents is then given as

number of equations = branches – (junctions-1)

In figure 2.41 there are seven branches and four junctions.

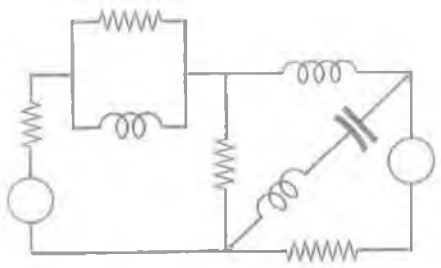

Figure 2.41A network.

The required number of mesh currents would be 7 – (4-1) = 4.

2.4.4 Mesh Equations by Inspection

The equations for a three mesh network in general notation are

$$\begin{array}{ccccccccc} & Z_{11}\,I_1 & \pm & Z_{12}\,I_2 & \pm & Z_{13}\,I_3 & = & V_1 \\ \pm & Z_{21}\,I_1 & + & Z_{22}\,I_2 & \pm & Z_{23}\,I_3 & = & V_2 \\ \pm & Z_{31}\,I_1 & \pm & Z_{23}\,I_2 & + & Z_{33}\,I_3 & = & V_3 \end{array}$$

$\mathbf{Z_{11}}$ is called the self-impedance of loop one, given by the sum of all impedances through which $\mathbf{I_1}$ passes. $\mathbf{Z_{22}}$ and $\mathbf{Z_{33}}$ are the self-impedances of loops two and three, given by the sums of the impedances in their respective loops. $\mathbf{Z_{12}}$ is the sum of all impedances common to mesh currents $\mathbf{I_1}$ and $\mathbf{I_2}$. It follows that $\mathbf{Z_{11}} = \mathbf{Z_{21}}$. The impedances $\mathbf{Z_{13}}$, $\mathbf{Z_{31}}$, $\mathbf{Z_{23}}$ and $\mathbf{Z_{32}}$ are the sums of the impedances common to the mesh currents indicated in their subscripts. The positive sign is used if both currents pass through the common impedance in the same direction, and the negative sign if they do not.

$\mathbf{V_1}$ is the sum of all voltages driving in loop one. The positive sign is used if the source drives in the direction of the mesh currents, and the negative sign if

it drives against the mesh current. $\mathbf{V_2}$ and $\mathbf{V_3}$ are the sums of the driving voltages in their respective loops.

2.4.5.1 Matrices

A matrix is a rectangular array of numbers or functions enclosed in a pair of brackets and is subject to certain rules of operation. In the matrix

$$A = \begin{bmatrix} a_{11} & a_{12} & \dots & a_{1n} \\ a_{21} & a_{22} & \dots & a_{2n} \\ \dots & \dots & \dots & \dots \\ a_{m1} & a_{m2} & \dots & a_{mn} \end{bmatrix}$$

the numbers or functions a_{ij} are called its elements. An element a_{ij} is in row i and column j. This matrix, of m rows and n columns, is of order "$m \times n$"and is called "the matrix A". Two matrices are equal if and only if one is the exact duplicate of the other.

2.4.5.2 Addition of Matrices

Two matrices of the same order are conformable for addition or subtraction; two matrices of different orders cannot be added or subtracted. The sum/difference of two $m \times n$ matrices, $A = \lfloor a_{ij} \rfloor$ and $B = \lfloor b_{ij} \rfloor$, is the $m \times n$ matrix C where each element of C is the sum/difference of the corresponding elements of A and B. Thus $A \pm B = \lfloor a_{ij} \pm b_{ij} \rfloor$.

2.4.5.3 Multiplication of Matrices

The product AB, in that order, of the $1 \times m$ matrix $A = \begin{bmatrix} a_{11} & a_{12} & \dots & a_{1m} \end{bmatrix}$ and the $m \times 1$ matrix $B = \begin{bmatrix} b_{11} \\ b_{12} \\ \dots \\ b_{1n} \end{bmatrix}$ is the 1×1 matrix C:

$$C = \begin{matrix} a_{11} & a_{12} & \dots & a_{1m} \end{matrix} \bullet \begin{matrix} b_{11} \\ b_{12} \\ \dots \\ b_{m1} \end{matrix} = a_{11}b_{11} + a_{12}b_{21} + \dots + a_{1m}b_{m1} = \sum_{k=1}^{m} a_{1k}$$

Note that each element of the row is multiplied into each corresponding element of the column and then the products are summed.

Matrix A is conformable to matrix B for multiplication, i.e. the product AB is defined, only when the number of columns of A is equal to the number of rows of B. Thus if A is a 3×2 matrix and B is a 2×5 matrix, then the product AB is defined but the product BA is not defined. If D is a 3×3 and E is a 3×3 matrix, both products AB and BA are defined.

2.4.5.4 Inversion

In an arrangement of positive integers, an inversion exists when a larger integer precedes a smaller integer. For example, in 132 the integer 3 precedes 1; hence there are 3 inversions. In 4213 the integer 4 precedes 2, 1 and 3, and the integer 2 precedes 1; thus there are 4 inversions. In 3421 the integer 3 precedes 2 and 1, the integer 4 precedes 2 and 1, and the integer 2 precedes 1; thus there are 5 inversions.

2.4.5.5 Determinant of a Square Matrix

Let us take n elements of the n-square matrix

$$A=\begin{bmatrix} a_{11} & a_{12} & \dots & a_{1n} \\ a_{21} & a_{22} & \dots & a_{2n} \\ \dots & \dots & \dots & \dots \\ a_{n1} & a_{n2} & \dots & a_{nn} \end{bmatrix}$$

and form a product $a_{1j_1}\ a_{2j_2}\ \dots\ a_{4j_4}$ such that one and only one element belongs to any row and one element belongs to any column. Note that the sequence of first subscripts is, for convenience, in the order 1, 2, …, n; then the sequence $j_1, j_2,\dots, j_n$ of second subscripts is one of the $n!$ permutations of the integers 1, 2, …, n. Associate a + or – sign with the product according to the number of inversions of the second subscripts is even or odd. Then the determinant of and n-square matrix A, written $|A|$, is the sum of all $n!$ such different signed products which can be formed from the elements of A. The determinant of a square matrix of order n is called a determinant of order n.

The value of the determinant $|A|$ of order n is the sum of the n products obtained by multiplying each element of any chosen row/column of $|A|$ by its cofactor. Thus

$$|A| = \begin{vmatrix} a_{11} & a_{12} & a_{13} \\ a_{21} & a_{22} & a_{23} \\ a_{31} & a_{32} & a_{33} \end{vmatrix} = a_{12}\Delta_{12} + \quad a_{22}\Delta_{22} + \quad a_{32}\Delta_{32}$$

$$= -a_{12}\begin{vmatrix} a_{21} & a_{23} \\ a_{31} & a_{33} \end{vmatrix} + a_{22}\begin{vmatrix} a_{11} & a_{13} \\ a_{31} & a_{33} \end{vmatrix} - a_{32}\begin{vmatrix} a_{11} & a_{13} \\ a_{21} & a_{23} \end{vmatrix}$$

is the expansion $|A|$ along the second column.

2.4.5.6 Solution of Linear Equations by Determinant and Cramer's Rule

The system of three linear equations in three unknowns x_1, x_2, x_3

$$\begin{aligned} a_{11}x_1 &+ a_{12}x_2 + a_{13}x_3 = k_1 \\ a_{21}x_1 &+ a_{22}x_2 + a_{23}x_3 = k_2 \\ a_{31}x_1 &+ a_{32}x_2 + a_{33}x_3 = k_3 \end{aligned}$$

may be written in matrix form as

$$\begin{bmatrix} a_{11} & a_{12} & a_{13} \\ a_{21} & a_{22} & a_{23} \\ a_{31} & a_{32} & a_{33} \end{bmatrix} \begin{bmatrix} x_1 \\ x_2 \\ x_3 \end{bmatrix} = \begin{bmatrix} k_1 \\ k_2 \\ k_3 \end{bmatrix}$$

The numerical value of the coefficient determinant, Δ_a, is multiplied by x_1 if each element of the first column is multiplied by x_1

$$\Delta_a = \begin{vmatrix} a_{11} & a_{12} & a_{13} \\ a_{21} & a_{22} & a_{23} \\ a_{31} & a_{32} & a_{33} \end{vmatrix} \text{ and } x_1\Delta_a = \begin{vmatrix} a_{11}x_1 & a_{12} & a_{13} \\ a_{21}x_1 & a_{22} & a_{23} \\ a_{31}x_1 & a_{32} & a_{33} \end{vmatrix}$$

Now to each element of the first column of the last determinant add x_2 times the corresponding element of the second column and x_3 times the corresponding element of the third column. Then

$$x_1\Delta_a = \begin{vmatrix} (a_{11}x_1 + a_{12}x_2 + a_{13}x_3) & a_{12} & a_{13} \\ (a_{21}x_1 + a_{22}x_2 + a_{23}x_3) & a_{22} & a_{23} \\ (a_{31}x_1 + a_{32}x_2 + a_{33}x_3) & a_{32} & a_{33} \end{vmatrix} = \begin{vmatrix} k_1 & a_{12} & a_{13} \\ k_2 & a_{22} & a_{23} \\ k_3 & a_{32} & a_{33} \end{vmatrix}$$

or

$$x_1 = \frac{\begin{vmatrix} k_1 & a_{12} & a_{13} \\ k_2 & a_{22} & a_{23} \\ k_3 & a_{32} & a_{33} \end{vmatrix}}{\Delta_a}$$

provided $\Delta_a \neq 0$. Similarly,

$$x_2 = \frac{\begin{vmatrix} a_{11} & k_1 & a_{13} \\ a_{21} & k_2 & a_{23} \\ a_{31} & k_3 & a_{33} \end{vmatrix}}{\Delta_a} \quad x_3 = \frac{\begin{vmatrix} a_{11} & a_{12} & k_1 \\ a_{21} & a_{22} & k_2 \\ a_{31} & a_{32} & k_3 \end{vmatrix}}{\Delta_a}$$

This method of solution, called *Cramer's Rule*, can be applied to any system of *n* linear equations in *n* unknowns provided the coefficient's determinant is not zero.

2.4.6.1 Matrix Methods and Circuit Analysis

The three mesh current equations

$$\begin{array}{ccccccccc} & Z_{11}\,I_1 & \pm & Z_{12}\,I_2 & \pm & Z_{13}\,I_3 & = & V_1 \\ \pm & Z_{21}\,I_1 & + & Z_{22}\,I_2 & \pm & Z_{23}\,I_3 & = & V_2 \\ \pm & Z_{31}\,I_1 & \pm & Z_{23}\,I_2 & + & Z_{33}\,I_3 & = & V_3 \end{array}$$

are now written in matrix form

$$\begin{bmatrix} Z_{11} & \pm Z_{12} & \pm Z_{13} \\ \pm Z_{21} & Z_{22} & \pm Z_{23} \\ \pm Z_{31} & \pm Z_{32} & Z_{33} \end{bmatrix} \begin{bmatrix} I_1 \\ I_2 \\ I_3 \end{bmatrix} = \begin{bmatrix} V_1 \\ V_2 \\ V_3 \end{bmatrix} \text{ or } [Z][I] = [V]$$

referred to as the matrix form of Ohm's law, were $[Z]$ is the impedance matrix, $[I]$ the current matrix and $[V]$ the voltage matrix.

The mesh currents I_1, I_2 and I_3 are found as the ratios of the two determinants:

$$I_1 = \frac{\begin{vmatrix} V_1 & \pm Z_{12} & \pm Z_{13} \\ V_2 & Z_{22} & \pm Z_{23} \\ V_3 & \pm Z_{32} & Z_{33} \end{vmatrix}}{\Delta_z} \quad I_2 = \frac{\begin{vmatrix} Z_{11} & V_1 & \pm Z_{13} \\ \pm Z_{21} & V_2 & \pm Z_{23} \\ \pm Z_{31} & V_3 & Z_{33} \end{vmatrix}}{\Delta_z} \quad I_2 = \frac{\begin{vmatrix} Z_{11} & \pm Z_{12} & V_1 \\ \pm Z_{21} & Z_{22} & V_2 \\ \pm Z_{31} & \pm Z_{32} & V_3 \end{vmatrix}}{\Delta_z}$$

When the numerator determinant of each is expanded about the elements of the column containing the voltages, we obtain the following set of equations for the mesh currents:

$$I_1 = V_1\left(\frac{\Delta_{11}}{\Delta_z}\right) + V_2\left(\frac{\Delta_{21}}{\Delta_z}\right) V_3\left(\frac{\Delta_{31}}{\Delta_z}\right) \qquad (1)$$

$$I_2 = V_1\left(\frac{\Delta_{12}}{\Delta_z}\right) + V_2\left(\frac{\Delta_{22}}{\Delta_z}\right) V_3\left(\frac{\Delta_{32}}{\Delta_z}\right) \qquad (2)$$

$$I_3 = V_1\left(\frac{\Delta_{13}}{\Delta_z}\right) + V_2\left(\frac{\Delta_{23}}{\Delta_z}\right) V_3\left(\frac{\Delta_{33}}{\Delta_z}\right) \qquad (3)$$

The terms on the right sides of equations *(1)*, *(2)* and *(3)* are phasor components which result from the various driving voltages. Thus in *(1)* the mesh current I_1 consists of three parts: $V_1(\Delta_{11}/\Delta_z)$ due to driving voltage V_1, $V_2(\Delta_{21}/\Delta_z)$due to driving voltage V_2, and $V_3(\Delta_{31}/\Delta_z)$due to driving voltage V_3.

2.4.6.2 Driving Point Impedance

Consider a passive or source-free network with two external connections as shown in the figure 2.42. Apply a voltage source V_1 and call the resulting mesh

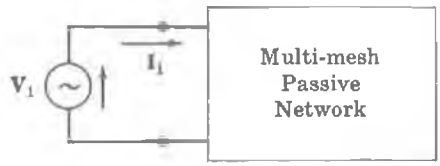

Figure 2.42 Multi-mesh passive network with attached voltage source.

current I_1. Since there are no other sources in the network the equation for mesh current I_1 is

$$I_1 = V_1\left(\frac{\Delta_{11}}{\Delta_z}\right) + (0)\left(\frac{\Delta_{21}}{\Delta_z}\right) + (0)\left(\frac{\Delta_{31}}{\Delta_z}\right) + \ldots = V_1\left(\frac{\Delta_{11}}{\Delta_z}\right)$$

The *input* or *driving point impedance* is the ratio of the applied voltage V_1 to the resulting current I_1. Thus

$$Z_1 = V_1/I_1 = \Delta_z/\Delta_{11}$$

The input impedance of an *active network* is defined as the impedance presented by the network to the specified terminals when *all internal sources are shorted but their internal impedances are retained.* Thus the ratio Δ_z/Δ_{11} is the driving

point impedance of loop one regardless of whether the network is passive or active.

2.4.6.3 Transfer Impedance

A voltage source driving in one mesh causes a current in each of the other meshes of a network. The transfer impedance is the ratio of a driving voltage in one mesh to the resulting current in another mesh, all other sources being set equal to zero. Consider the network in the figure below with a voltage V_r driving in mesh r and

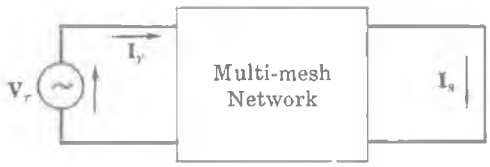

Figure 2.43 Multi-mesh passive network with attached voltage source with resulting current.

the resulting current I_s in mesh s. Then

$$I_s = (0)\frac{\Delta_{1s}}{\Delta_z} + \ldots + (V_r)\frac{\Delta_{rs}}{\Delta_z} + \ldots + (0)\frac{\Delta_{ns}}{\Delta_z} = (V_r)\frac{\Delta_{rs}}{\Delta_z}$$

and

$$Z_{transfer_{rs}} = V_r / I_s = \Delta_z / \Delta_{rs}$$

The double subscripts of the transfer impedance, rs, indicate the direction of the action, i.e. the source is in mesh r and the resulting current is in mesh s. And the determinant of the denominator is the cofactor of the rs position, Δrs, with the same subscripts as the transfer impedance.

2.4.7 The Simplex Method

The Simplex Method is a practical linear programming algorithm. It was designed in 1947 by G. Dantzig and can be used to solve linear programs. It typically is used to solve problems with many variables and constraints. Conceptually it is very simple. Linear programming is a finite problem. When an objective function is bounded below only the vertices of a given polytope need to be scanned in order to find an optimal point. The Simplex method is an orderly way of scanning such vertices.

The algorithm starts from an arbitrary vertex of the feasible region and finds a better neighbouring vertex. ("Better" is defined as closer to the frequency

sweep, in our case). If no neighbouring vertex is "better", the current vertex can be proven globally optimal. For a more in depth explanation of the Simplex Method refer to reference [8].

Chapter 3 System Set-up

3.1 Introduction

A basic block diagram of the system used for this thesis is shown in figure 3.1. Each block will be described in detail in the proceeding sections of this chapter.

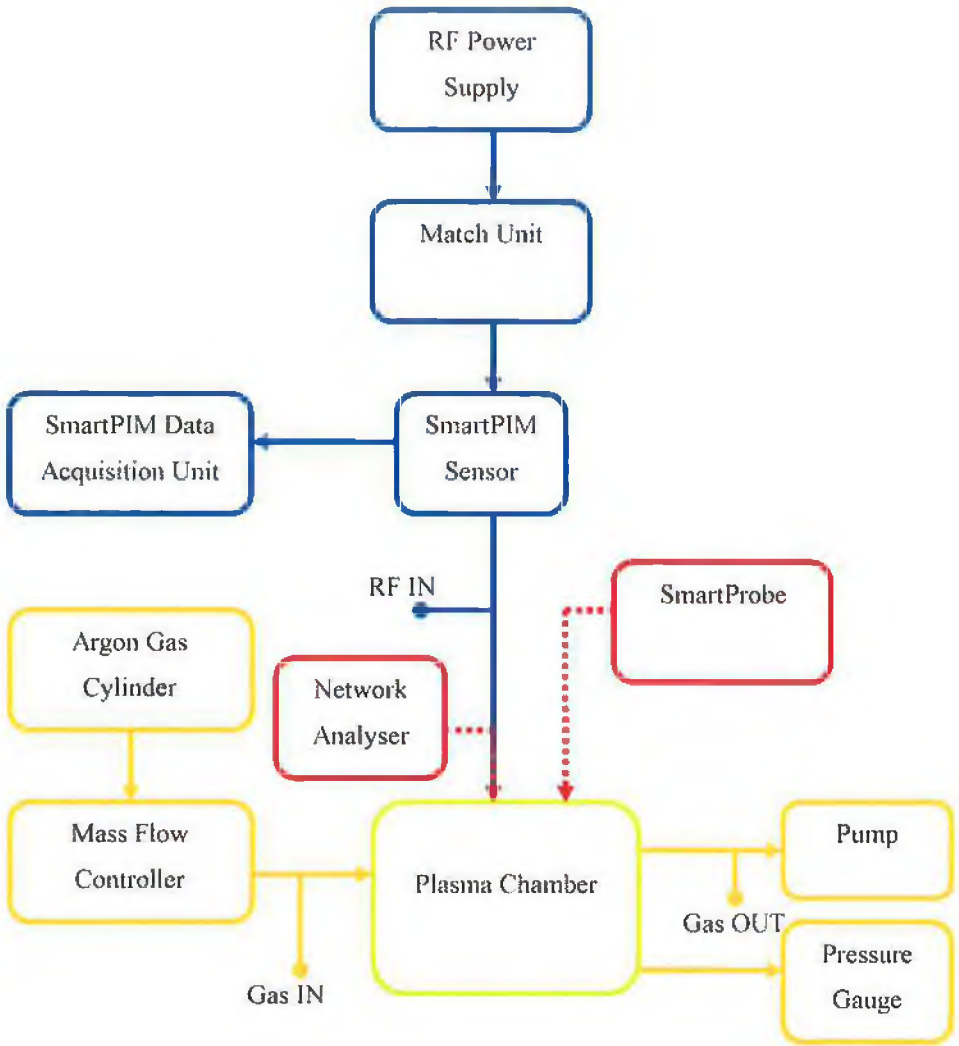

Figure 3.1 Block diagram of plasma chamber system

There were three factors taken into consideration in the design of the system:

- **Safety**

  There are many safety concerns associated with plasma chamber systems. High powered electrical radiation and high temperatures are two examples

of hazardous energies present. Different gases are used to generate plasmas in the chamber. Only argon and nitrogen are used in this system as they are not combustible. However they still are hazardous as they can cause asphyxiation. Ergonomic safety issues are also a major concern. Parts of the system such as the radio frequency generator and gas cylinders are very heavy and should not be carried.

These are just some of the safety issues that must be addressed in the design of a plasma chamber system. By employing proper safety measures, the risk of injury will be greatly reduced. This is a key element in the design of any hazardous system.

- **Cost**

  There was a limited budget for the design of this system. There is no point in building a system that will cost too much to maintain anytime something fails. The engineer should always balance between performance and cost. The system will have to achieve a definite specification. If the system operates at a much better specification than required but cost has been compromised to achieve this then the system is of poor design. Safety must never be compromised for cost.

- **Performance**

  It is essential that a plasma chamber system has a stable performance, otherwise repeatable and reproducible measurements cannot be taken. Conclusions about experiments cannot be made as the data taken from the system cannot be trusted. It is important that any data from an experiment can be reproduced. The performance of the experiment should match its initial performance if the experiment is set up, as per a given specification, in any other laboratory.

3.2 System Components

3.2.1 The Power Supply

The power supply used was an Advanced Energy RF Power Delivery System, model number RFX-600. It is capable of driving a single frequency signal of 13.56 MHz within the range of 6 to 600 Watts into a 50 Ω load. A typical power

range of between 10 Watts and 150 Watts was used for driving the plasma in the chamber.

3.2.2 The Network Analyser

The HP 8753D network analyser was used for collecting data from the plasma chamber system. It is a high performance vector network analyser for laboratory or production measurements of reflection and transmission parameters. It integrates a high resolution synthesised RF source, an S-parameter test set and a dual channel three-input receiver to measure and display magnitude, phase and group delay responses of active and passive RF networks.

3.2.3 The Plasma Chamber

A capacitively coupled plasma chamber was designed for this work (refer to § *2.3.3 RF Diodes*). A mechanically similar design was used for the grounded electrode and the RF-live electrode. Copper sheets, pipes, rods and finger-strip were used for the conducting parts of the electrodes. PTFE was used for the insulating parts of the electrodes. Figures 3.2 through 3.11 illustrate the assembly of the grounded electrode. The RF-live electrode is assembled in the same manner. An N-type (female) QC connector is also attached to the RF-live electrode. N-type (male) transmission line cables are connected from here to the power generator via the matching unit.

A minimum stand-off distance of 10mm through PTFE and vacuum was observed between RF-live components and grounded components. This precaution was taken to stop dielectric breakdown and hence shorting between RF-live and grounded components.

It was desired to contain the plasma between the two electrode plates, thus achieving the RF diode setup as described in § *2.3.3*. The shield in the electrode, shown in figure 3.4, stops electromagnetic radiation from the electrode plates permeating into the cavity behind the electrode assembly. As a result, gas present here will not be excited into the plasma state. Plasma only forms between the two electrode plates shown in figure 3.11.

Figure 3.2 Copper rod connected to outer wall.

Figure 3.3 PTFE insulator separates inner and outer conductors.

Figure 3.4 Grounded shield prevents plasma forming in the cavity behind electrode plate.

Figure 3.5 4cm thick PTFE block insulates the electrode plate from the grounded shield.

Figure 3.6 Aluminium plate is used to attach the grounded electrode to the outer wall.

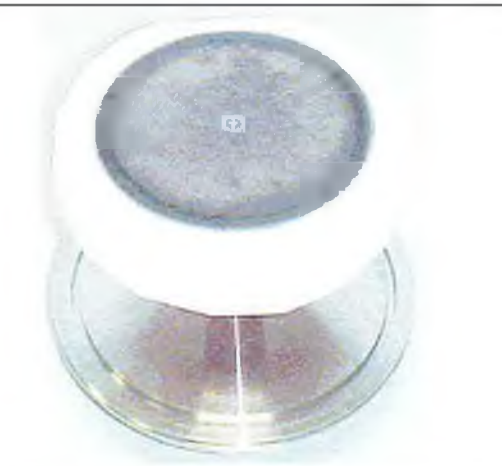

Figure 3.7 A flat disc is attached to the centre rod.

Figure 3.8 The grounded electrode is clamped to the rest of the chamber for good connectivity.

Figure 3.9. Grounded electrode inside the chamber.

Figure 3.10 The RF-live electrode is clamped to the rest of the chamber for good connectivity. Note the N-type connector.

Figure 3.11 Grounded electrode and RF-live electrode assembled inside the chamber.

The addition of a quartz cylinder around the two discs was also considered. This would have the effect of further containing the plasma, provided an extra pumping system was added to cause a pressure difference between outside and inside the quartz cylinder. It was decided against adding these features because of cost and the long lead time for a quartz cylinder.

3.2.4 The Match Unit

The impedance of the plasma chamber (as assembled in § *3.2.3*) was measured using the network analyser. It was found to have an impedance of 66 Ω and -77 degrees at 13.56 MHz.

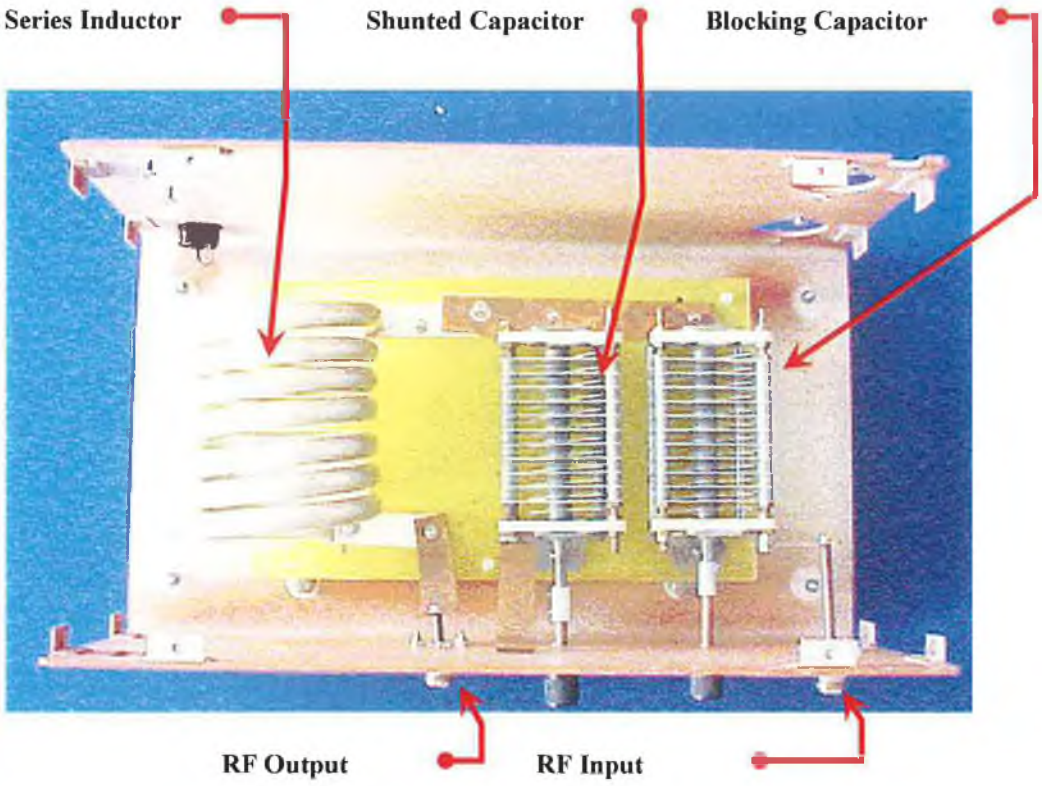

Figure 3.12 Inside layout of match unit

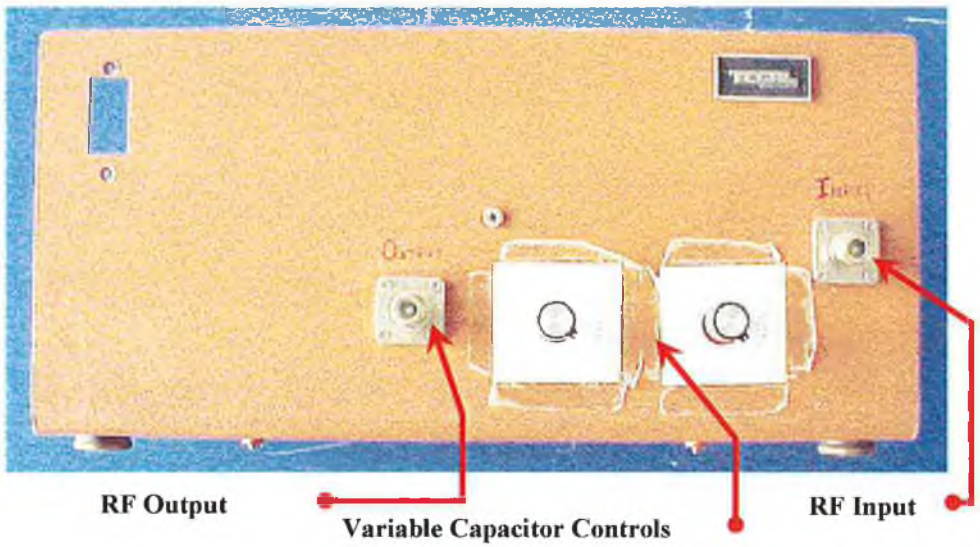

Figure 3.13 Front panel of match unit

A match unit was designed to match the impedance of the plasma chamber to the 50 Ω input impedance of the RF generator. The components of the match unit are shown in figures 3.12 and 3.13 and are contained within a grounded box. Good contact between the grounded surfaces is essential to prevent leakage of RF electromagnetic radiation into the surrounding area. Good connectivity between conducting paths as well as an ability to carry the high currents (maximum of

10A) delivered is required, otherwise the conducting path will burn out. This is the reason why the components are so large; for instance the copper straps connecting the different components have a width of 10mm. A circuit diagram of the match unit is shown in figure 3.14.

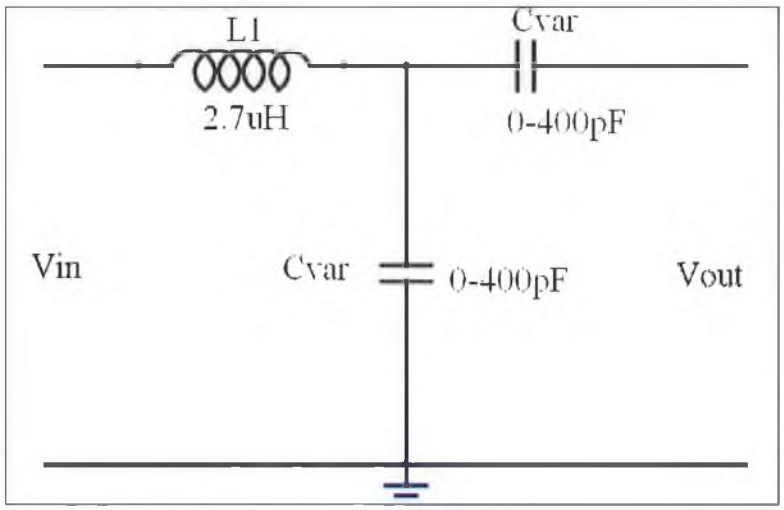

Figure 3.14 Circuit diagram of the match unit

The series inductor has a fixed value of 2.7uH. It nullifies the imaginary component of the plasma chamber. The blocking capacitor prevents DC current, generated in the plasma, passing back through the matching unit and damaging the RF generator. Both the blocking capacitor and the shunt capacitor are variable and are used to fine tune the matching unit so that the maximum power can be delivered from the RF generator to the plasma chamber. The Smith chart in figure 3.15 (see also § *2.2.6 Smith Charts*) shows the range of impedances at 13.56 MHz that the matching unit can match. The points were measured by placing a 50 Ω terminator on the input of the matching unit (simulating the RF generator input impedance) and connecting the network analyser to the output of the matching unit. The two capacitors were varied across their ranges and the points measured were plotted on the Smith chart. The impedance of the plasma chamber is also shown as the blue dot. Table 3.1 lists the data points plotted on the Smith Chart.

Point	Real	imaginary	$Real_{normalised}$	$Imaginary_{normalised}$
1	4	-17	0.1	-0.3
2	4.2	-5.2	0.1	-0.1
3	3.4	17.4	0.1	0.3
4	3.3	34	0.1	0.7
5	3.2	65	0.1	1.3
6	2.3	76	0.0	1.5
7	3.4	90	0.1	1.8
8	6.5	100	0.1	2.0
9	7.3	111	0.1	2.2
10	13.8	157	0.3	3.1
11	36.7	111	0.7	2.2
12	25.3	80	0.5	1.6
13	21.7	70	0.4	1.4
14	19.5	56	0.4	1.1
15	13.7	34	0.3	0.7
16	9.3	11.9	0.2	0.2
Chamber	14.8	64.3	0.3	1.3

Table 3.1 Match unit data points shown on Smith chart in figure 3.15

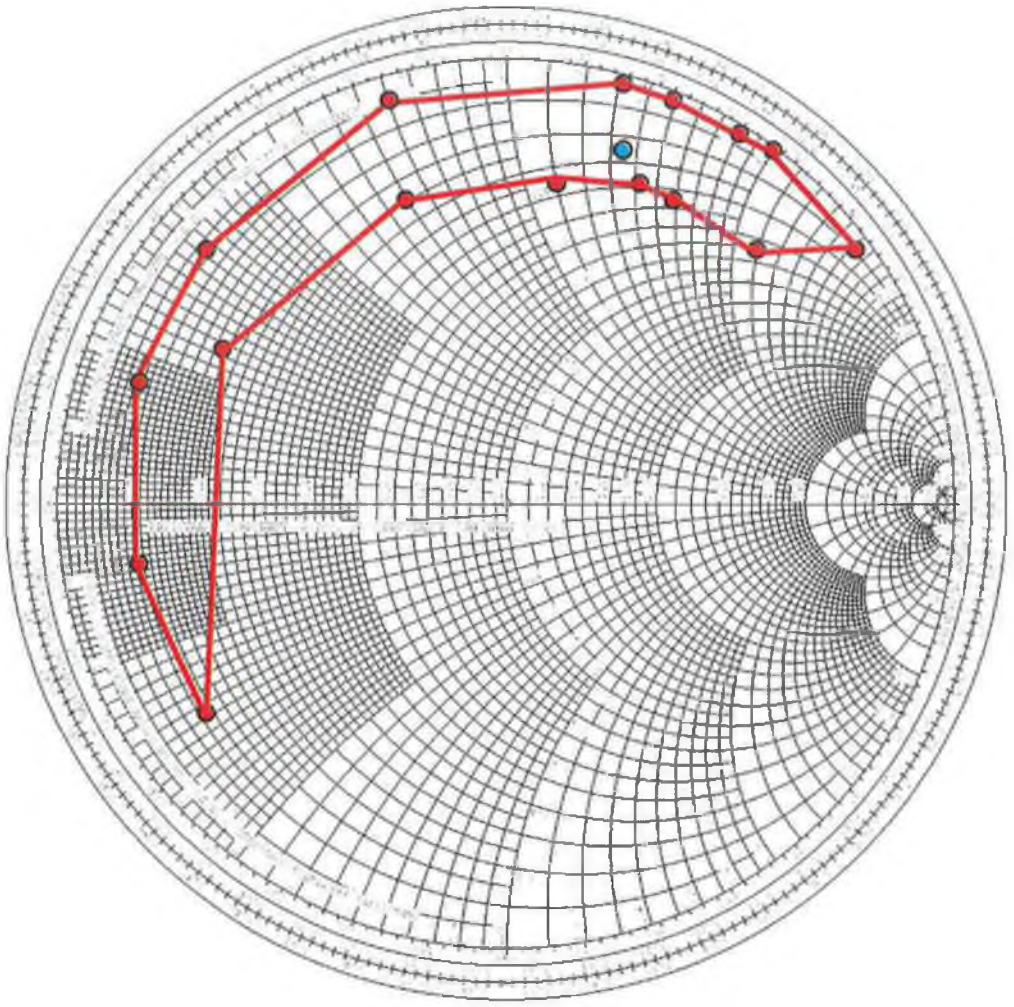

Figure 3.15 Smith Chart showing the range of impedance covered by the match unit (red) and the chamber impedance (blue).

As with the plasma chamber, N-type (female) QC connectors were used to connect the matching unit to the rest of the system via N-type (male) transmission line cables.

3.2.5 The SmartPIM System

In the plasma research and plasma based manufacturing communities it is well known that measuring the plasma is key to understanding and improving on new and existing plasma processes. Achieving such understanding involves using plasma diagnostic sensors which can be intrusive in nature and in some cases can perturb the plasma which is being monitored. The ideal plasma diagnostic is one which can monitor what is happening inside a plasma chamber and yet does not have to be inserted inside the plasma.

SmartPIM™, Scientific Systems Plasma Impedance Monitor is such a non-intrusive plasma diagnostic. It resides on the RF power line post match unit. SmartPIM™ measures the plasma impedance at the fundamental frequency and the four higher harmonics. The SmartPIM™ system comprises an acquisition electronics unit, RF transmission line sensor and PIMSoft™ software. Communication between the acquisition electronics unit and PIMSoft™ is via RS232. PIMSoft™ is used to acquire and display the current, voltage and phase of the fundamental and four higher harmonics. Power and impedance are then calculated from the current, voltage and phase values.

3.2.6 The SmartProbe

SmartProbe™ from Scientific Systems is a commercial Langmuir probe system and is used to measure a wide range of plasma parameters such as plasma density, uniformity and electron temperature distribution. It enables plasma researchers to understand the complexity and characteristics of a plasma and how they relate to the plasma process they are trying to develop. SmartSoft™, the software application that comes packaged with the SmartProbe™, is a powerful Microsoft Windows compatible software package that provides immediate data acquisition and analysis.

3.3.1 Mechanical Systems

An Edwards, 2-stage, 12 litre pump was used to bring the chamber down to vacuum. Edward Pre-10k pressure gauges were used to monitor the pressure within the chamber. A Spectra Vascan Plus chemical detector was used to find leaks in the chamber. A Tylan Mass Flow controller was used to set the flow of gas into the plasma chamber.

Chapter 4 Method

4.1 Introduction

The goal of this thesis was to design a simple capacitively coupled plasma discharge. A detailed electronic component model was then to be developed to better understand how the radio frequency energy was dissipated within the chamber. Two experiments were set-up to demonstrate these two goals. The first experiment demonstrates that the chamber does indeed produce capacitively coupled plasma, i.e. it displays the characteristics of the RF-diode discussed in § *2.3.3*. The second experiment describes how the electronic component model of the chamber is developed. Empirical data is gathered to demonstrate that the model accurately reflects how the radio frequency radiation is dissipated in the plasma chamber system. The following sections detail the two experiments and their results.

4.2 Experimental Set-up and Results

4.2.1 SmartProbe and SmartPIM measurements of an Argon Plasma

The typical I-V characteristic for a given plasma in an RF-Diode system, taken with a Langmuir probe, is shown in figure 4.1.

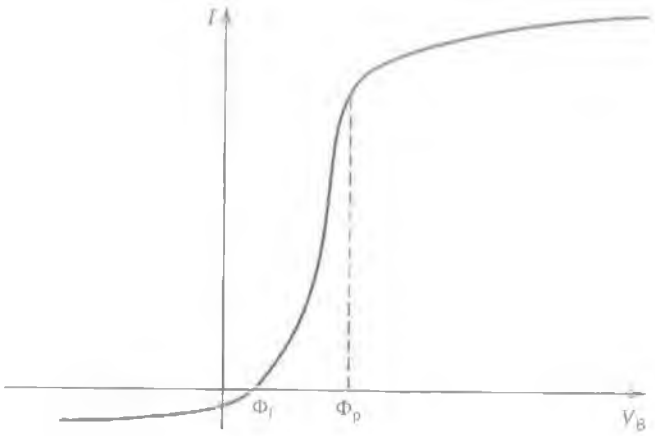

Figure 4.1 Typical I-V characteristic of an argon plasma taken with a Langmuir Probe

A typical I-V Scan of an Argon Plasma driven in the chamber system is shown in figure 4.2.

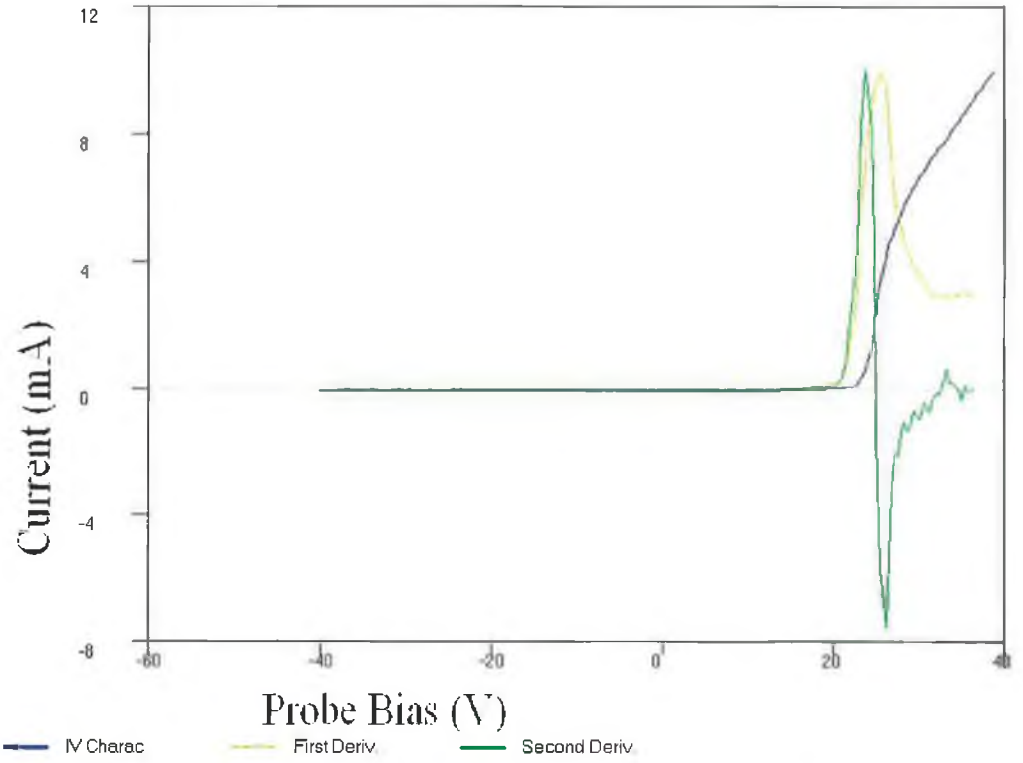

Figure 4.2 I-V characteristic of an argon plasma in the plasma chamber designed for this thesis

The I-V profile of the argon plasma in the plasma chamber has all the characteristics of a typical capacitively coupled plasma discharge. This gives a high level of confidence that the chamber is functioning as required.

4.2.2 Electronic Component Model of the Plasma Chamber System

The derivation of the electronic components model requires empirical measurements of the plasma chamber, an intuitive circuit representation of the plasma chamber and matrix analysis to compare the model's output to the empirical measurements. The RF theory described in *§2.2.1* to *§2.2.5.6* is extensively used to develop the model. The mesh current analysis and matrix theory described in *§2.4.1* to *§2.4.7* is used to develop a *Scilab* program (see *§4.2.2.4*) to compare the model's output to empirical measurements.

4.2.2.1 Frequency Response of the Chamber

The first step is to obtain a frequency sweep of the impedance of the plasma chamber. The network analyser is attached to the N-type (female) connector of the RF-live electrode in the plasma chamber. The network analyser is set to record the impedance of the plasma chamber over a frequency range of 3MHz to 180MHz. Figure 4.3 shows the frequency response of the chamber.

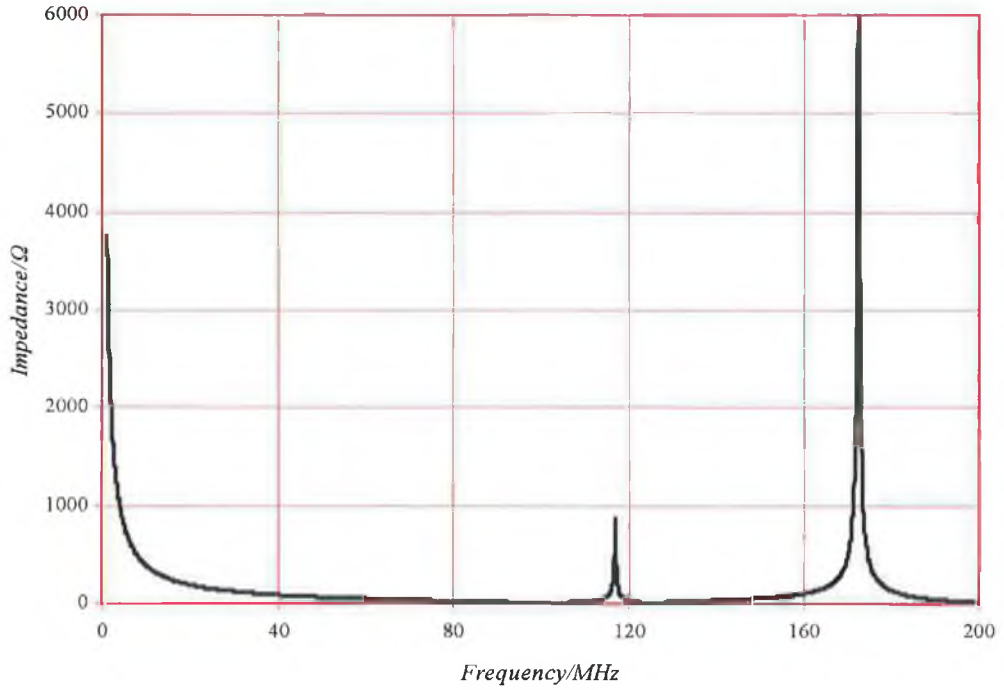

Figure 4.3 Impedance plot of the plasma chamber over the frequency range 3MHz to 180MHz.

It can be seen that impedance is decreasing in the frequency range of 3MHz to 90MHz. The phase of the impedance is approximately -90° throughout this range. The impedance of the plasma chamber $Z_{chamber}$ is being dominated by capacitive impedance. At 100MHz and 125MHz the impedance is approximately 0 Ω. These are series resonance points and some capacitance in series with some inductance dominates the impedance. At 117MHz and 172MHz a parallel resonance circuit dominates and the impedance magnitude is approaching ∞ (limited by the resistance of the parallel resonance circuit).

The profile of the plasma chamber's impedance-frequency sweep indicates that a model of the chamber will contain more than one or two components. Therefore, to assist developing the model of the chamber, measurements of the chamber were taken with various mechanical parts removed. Table 4.1 summarises the measurements taken of the chamber with the different parts removed. Figures 4.4 through 4.7 show the impedance of the chamber for the various set-ups. Refer to the pictures in *§3.2.3* for the different parts.

Figure	Chamber Set-up
4.4	RF-live electrode without disc attached; grounded electrode removed.
4.5	RF-live electrode with disc attached; grounded electrode removed.
4.6	RF-live electrode with disc attached; grounded electrode attached.
4.7	RF-live electrode without disc attached; grounded electrode attached.

Table 4.1 Impedance-frequency sweep for the plasma chamber with various set-ups.

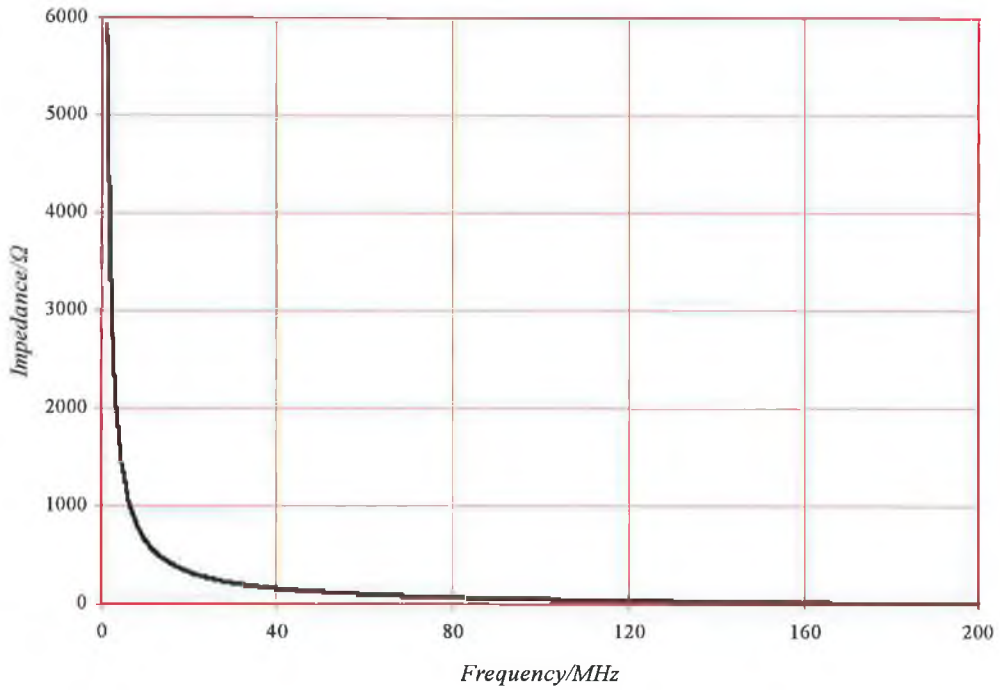

Figure4.4 RF-live electrode without disc attached; grounded electrode removed.

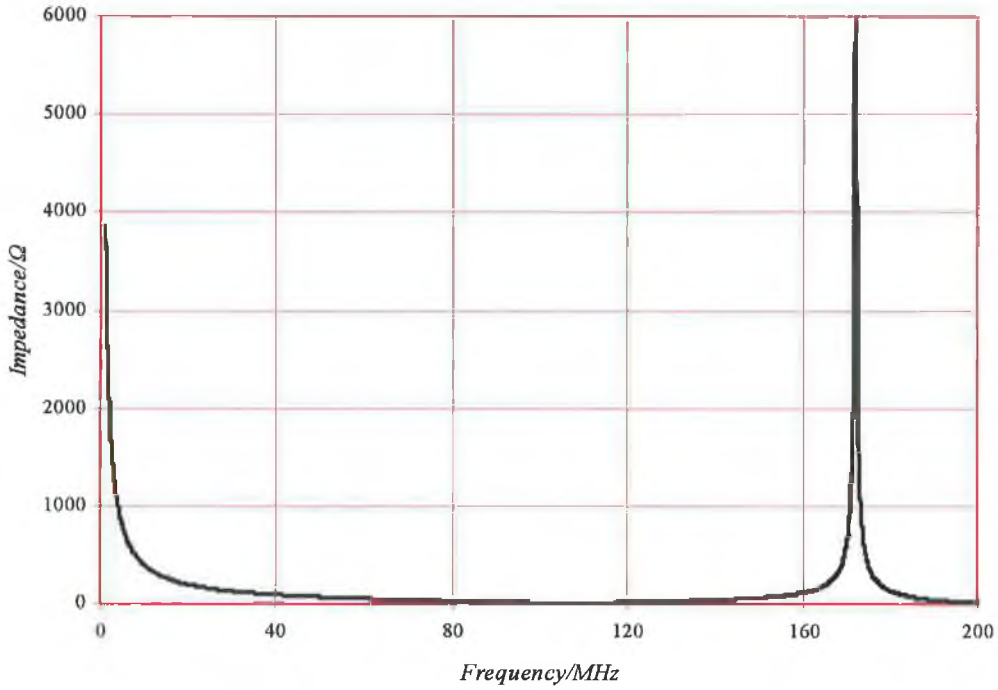

Figure 4.5 RF-live electrode with disc attached; grounded electrode removed.

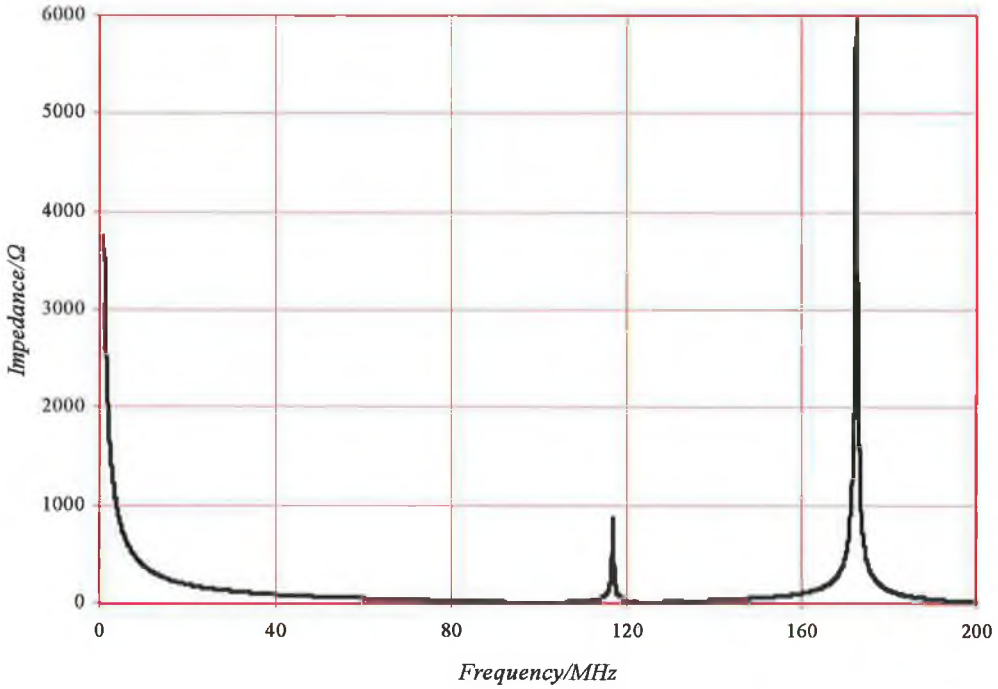

Figure 4.6 RF-live electrode with disc attached; grounded electrode attached.

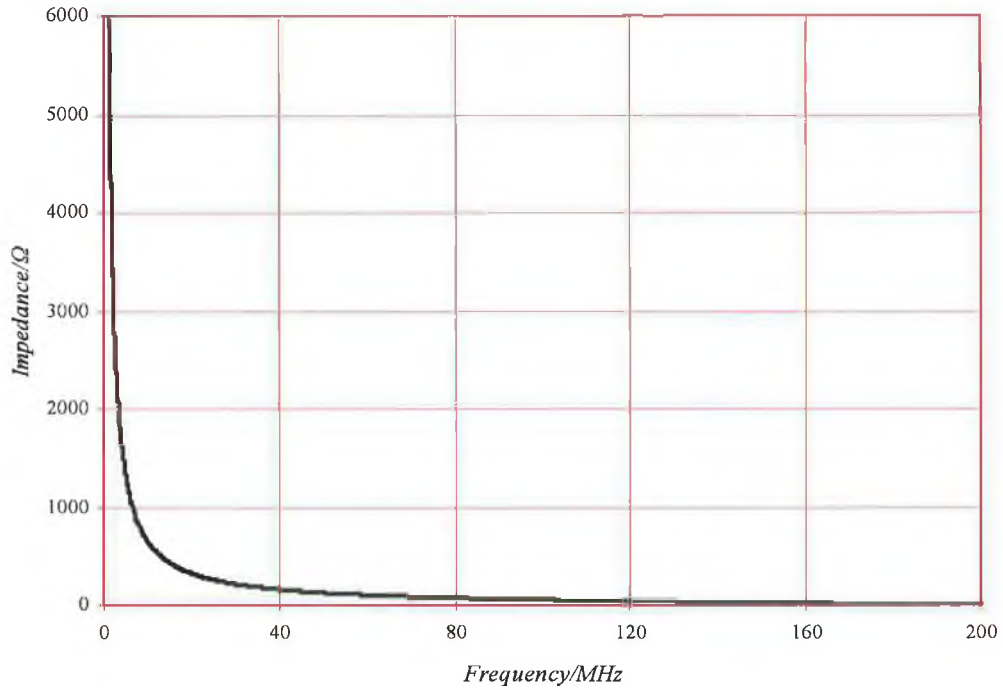

Figure 4.7 RF-live electrode without disc attached; grounded electrode attached.

Figure 4.4 illustrates that the corresponding chamber set-up is predominantly capacitive. The capacitance that gives this impedance response can be approximately calculated using the equation $C_{set-up1} = \frac{1}{2\pi f Z_{set-up1}}$ and applying it to all the points of a linear section of the frequency sweep. The value is found to be approximately 24pF.

Figure 4.5 has a parallel resonance point. The disc now attached to the RF-live electrode has added an inductance that is causing the resonance peak. Figure 4.6 shows that the addition of the grounded electrode with disc causes another resonance peak at 117MHz. Figure 4.7 is very similar to figure 4.3. The disc from the RF-live electrode has been removed. The effect of the grounded electrode is no longer significant because radio frequency radiation cannot easily travel from the RF-live electrode to the grounded electrode.

The graphs above give clues to the final circuit layout for the chamber. The measurements are also used to give good first guess values for the *Scilab* program discussed in *§4.2.2.3*.

4.2.2.2 Electronic Component Model

The circuit diagram shown in figure 4.8 is the electronic component model that was developed for the plasma chamber system. A list of the components and the parts of the chamber that they represent is given in Table 4.2.

Component	Chamber Part
R_c	Resistance of the RF-live electrode from the inner conductor of the N-type connector to the edge of the RF-live electrode disc.
L_c	Inductance of the RF-live electrode from the inner conductor of the N-type connector to the edge of the RF-live electrode disc.
C_c	Capacitance between the RF-live parts of the RF-live electrode and the grounded shield of the RF-live electrode.
C_{pw}	Capacitance between the RF-live parts of the RF-live electrode and the grounded walls of the chamber.
R_w	Resistance of the grounded walls of the chamber near the powered electrode.
L_w	Inductance of the grounded walls of the chamber near the powered electrode.
C_{pg}	Capacitance between the RF-live parts of the RF-live electrode and the grounded electrode.
R_e	Resistance from the grounded wall near the grounded electrode to the grounded walls near the powered electrode.
L_e	Inductance from the grounded wall near the grounded electrode to the grounded walls near the powered electrode.
C_e	Capacitance across the inductance L_e.
C_{gw}	Capacitance between disc of the grounded electrode and the grounded walls of the chamber.
R_g	Resistance of the grounded electrode i.e. along the disc, rod and grounded shield of the grounded electrode.
L_g	Inductance of the grounded electrode i.e. along the disc, rod and grounded shield of the grounded electrode.

Table 4.2 List of electronic components in the model of the plasma chamber

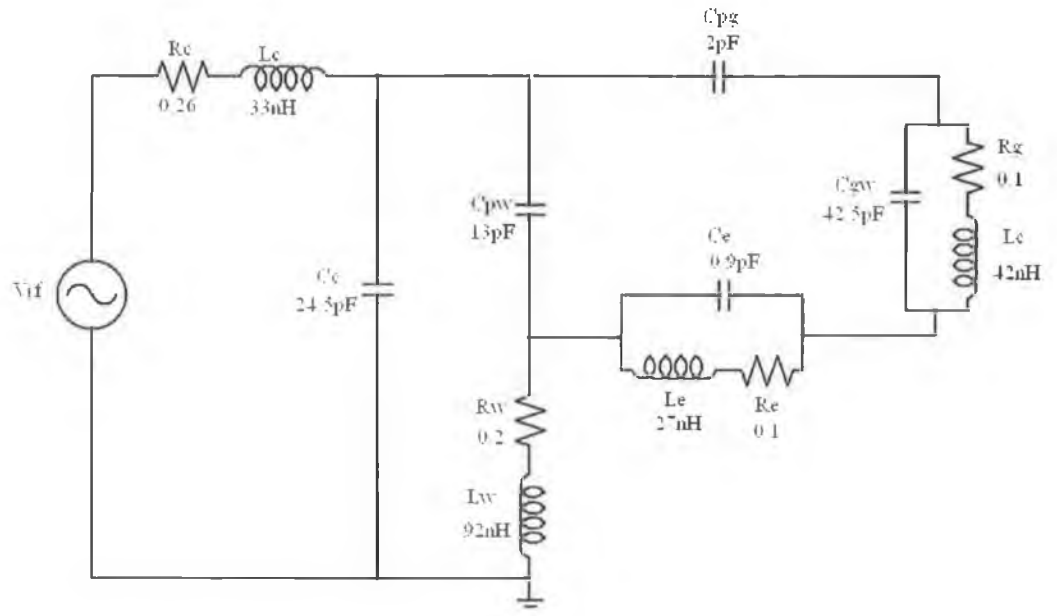

Figure 4.8 Circuit diagram of electronic component model of the plasma chamber.

4.2.2.3 Scilab Program

Scilab is a freeware tool that can be used for matrices analysis. More information about this application can be found at www.scilab.org. Print outs of the Scilab program files used in this thesis are given in Appendix A.

The block diagram in figure 4.9 shows the basic flow of the program. The program is initiated and the user inputs the frequency sweep data file for the chamber's impedance. The user then applies the circuit shown in figure 4.7 above with best guess initial conditions for each of the components. The simplex algorithm is initiated and the parameters of the components in the model are varied so as to achieve a match between the actual frequency sweep data of the plasma chamber's impedance and the frequency response of the electronic component model's impedance. The actual frequency sweep of the chamber's impedance and the characteristic frequency response of the electronic component model's impedance are plotted. An output is given of the root mean square value of the difference between all data points of the actual frequency response of the chamber and the frequency response of the electronic component model.

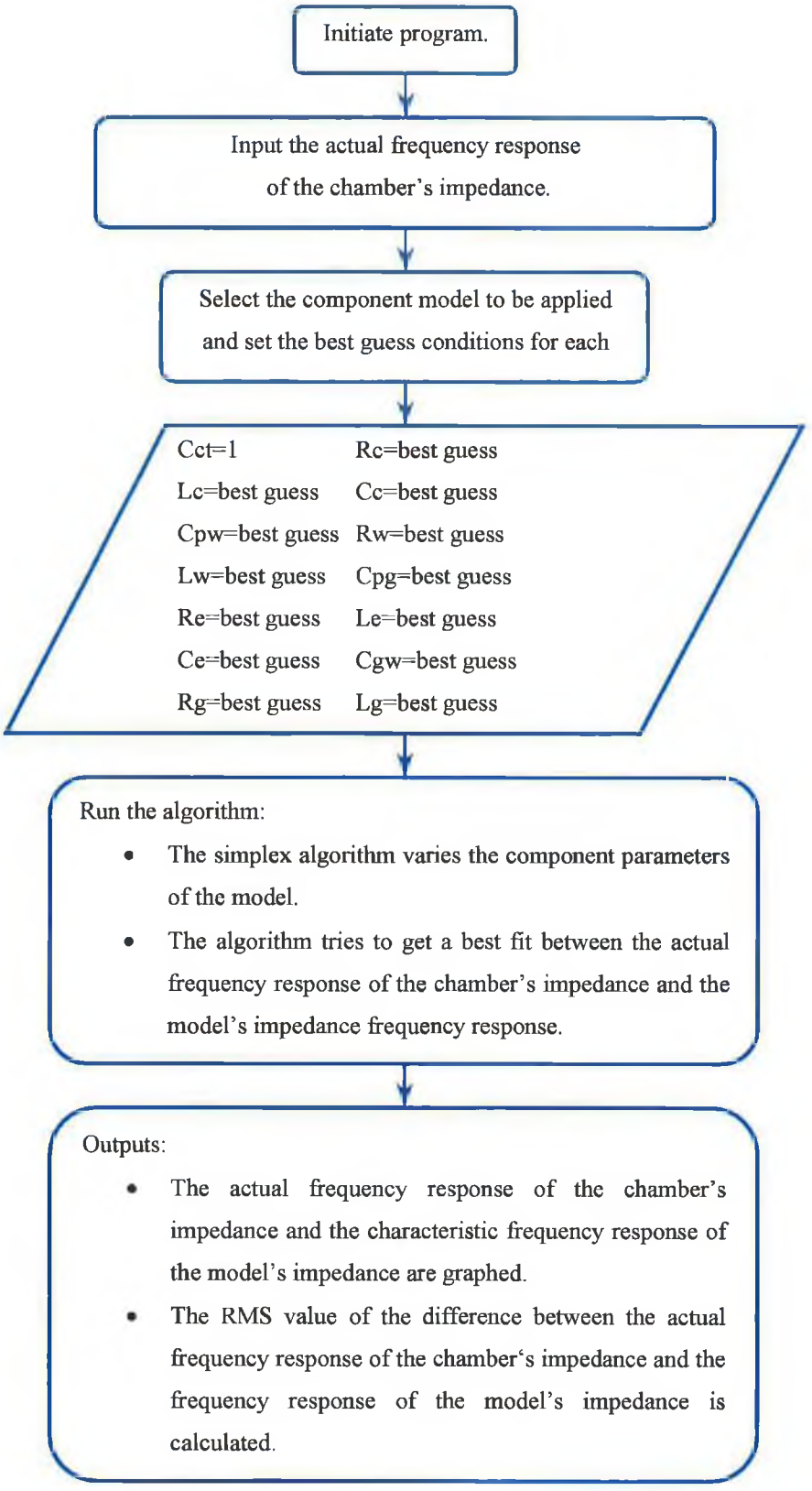

Figure 4.9 Block diagram of the program.

Chapter 5 Results and Conclusions

5.1 Introduction

The results generated from the experiments run in chapter 4 are given in chapter 5. Conclusions are drawn and ideas for further experimental work are discussed. Finally, a synopsis is given of the applications of the work in this thesis for the semiconductor microchip manufacturing processes.

5.2 SmartProbe Analysis of the Plasma Chamber

A comparison of figure 4.1 (a typical I-V characteristic scan of an argon plasma) and 4.2 (I-V characteristic of the argon plasma the chamber designed for this thesis) indicates that the plasma discharge is demonstrating the characteristics of a capacitively coupled rf discharge. The probe bias voltage V_B is approximately the same as the plasma potential Φ_p (see figure 4.2) at $V_B = 26$ Volts. The probe is mainly drawing current from the mobile electrons in the plasma and this is designated by a positive current flow from the probe to the plasma. As the probe voltage increases above 26 Volts the current starts to saturate at the electron saturation current. However, due to the probe geometry, the effective collection area is increasing as V_B is increasing and therefore the current still increases. This is different to the typical I-V characteristic shown in figure 4.1 where the current levels off as the probe bias voltage increases.

As the probe bias voltage decreases below 26 Volts electrons start to be repelled as per the Boltzmann relation,

$$n_e = n_o e^{-\Phi/T_e},$$

i.e. electrons are attracted to more positive areas of potential. The total current equals zero when the probe is sufficiently negative with respect to the plasma such that the electron current is equal to the ion current. The voltage that this occurs at is called the floating potential Φ_f, and from figure 4.2 it can be seen that this is at 16 volts for the given argon plasma. At this potential the probe cannot draw current and therefore floats. As the probe bias voltage is decreased further ion current increases, leading to ion saturation current. The ion saturation current

is much smaller than the electron saturation current due to the much greater ion mass relative to the electron mass.

5.3 *Electronic Component Model of the Plasma Chamber*

The electronic component model shown in figure 4.7 was applied to the chamber. As can be seen in figure 5.1, the frequency response of the circuit's impedance has the same characteristic profile as the actual frequency sweep of the chamber's

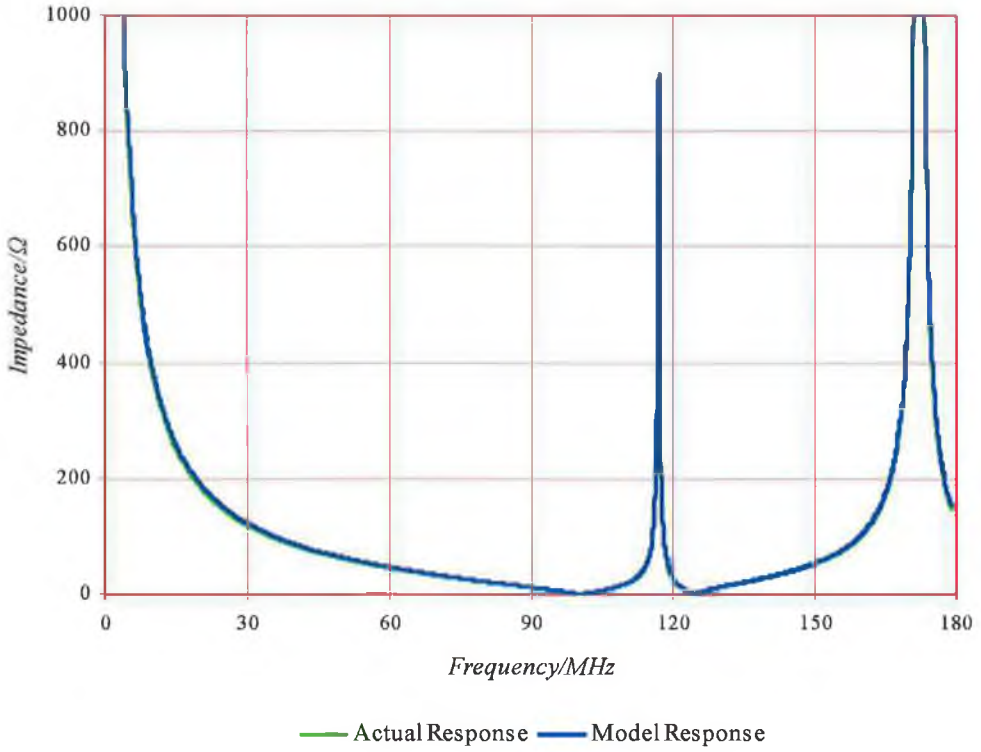

Figure 5.1Characteristic profiles of the chamber's impedance and the electronic components model's impedance.

impedance. The close correlation between the two profiles can be seen by looking specifically at the resonance points in the profiles (see figures 5.2 through to 5.4)

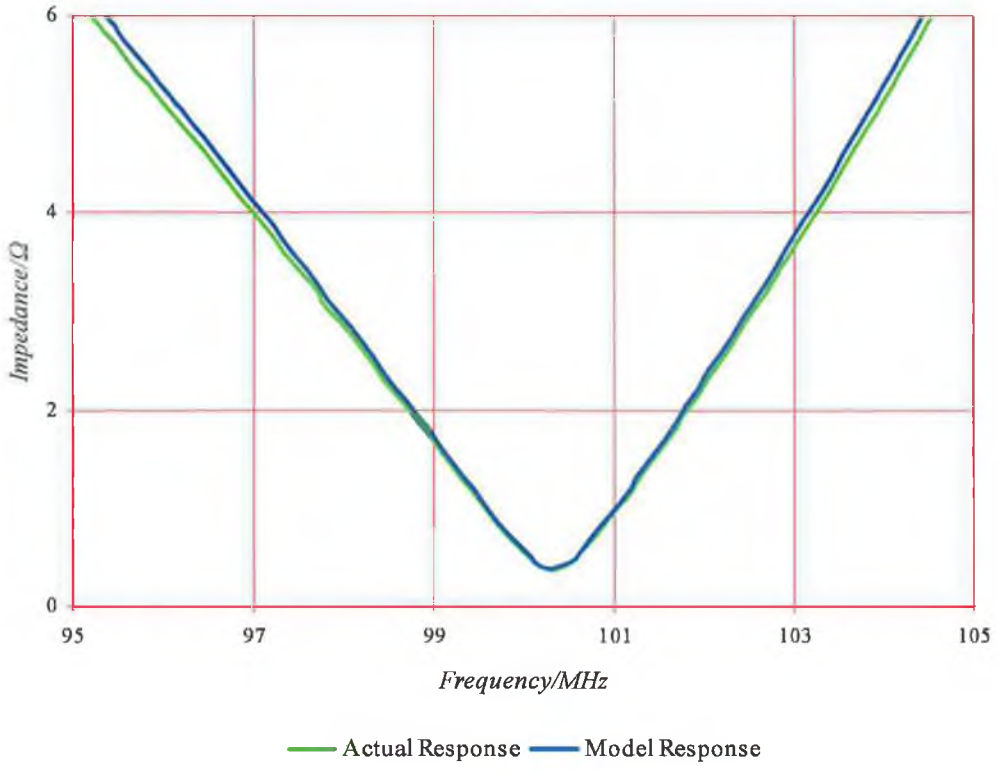

Graph 5.2 Resonance point at ~100MHz

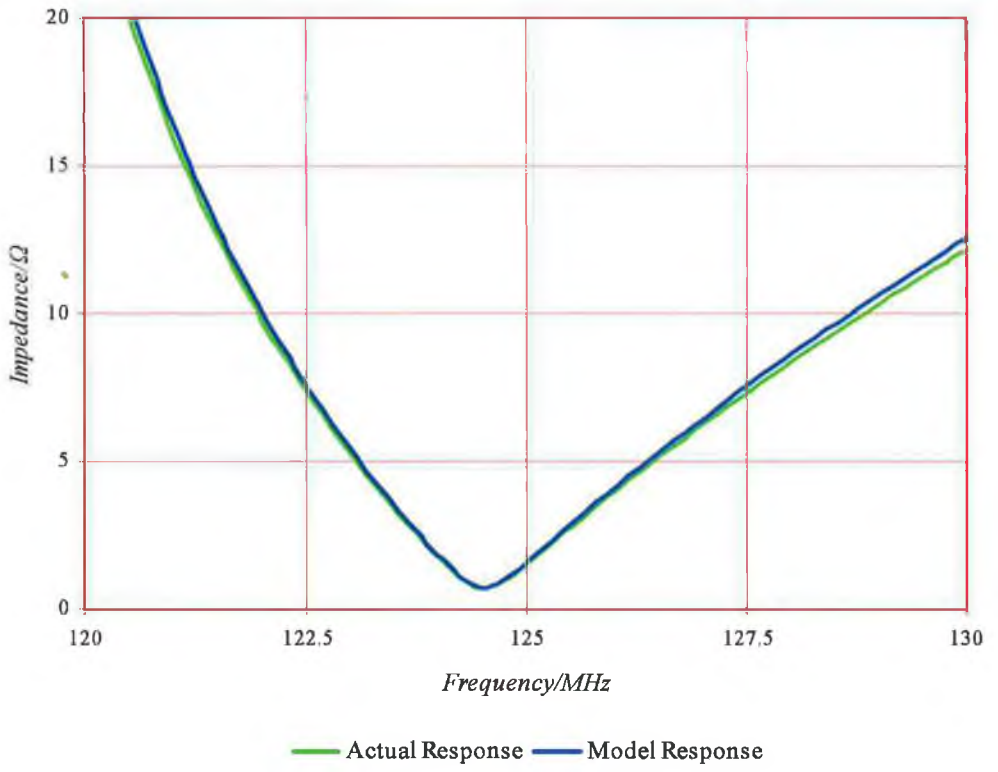

Graph 5.3 Resonance point at ~125MHz

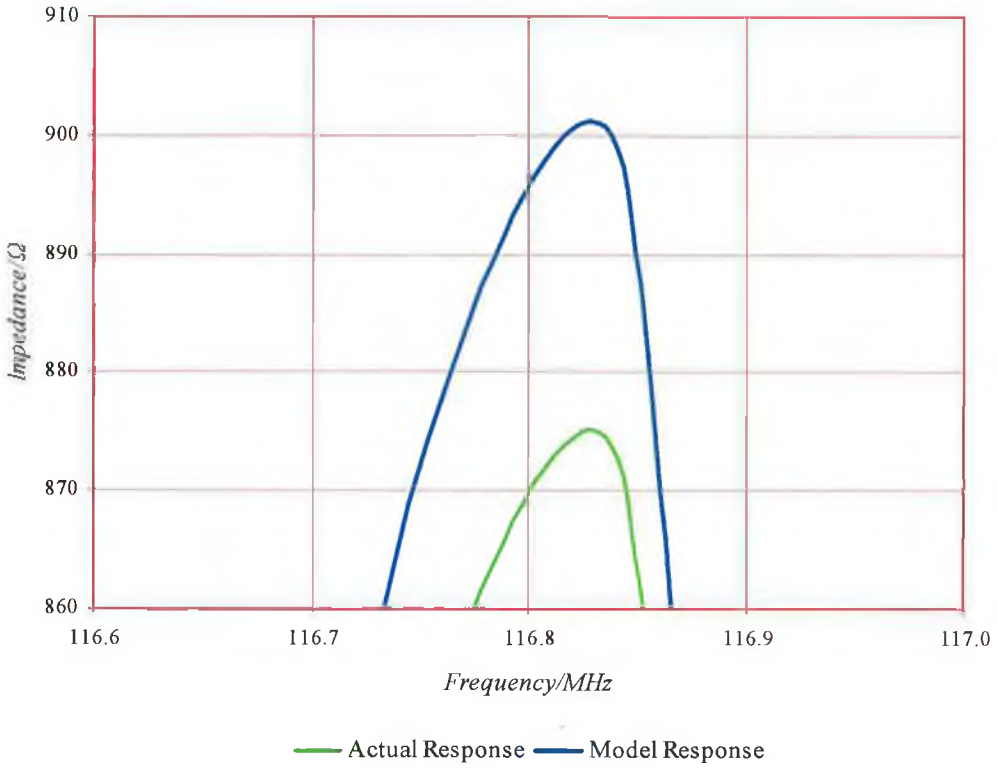

Graph 5.4 Resonance point at ~116.8MHz

The root mean square value of the difference between the actual chamber impedance and the electronic component model's impedance for each frequency point was better than 3% (2.8% to be precise). This figure, Δ_{rms}, was calculated using the formula:

$$\Delta_{rms} = \sqrt{\sum_{1}^{n} (x_{actual} - x_{circuit})^2}$$

where n is the number of sample points in the frequency sweep of the actual chamber impedance, x_{actual} is the actual impedance of the chamber at a given frequency point and $x_{circuit}$ is the electronic component model's impedance at the same given frequency. Therefore, the way in which the applied radio frequency electromagnetic radiation propagates through the chamber is accurately described by the intuitive electronic component model of the chamber.

At 13.56MHz the impedance of the chamber is 277 Ω with a phase of -90°. The electronic component model gives an impedance value of 285 Ω and -90°. This constitutes a 3.4% difference at 13.56MHz (see figure 5.5).

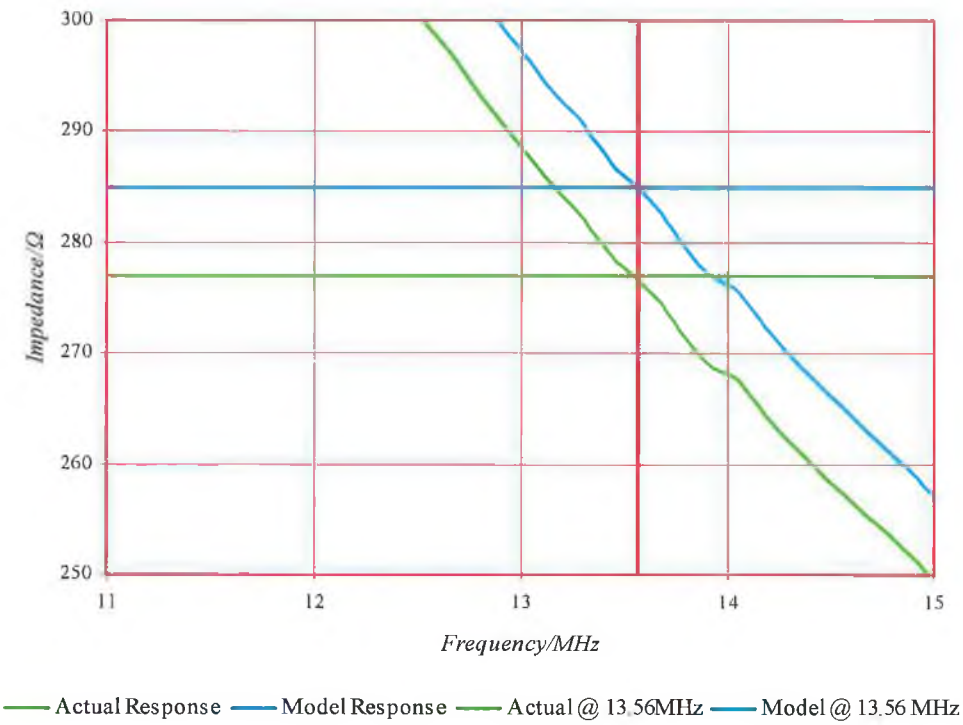

Figure 5.5 Impedance values at 13.56MHz for electronic component model and plasma chamber.

The SmartPIM™ (see §*3.2.5*) was used to measure the impedance of the chamber while an Argon plasma was ignited between the electrodes of the chamber. The SmartPIM™ was placed between the match unit and the plasma chamber. It was connected to the N-type connector on the chamber, the same point where the network analyser was connected to take the frequency sweep of the chamber. Table 5.1 lists the settings and readings taken for the argon plasma.

Pressure/mTorr	**Generator Power/W**	**Impedance/ Ω**	**Phase/°**
263-267	40	93.7	-87.1
263-267	70	97.2	-87.8
263-267	100	95.4	-84.9
324-326	40	90.4	-83.4
324-326	70	90.8	-85.2
324-326	100	89.5	-84.9
388-390	40	89.2	-79.1
388-390	70	86	-85.3
388-390	100	87	-85.7

Table 5.1 PIM measurements of an Argon plasma.

Figures 5.6 and 5.7 show the variation in impedance and phase as measured by the SmartPIM^{TM} for the different settings.

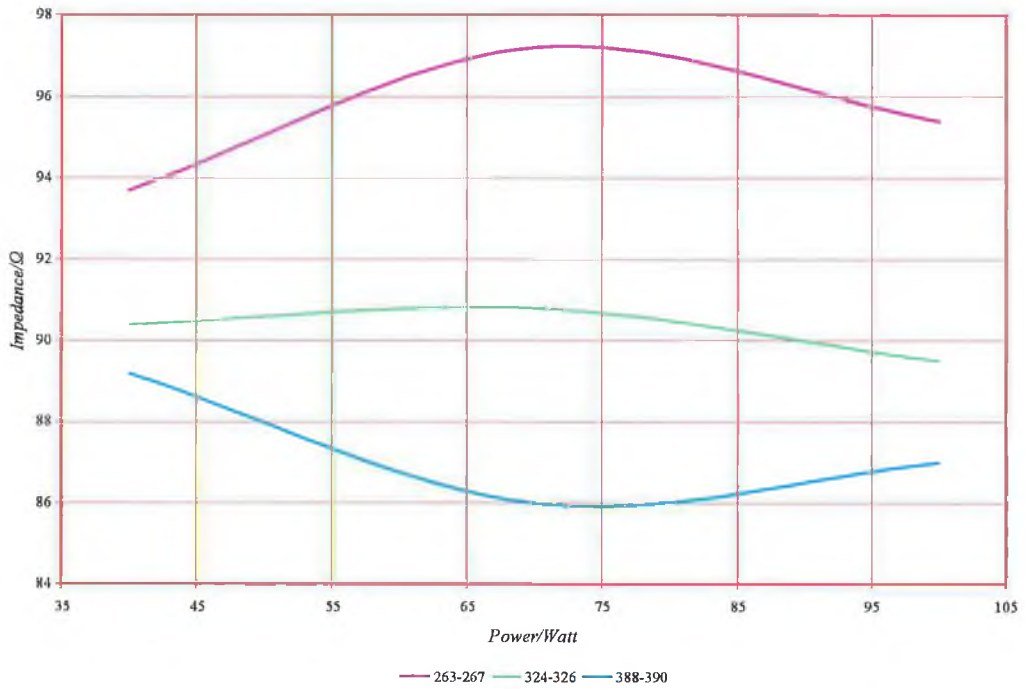

5.6 Impedance of Argon Plasma versus generator power.

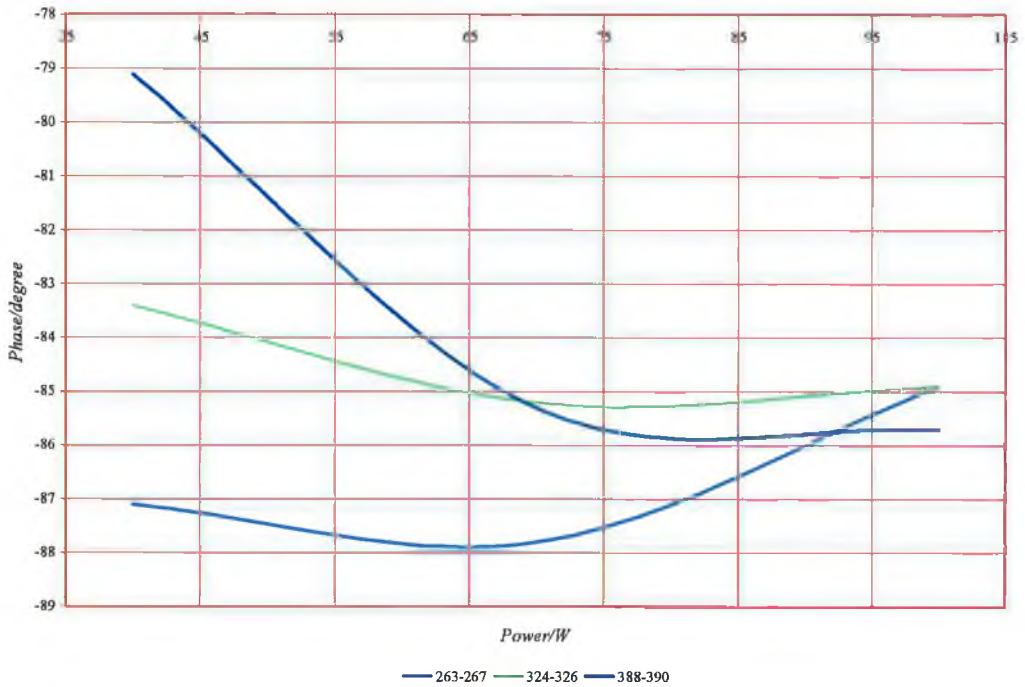

5.7 Phase versus power for argon plasma.

If the assumption is made that the ignited plasma is contained within the electrode plates, then the difference in impedance at 13.56MHz between the SmartPIM^{TM} measurements and the impedance of the chamber given by the

network analyser measurements is solely due to the plasma that exists between the two electrodes. The introduction of the plasma has dramatically reduced the overall chamber impedance (at 13.56 MHz) from 277 Ω to between 87 Ω and 98 Ω, depending on the controllable parameter settings i.e. power and pressure. The amount of current now drawn by the chamber has increased because the plasma is providing a path for current to flow. The impedance between the parallel plates in the chamber with plasma present dominates the chamber impedance.

Figure 5.6 shows that as pressure increases the chamber impedance decreases. The increased pressure is due to a controlled increase in the flow rate of argon into the chamber and effectively increases n_e and n_i, the number of electrons and ions in the chamber. Therefore the number of current carriers between the parallel plates is increased and the impedance is reduced. At low powers and high pressures the phase of the impedance is less capacitive than at any other parameter setting as seen in figure 5.7. This would suggest that the plasma impedance at this point is being affected by the inductive component of the bulk plasma (see *§2.3.4.1*).

The next logical step would be to develop a model for the chamber with the plasma present between the electrodes. The model could define the plasma for specific parameter settings such as pressure, applied power and even the chemistry of the gas used to generate the plasma. An in-line sensor with the ability to measure over a frequency range would be needed to generate the necessary empirical data. This would be placed between the matching unit and the plasma chamber. The modelling techniques discussed in this thesis would then be applied to generate the model for the plasma chamber with plasma present.

The model for the plasma chamber with plasma present would include all the values for the components shown in figure 4.7. However, the C_{pg} parameter would be replaced by a more complex circuit. A suggestion for the replacement circuit for C_{pg} would be a series RLC circuit. The capacitance due to the DC sheaths that form at each electrode (see *§2.3.2*) would be represented by the series capacitor. The resistance and inductance due to the current that crosses the bulk plasma would be represented by the series resistance and inductance. Unfortunately there is not yet an in-line sensor commercially available that can

measure the impedance of a plasma chamber, while there is a plasma present, over a frequency range that could generate the required empirical data. If such a sensor were to be developed then modelling and hence control of plasma processing could be brought to a new level.

5.4 *Further Experimentation and Work*

The experiments in this thesis have shown that it is possible to generate an equivalent electronic component model for a given plasma chamber. A next step in this work would be to develop a model for an industrial plasma chamber that is actively used to manufacture microchips. The model again would be based on the electro-mechanical set up of the given chamber. The model could then be applied to the second/third/fourth of a kind of a cluster of plasma chamber tools. Detailed data on the variation between tools could be generated; differences could be pin pointed to distinct parts of the tools and an operation window for the cluster of tools could be determined.

Chamber design could be aided by the use of the modelling techniques used in this thesis. In the design of a new plasma chamber, efforts could be made to ensure that the area where the plasma exists (between electrodes for example) will dominate the impedance at the frequency of the input power. Therefore impedance of the plasma chamber would be dominated by the impedance of the plasma inside the chamber and not the chamber components. This would lead to more effective modelling of the plasma as small variations in the plasma would be detected more easily. The ability to observe small changes in the plasma impedance would lead to easier detection of events in a plasma process such as endpoint.

5.5 *Applications*

A monitoring system for plasma chambers could be developed based on the work in thesis. The basic outline of the monitoring system is as follows:

- An acquisition unit measures the electrical impedance of a chamber over a frequency bandwidth.
- The frequency response is simulated by an electrical network of components based on the physical arrangement of the chamber.

- Software is used to analyse the chamber state and diagnose faults.

Immediate applications would be:

- The state of a given plasma chamber can be monitored as it ages to detect when cleaning or repair is required.
- The characteristics of the chamber can be checked to see if they are as expected after manufacture, rebuild or modification.

The advantages of such a monitoring system are:

- It can be integrated into the normal process flow of a chamber system; when the plasma is not powered up, e.g. during wafer loading, the monitoring system can be switched in and measurements made.
- It is non-intrusive unlike, for example, a Langmuir probe.
- It can be applied to any type of plasma etching/deposition chamber system.

References

1. J. Proud, R.A. Gottscho, J. A Bondur, A. Garscadden, J. V. Heberlein, G.K. Herb, M.J. Kushner, J.E. Lawler, M.A. Lieberman, T.M. Mayer, A. V. Phelps, W. Roman, H. H. Sawin and H.F. Winters, *Plasma Processing of Materials: Scientific Opportunities and Technological Challenges*, Washington D.C.: National Academy Press, 1991.
2. R.A. Gottscho, M.E. Barone and J.M. Cook, *MRS Bulletin*, vol. 21 p.38, 1996.
3. M. A. Lieberman, *IEEE Transactions on Plasma Science*, vol. 16 no. 6, p. 638, December 1988.
4. V. A. Godyak, R. B. Piejak, B. M. Alexandrovich, *IEEE Transactions on Plasma Science*, vol. 19, no. 4, p. 660, August 1991.
5. M. A. Soblewski, *Journal of Vacuum Science Technology A*, 10(6), November/December 1992.
6. M. A. Soblewski, *IEEE Transactions on Plasma Science*, Vol. 23, No. 6 December 1995.
7. S. Rauf, M. J. Kushner, *Journal of Applied Physics*, Volume 83, Number 10, 15 May 1998, p. 5087.
8. H. Karloff, *Progress in Theoretical Computer Science-Linear Programming*, Birkhauser 1991.
9. H. H. Skilling, *Fundamentals of Electric Waves*, Florida: Roberts E. Krieger Publishing Co., Inc., 1942.
10. F. T. Ulaby, *Fundamentals of Applied Electromagnetics*, New Jersey: Prentice Hall, 1999.
11. M. M. Radmanesh, *Radio Frequency and Microelectronic Electronics*, New Jersey: Prentice Hall, 2001.
12. M. A. Lieberman and A. J. Licthenberg, *Principles of Plasma Discharges and Materials Processing*, New York: John Wiley and Sons Inc., 1994.
13. B. Chapman, *Glow Discharge Processes*, New York: John Wiley and Sons Inc., 1980.

14. J. A. Edminister, *Shaum's Outline Series of Theory and Problems of Electric Circuits*, New York: McGraw-Hill Book Company, 1965.
15. H. Anton, *Elementary Linear Algebra Edition 7*, New York: John Wiley and Sons, Inc., 1994.

Appendix A Scilab Program Files

Column1

```
// Columnises circuit branches parameter data and circuit branches type data
//
// copyright Brian Cregan
//
// 5/3/03
function [Params,CBtype]=column1(Cct_Branch,cb);
Params=Cct_Branch(1:5,2:14)'; // Puts the params R1, L1 etc for each circuit branch into columns,
                    // to get a 6(params) X cb(no. of cct branches) matrix
                    // that reads down first column of Cct_Params,
                    // then down second column etc
CBtype=Cct_Branch(:,1);          // Sets CBtype to the type of circuit for each
                                 // branch, a 5 X 1 matrix
```

Error2

```
// Calculates error signal
//
// copyright Brian Cregan
//
// 5/3/03
function
[err]=Error2(Cct_Branch,Magnitude,Envelope,Frequency,np,cnt,maxcnt);

[Envelope]=pshape1(Cct_Branch,Envelope,Frequency,cb,Trows);

CB_Total=makesum(Envelope);
// CB_Total is a Trows X 1 matrix giving the total effect of
```

```
// all circuit branches at each frequency point
err=sqrt((sum((((Magnitude-CB_Total)./(Magnitude))*100)^2))./Trows);
// Gives addition of the square of the difference between Mag and CB_Total
// The next part draws the "time elapsed indicator"
xset('window',1);
colours=[1];
xset('pattern',colours);
xfrect((cnt-1)/maxcnt,-0.5,1/maxcnt,-1.5);
[Envelope]=pshape1(Cct_Branch,Envelope,Frequency,cb);
// Gets Envelope ready to be drawn
```

makesum

```
// Calculates
//
// copyright Brian Cregan
//
// 5/3/03
function [CB_Total]=makesum(Envelope);
CB_Total=sum(Envelope,'c');
// The sum operator adds every value in a given row of Envelope
// Adds effect of all circuit branches at each frequency point
// and columates with increasing frequency
```

Parallel

```
// Circuit fitting program
//
// copyright Brian Cregan
//
// 5/3/03
clear        // Clears all variables at the start of the program
errclear(-1);
```

```
// All errors are cleared, for (n), n=+ it clears error no. n, for n=- clears all errors
// global flg;
// This means that the flg variable is a global variable across all functions

// Reads in file and arranges in ascending order
getf('C:\AAA\DCU HARDDRIVE\ATHESIS\Scilab Files\Progam
Files\simplex4.txt','c'); // Gets the file at given location, 'c'
getf('C:\AAA\DCU HARDDRIVE\ATHESIS\Scilab Files\Progam
Files\error2.txt','c'); // means it is complied to be more efficient
getf('C:\AAA\DCU HARDDRIVE\ATHESIS\Scilab Files\Progam
Files\update.txt','c');
getf('C:\AAA\DCU HARDDRIVE\ATHESIS\Scilab Files\Progam
Files\column1.txt','c');
getf('C:\AAA\DCU HARDDRIVE\ATHESIS\Scilab Files\Progam
Files\pshape1.txt','c');
getf('C:\AAA\DCU HARDDRIVE\ATHESIS\Scilab Files\Progam
Files\plotshape2.txt','c');
getf('C:\AAA\DCU HARDDRIVE\ATHESIS\Scilab Files\Progam
Files\makesum.txt','c');

Filename=xgetfile('*.txt','C:\AAA\DCU HARDDRIVE\ATHESIS\Scilab
Files\Chamber Data','Enter input Params file name');
 // Creates a dialog window for file selection
read(Filename,-1,2);
// Reads Filename, m,n are integers of the matrix x, when m=-1 as here it means
// that we don't know what the value of m is
Inputfile=read(Filename,-1,2); // Defining inputfile variable
Filesize=size(Inputfile);  // Defining Filesize variable, o/p is a mX2 matrix
nrows=Filesize(1,1);
// Defining nrows the as 1,1 index of filesize, nrows is a single number
```

```
if Inputfile(nrows,1)<Inputfile(1,1) then // Arranges Inputfile in ascending order
[m,n]=size(Inputfile);
        Infile=Inputfile(m:-1:1,:);
else
        Infile=Inputfile; // Infile is a mX2 matrix
end; // "end" of "if Inputfile(nrows,1)<Inputfile(1,1)"
// Chooses limited range for plotting Magnitude versus Frequency
xdel(0);              // Closes any open windows
xset('window',0);       // Sets current window to the window window-number +
creates the window if it doesn't exist
xmax=max(Infile(:,1)); // Defines xmax variable as the max of the Frequency,
max gets the max value of x readings
xmin=min(Infile(:,1)); //
ymax=max(Infile(:,2)); // Defines ymax variable as the max of the Magnitude

ymin=0;               // Defines ymin as 0

rect=[xmin,ymin,xmax,ymax];
// Defines a matrix rect as xmin,ymin,xmax,ymax, four points
plot2d(Infile(:,1), Infile(:,2),[1],'051',' ',rect); // Plots the infile on a graph
// Generation of all the circuit branches defined by the user
Loop1=0; // Setting Loop1 to 0. This loop allows user to add circuit branches
cb=0;   // cb is the number of circuit branches
Frequency=Infile(:,1);   // Frequency is all the rows in the first column of Infile
Magnitude=Infile(:,2);    // Frequency is all the rows in the second column of
Infile
Trows=length(Frequency); // Trows is simply the lenght of Frequecny
Envelope=zeros(Trows,5); // Defines envelope as a matrix of Trows by 5 zeros,
again Trows is a single number
```

```
Cct_Branch=zeros(5,14);          // Defines Cct_Branch as a zero matrix of 5 (max
no of cct branches) by 7 (no of params)
Single_Cct_Branch=zeros(Trows,5); // Defines Single_Cct_Branch as a matrix of
Trows by cb zeros
// Start of Loop1 loop
while Loop1<>1
        add_cct_branch=x_message(['Add Circuit Branch?'],['Yes','No']);
        if add_cct_branch==1 then
                cb=cb+1;
                text=['Cct (1), Cct (2), Cct (3), Cct
(4)';'Rc';'Lc';'Cc';'Cpw';'Rw';'Lw';'Cpg';'Re';'Le';'Ce';'Cgw';'Rg';'Lg'];
                if cb==1 then
        values=['1';'0.2614960';'0.00000003297';'0.00000000002451';'0.00000000
001308';'0.2242817';'0.00000009173';'0.000000000001996';'0.0177132';'0.00000
002691';'0.0000000000009138';'0.00000000004251';'0.0690086';'0.00000004162'
];
// For fisrt Circuit Branch default values set to as above
                else
                        values=[string(Cct_Branch(cb-1,1));string(Cct_Branch(cb-
1,2));string(Cct_Branch(cb-1,3));string(Cct_Branch(cb-
1,4));string(Cct_Branch(cb-1,5));string(Cct_Branch(cb-
1,6));string(Cct_Branch(cb-1,7));string(Cct_Branch(cb-
1,8));string(Cct_Branch(cb-1,9));string(Cct_Branch(cb-
1,10));string(Cct_Branch(cb-1,11));string(Cct_Branch(cb-
1,12));string(Cct_Branch(cb-1,13));string(Cct_Branch(cb-1,14))];
// For second, third etc Circuit Branches,
// values are given by previous Circuit branch
// initially until user changes them
                end; // "end" of "if cb==1"
```

```
        props=x_mdialog('Enter Circuit Branch
Parameters',[text],[values]); // Interactive input function
        Cct_Branch(cb,1)=eval(props(1)); // Circuit type selected inputted
                                         // for props(1)
        Cct_Branch(cb,2)=eval(props(2)); // Cpw of circuit branch cb
        Cct_Branch(cb,3)=eval(props(3)); // Rgw of circuit branch cb
        Cct_Branch(cb,4)=eval(props(4)); // Lgw of circuit branch cb
        Cct_Branch(cb,5)=eval(props(5)); // Lgw of circuit branch cb
        Cct_Branch(cb,6)=eval(props(6)); // Lgw of circuit branch cb
        Cct_Branch(cb,7)=eval(props(7)); // Lgw of circuit branch cb
        Cct_Branch(cb,8)=eval(props(8)); // Lgw of circuit branch cb
        Cct_Branch(cb,9)=eval(props(9)); // Lgw of circuit branch cb
        Cct_Branch(cb,10)=eval(props(10)); // Lgw of circuit branch cb
        Cct_Branch(cb,11)=eval(props(11)); // Lgw of circuit branch cb
        Cct_Branch(cb,12)=eval(props(12)); // Lgw of circuit branch cb
        Cct_Branch(cb,13)=eval(props(13)); // Lgw of circuit branch cb
        Cct_Branch(cb,14)=eval(props(14)); // Lgw of circuit branch cb
    else
        if cb==0 then abort
        end;
// This part gives you the option of putting the newer starting
// values for a given cicuit branch
        number=[];
        for n=1:cb
            number(n)=string(n); // Converts a matrix into a matrix of
                                 // strings
            end; // "end" of "for n=1:cb"
        number(cb+1)='finished';
        l1=list('',cb+1,number');
        finished=0;
```

```
while finished~=1 then
        numbranch=x_choices('Enter Circuit Branch number to
change',list(11));
        if numbranch == cb+1 then finished=1;
// This is if the user chooses Finished in the window
        else
            fmished=0;
            text=['Cct (1), Cct (2), Cct (3), Cct
(4)';'Rc';'Lc';'Cc';'Cpw';'Rw';'Lw';'Cpg';'Re';'Le';'Ce';'Cgw';'Rg';'Lg'];
    values=[string(Cct_Branch(numbranch,1));string(Cct_Branch(numbranch,
2));string(Cct_Branch(numbranch,3));string(Cct_Branch(numbranch,4));string(C
ct_Branch(numbranch,5));string(Cct_Branch(numbranch,6));string(Cct_Branch(n
umbranch,7));string(Cct_Branch(numbranch,8));string(Cct_Branch(numbranch,9
));string(Cct_Branch(numbranch,10));string(Cct_Branch(numbranch,11));string(
Cct_Branch(numbranch,12));string(Cct_Branch(numbranch,13));string(Cct_Bran
ch(numbranch,14))];
            props=x_mdialog('Enter Circuit Branch
parameters',[text],[values]);
            Cct_Branch(numbranch,1)=eval(props(1));
            Cct_Branch(numbranch,2)=eval(props(2));
            Cct_Branch(numbranch,3)=eval(props(3));
            Cct_Branch(numbranch,4)=eval(props(4));
            Cct_Branch(numbranch,5)=eval(props(5));
            Cct_Branch(numbranch,6)=eval(props(6));
            Cct_Branch(numbranch,7)=eval(props(7));
            Cct_Branch(numbranch,8)=eval(props(8));
            Cct_Branch(numbranch,9)=eval(props(9));
            Cct_Branch(numbranch,10)=eval(props(10));
            Cct_Branch(numbranch,11)=eval(props(11));
            Cct_Branch(numbranch,12)=eval(props(12));
```

```
                    Cct_Branch(numbranch,13)=eval(props(13));
                    Cct_Branch(numbranch,14)=eval(props(14));
                end; // "end" of "if numbranch == cb+1"
            end; // "end" of "while finished~=1" loop
        end; // "end" of "if add_cct_branch==1"
        xdel(0); // Closes all windows
// This should be a 5 X 7 matrix with each circuit branch and the
// corresponding parameters
// This is a Trows X 5 zeros matrix at this point
        //disp(Frequency);  // This is a Trows X 1 column matrix
        //disp(Magnitude);  // This is a Trows X 1 column matrix
        //disp(cb);         // This is a single number giving the number of circuit branches
        //disp(Trows);      // This is a single number giving the number of points in Frequency
// Calculates Circuit Branch Magnitude versus Frequency
// and outputs it as Envelope


[Envelope]=pshape1(Cct_Branch,Envelope,Frequency,cb,Trows);
// Outputs Envelope in a new format
// Plots Cct_Branch
plotshape(Envelope,Frequency,Magnitude,cb); // Plots Magnitude and Envelope
// Peak fitting routine
        Fitcircuit=x_message(['Do you want to run circuit fitting routine?'],['Yes','No']); // You click on yes or no, yes=1 no=0
        xdel(1);
        xset('window',1);
        xset('wdim',700,40);
        xset('pattern',1);
```

```
        plot2d(0,0,2,'010',' ',[0,-1,1,1]);
        xrect(0,-0.5,1,-1.5); // xrect draws a rectangle defined by
// [x,y,w,h] (upper-left point, width, height) using the current scale and style.
        if Fitcircuit==1 then
                [Cct_Branch,fv]=simplex4(cb,Cct_Branch,Envelope,Frequency);
// Modifies Envelope to fit onto Magnitude
                [Envelope]=pshape1(Cct_Branch,Envelope,Frequency,cb);
// New "better fit" Envelope is reorganised
                xbasc(0);
// Clears the current graphics window and erases the recorded graphics
                plotshape(Envelope,Frequency,Magnitude,cb);
// Plots Magnitude and "better fit" Envelope
                errtot=min(fv);
                disp(errtot,'Error = ');
        end; // "end" of "if Fitcircuit==1"
        //xclear(1); // This function clears the current window. Otherwise it clears
        // the graphics windows whose numbers are included in the vector
        xset('window',0);  // Closes window
        // Gives the user the option to terminate the Circuit Fitting Program
        Loop1=x_message(['Do you want to terminate programme?'],['Yes','No']);
        if Loop1 ~=1 then
        end;
end; // "end" of "Loop1"
//xdel(1);
// xdel deletes graphics windows win-nums or the current graphics window if no
// argument is given.
//F=ones(1:cb);
//Expback=Backgrd(:,F);
//G=zeros(Trows,10-cb);
//H=[Expback G];
```

```
//Individs=Envelope+H;
// Gives the user the option to save the Params
if cb~=0 then
        AllParams=[Frequency Magnitude];
        saveParams=x_message(['Do you want to save Params?'],['Yes','No']);
        if saveParams==1 then
                filename=xgetfile('*.dat','d:\scilab\raman\Params\','Enter a file
name');
                errcatch(240,"continue","nomessage");
                if filename ~= '' then
                        write(filename,AllParams,'(13(e10.3))');
                        while iserror(240)==1
                                errclear(240);
                                text='File already exists: choose new name.';
                                filename=xgetfile('*.dat','E:\Program Files\Scilab-
2.7\Programs\Params\','Enter another file name');
                                if filename == '' then
                                        break
                                end; // "end" of "if filename ==""
                                write(filename,AllParams,'(13(e10.3))');
                        end; // "end" of "while iserror(240)==1"
                end; // "end" of "if filename ~= ""
        end; // "end" of "if saveParams==1"
        // Gives the user the option to see the Params in the Scilab window
        display=x_message(['Do you want to see circuit branch Params';'(in
command window)?'],['Yes','No']);

        for n=1:5
                BranchData=Cct_Branch(n,1);
                if BranchData==0 then
```

```
                    Area(n)=0;
                else
                    A=0;
                    for m=2:Trows
                        A=A+(Frequency(m)-Frequency(m-
1))*(Envelope(m,n)+Envelope(m-1,n))/2;
                    end; // "end" of "for m=2:Trows"
                    Area(n)=A;
                end; // "end" of "if BranchData==0"
        end; // "end" of "for n=1:5"
        errtot=min(fv);
        Branch_Params=[Cct_Branch Area];
        if display==1 then
            disp('Branch Params = ',Branch_Params);
            disp('Error = ',errtot);
        end; // "end" of "if display==1"
end; // "end" "if cb~=0"
```

plotshpape2

```
// Plots the Magnitude versus Frequency again and then plots each branch and
their Envelope versus Frequency
//
// copyright Brian Cregan
//
// 5/3/03
function []=plotshape(Envelope,Frequency,Magnitude,cb);
Sum=sum(Envelope,'c'); // Sum is a trows X 1 matrix
Xscale=[Frequency Frequency];
// Used to draw overall Magnitude and overall effect of cirtuit branches
Yscale=[Magnitude Sum];
// Used to draw overall Magnitude and overall effect of cirtuit branches
```

```
colours=[1 2];
for x=1:cb
        Yscale=[Yscale Envelope(:,x)];
// Plot of Magnitude, Sum effect of all circuit branches, effect of each branch
        Xscale=[Xscale Frequency];
// Simply the Frequency Sweep as the x-axis
        colours=[colours x+2];
end;
X1=Frequency(1);
// Defining points for window, X1 is the first entry
// in the 1 column matrix Frequency
X2=Frequency(Trows);
// Defining points for window, X2 is the second entry in the
// 1 column matrix Frequency
Y1=0;                   // Defining points for window, Y1 is 0
Ymag=max(Magnitude); // Defining points for window
Ysum=max(Sum);       // Defining points for window
Y2=max(Ymag,Ysum);   // Defining points for window,
// Y2 is the max Magnitude between Magnitude and Envelope
rect=[X1,Y1,X2,Y2];  // Defining points for window
xset('window',0);
xclear(0);
xbasc(0);
plot2d([Xscale],[Yscale],[colours],'051',' ',rect);
```

pshape1

```
// Calculates Frequency response of theoretical circuit
//
// copyright Brian Cregan
//
// 5/3/03
```

```
function [Envelope]=pshape1(Cct_Branch,Envelope,Frequency,cb,Trows);
for n=1:cb              // cb is the number of circuit branches
BranchData=Cct_Branch(n,:);
// Sets BranchData as a variable that goes through the columns
// of each row of Cct_Branch matrix

        select Cct_Branch(n,1)
 // Uses column 1 of Cct_Branch, which represents the user's choice of circuit,
// to choose which case statement below will be used as a solver.
        case 1 then  // Magnitude of Plasma Circuit
                Rc=BranchData(2);
                Lc=BranchData(3);
                Cc=BranchData(4);
                Cpw=BranchData(5);
                Rw=BranchData(6);
                Lw=BranchData(7);
                Cpg=BranchData(8);
                Re=BranchData(9);
                Le=BranchData(10);
                Ce=BranchData(11);
                Cgw=BranchData(12);
                Rg=BranchData(13);
                Lg=BranchData(14);
                XLc=(2*%pi*Lc)*Frequency;
                XCc=((2*%pi*Cc)*Frequency)^(-1);
                XCpw=((2*%pi*Cpw)*Frequency)^(-1);
                XLw=(2*%pi*Lw)*Frequency;
                XCpg=((2*%pi*Cpg)*Frequency)^(-1);
                XLe=(2*%pi*Le)*Frequency;
                XCe=((2*%pi*Ce)*Frequency)^(-1);
```

```
XCgw=((2*%pi*Cgw)*Frequency)^(-1);
XLg=(2*%pi*Lg)*Frequency;
A=XLc-XCc;
B=XLw-XCe-XCpw;
C=XLe-XCpw-XCpg-XCgw;
D=XLg-XCgw;
E=XLe-XCe;
F=Re.*Rg-D.*E;
G=D.*Re+E.*Rg;
H=F.*Re-C.*G;
I=C.*F+G.*Re;
J=H.*Rw-B.*I;
K=B.*H+I.*Rw;
L=J.*Rc-A.*K;
M=A.*J+K.*Rc;
N=-E.*XCgw;
O=Re.*XCgw;
P=-O.*XCgw;
Q=N.*XCgw;
R=P.*Rw-B.*Q;
S=B.*P+Q.*Rw;
T=R.*Rc-S.*A;
U=Rc.*S+A.*R;
V=-Re.*Rg+D.*XLe;
W=-D.*Re-Rg.*XLe;
X=-Re.*V+W.*XLe;
Y=-V.*XLe-Re.*W;
Z=Rw.*X-B.*Y;
Aa=B.*X+Rw.*Y;
Ab=Rc.*Z-A.*Aa;
```

```
Ac=A.*Z+Aa.*Rc;
Ad=-G.*XCpw;
Ae=F.*XCpw;
Af=-Ae.*XCpw;
Ag=Ad.*XCpw;
Ah=Af.*Rc-A.*Ag;
Ai=A.*Af+Ag.*Rc;
Aj=-H.*(XCc^2);
Ak=-I.*(XCc^2);
Al=-P.*(XCc^2);
Am=-Q.*(XCc^2);
An=-X.*(XCc^2);
Ao=-Y.*(XCc^2);
Ap=L-T-Ab-Ah-Aj+Al+An;
Aq=M-U-Ac-Ai-Ak+An+Ao;
Ar=J-R-Z-Af;
As=K-S-Aa-Ag;
At=((Ap.*Ar-Aq.*As)./(Ar^2+As^2));
Au=((Aq.*Ar+Ap.*As)./(Ar^2+As^2));
Zlmag=sqrt(At^2+Au^2);
Outline=(Zlmag);
// Outline is a Trows by 1 column variable matrix
// It gives the outline calculated from the function
// versus increasing frequency
        case 2 then // Phase of Plasma Circuit

Rc=BranchData(2);
Lc=BranchData(3);
Cc=BranchData(4);
Cpw=BranchData(5);
```

```
Rw=BranchData(6);
Lw=BranchData(7);
Cpg=BranchData(8);
Re=BranchData(9);
Le=BranchData(10);
Ce=BranchData(11);
Cgw=BranchData(12);
Rg=BranchData(13);
Lg=BranchData(14);
XLc=(2*%pi*Lc)*Frequency;
XCc=((2*%pi*Cc)*Frequency)^(-1);
XCpw=((2*%pi*Cpw)*Frequency)^(-1);
XLw=(2*%pi*Lw)*Frequency;
XCpg=((2*%pi*Cpg)*Frequency)^(-1);
XLe=(2*%pi*Le)*Frequency;
XCe=((2*%pi*Ce)*Frequency)^(-1);
XCgw=((2*%pi*Cgw)*Frequency)^(-1);
XLg=(2*%pi*Lg)*Frequency;
A=XLc-XCc;
B=XLw-XCc-XCpw;
C=XLe-XCpw-XCpg-XCgw;
D=XLg-XCgw;
E=XLe-XCe;
F=Re.*Rg-D.*E;
G=D.*Re+E.*Rg;
H=F.*Re-C.*G;
I=C.*F+G.*Re;
J=H.*Rw-B.*I;
K=B.*H+I.*Rw;
L=J.*Rc-A.*K;
```

```
M=A.*J+K.*Rc;
N=-E.*XCgw;
O=Re.*XCgw;
P=-O.*XCgw;
Q=N.*XCgw;
R=P.*Rw-B.*Q;
S=B.*P+Q.*Rw;
T=R.*Rc-S.*A;
U=Rc.*S+A.*R;
V=-Re.*Rg+D.*XLe;
W=-D.*Re-Rg.*XLe;
X=-Re.*V+W.*XLe;
Y=-V.*XLe-Re.*W;
Z=Rw.*X-B.*Y;
Aa=B.*X+Rw.*Y;
Ab=Rc.*Z-A.*Aa;
Ac=A.*Z+Aa.*Rc;
Ad=-G.*XCpw;
Ae=F.*XCpw;
Af=-Ae.*XCpw;
Ag=Ad.*XCpw;
Ah=Af.*Rc-A.*Ag;
Ai=A.*Af+Ag.*Rc;
Aj=-H.*(XCc^2);
Ak=-I.*(XCc^2);
Al=-P.*(XCc^2);
Am=-Q.*(XCc^2);
An=-X.*(XCc^2);
Ao=-Y.*(XCc^2);
Ap=L-T-Ab-Ah-Aj+Al+An;
```

```
                Aq=M-U-Ac-Ai-Ak+An+Ao;
                Ar=J-R-Z-Af;
                As=K-S-Aa-Ag;
                At=((Ap.*Ar-Aq.*As)./(Ar^2+As^2));
                Au=((Aq.*Ar+Ap.*As)./(Ar^2+As^2));
                Z1mag=atan(Au./At);
                Outline=(Z1mag);
// Outline is a Trows by 1 column variable matrix
// It gives the outline calculated from the function
// versus increasing frequency
        else
                disp('Faulty Circuit (Outline Faulty');
                abort;
end;
Envelope(:,n)=Outline;
// Lists the outline for each cct branch (max of 5) in columns 1 to 5 of Envelope
end;
```

Simplex4

```
// Simplex fitting programme
//
// copyright Brian Cregan
//
// 5/3/03
//
//
function [Cct_Branch,fv]=simplex4(cb,Cct_Branch,Envelope,Frequency);
errclear(-1);
// All errors are cleared, for (n), n=+ it clears error no. n, for n=- clears all errors
[Params,CBtype]=column1(Cct_Branch,cb);
// Params gives 1 column with parameter i/p for each circuit branch ADDED only
```

```
// CBtype gives type of circuit for each circuit branch in a 5 X 1 matrix
n=length(Params);
// Tells how many param values to be changed, as length of Params varies with no. of branches added
maxcnt=120*n;
// Counter max, limits number of iterations so that the program does not go on indefinitely
tol=.000001;      // Tolerance set for acceptable fit of calculated curve
tol2=0.00001;     // Tolerance set for acceptable fit of calculated curve
xin=Params;     // This is done so that Params can be updated throughout the program
v=Params(:);      // v is a 30X1 (i.e. 1 column) matrix listing all the params of the cct branches
cnt=0;


fv=Error2(Cct_Branch,Magnitude,Envelope,Frequency,cb,cnt,maxcnt);
// Function, fv is just one number
// It is the sum of the square of the differences
// between Mag and CB_total at each freq point
// Also the time indicator window is drawn at this
// point as it is part of the o/p of Error2
for j=1:n                         // n is length of Params
        delta=0.001;                    // Used to tell how much you vary a parameter by, here variation is %50
        zero_term_delta=0.25;           // Just for when a paramamter value is zero
        //disp(Params,'Params before y=');
        y=Params(:);
// y is a 30X1 (i.e. 1 column) matrix listing all the params of the cct branches
        if y(j)~=0 then                 // Individual point in Params
```

```
                y(j)=(1+delta)*y(j);      // Changes value of individual point
        else
 //y(j)=zero_term_delta;
// If a parameter is zero it is incremented to zero_term_delta
        end;
        v=[v y];
// A j+1 column matrix with y changing. v is the initial params. We end up with a
matrix
// that has the original parameters in the first column, then
// it has the the parameters
// in the next columns with each successive parameter changed by 50%
        Params(:)=y; // Updated Params matrix
        cnt=n;
        [Cct_Branch]=update(Params,CBtype);
// Updates the Cct_Branch matrix with the new Param matrix
// with 1 param changed by %50
        f=Error2(Cct_Branch,Magnitude,Envelope,Frequency,cb,cnt,maxcnt);
 // f is just 1 valued error signal and is
// calculated for the particular Cct_Branch
// with one parameter changed by %50
        fv=[fv f];
// A matrix that gives the original error (fv) and then the error due to the change
// in 1 parameter (f)
end;
[fv,j]=sort(fv);
// fv is now a matrix that gives the intial error and the error by a change in a given
parameter of %50
// fv is a 1 X n+1 matrix that is in decreasing order
// fv is actual error in descending order, j is the index of each fv term
// This part finds the param that has the biggest effect on the error
```

```
v=v(:,j);
// Picks out Params that gives smallest error, j equals n at this stage so we have a
n X n+1 matrix
// that gives the params of all 6 cct branches in each column, the first column is
// unchanged, and the
 // next column has each consecutive parameter changed by 50%
 // At the moment there are zeros for if the user inputs less than 6 cct branches
cnt=n+1;
alpha=1; beta=0.5;Gamma=2;
[n,npl]=size(v); // size function tells the dims of the matrix v, it will be nXn+1,
n= no. of rows, npl=> columns, i.e n+1
onesn=ones(1,n); // A 1 X n ones matrix
ot=2:n+1;        // Simply a counter to run through 2 to n+1, for going through the
columns of v
on=1:n;
 // Simply a counter to run through 1 to n, for going through the rows of v
// v is a 30X31 matrix.
// This takes the first column of v containing the user inputted
// paramters and generate
// a matrix that has the same values in all the columns as in the first column
while cnt<maxcnt
// maxcnt is 120*n and limits number of iterations so that the program does not
// go on indefinitely

        if max(max(abs(v(:,on)-v(:,onesn)))) <= tol & ... //
                max(max(abs(fv(1)-fv(on)))) <= tol2 then
// This is the max of the absolute differences in error break
// before and after a change in the parameters
// if all the values are within the tolerance stop program
```

```
// Inside the while cnt<maxcnt loop, the command break
// forces the end of the loop
        end;
// Simplex algorithm starting
        vbar=(sum(v(:,ot),'c')/n);
// Takes the average of all parameter 1, parameter 2 etc
// excluding the inputted parameters
                        // vbar is a 30X1 matrix
        vr=(1+alpha)*vbar - alpha*v(:,1);
// vr is a 30X1 matrix with each index of vbar increased by 200% and
// the original inputted parameters subtracted
        Params(:)=vr; // Updated Params matrix
        [Cct_Branch]=update(Params,CBtype);
// This just puts the parameters and cct branch type back into 1 matrix
// i.e. Cct_Branch for use later on in the program (see next line)

        fr=Error2(Cct_Branch,Magnitude,Envelope,Frequency,cb,cnt,maxcnt);
// error is calculated with changed params
        cnt=cnt+1;
        vk=vr;          // new matrix vk is defined as vr
        fk=fr;
// new matrix fk is defined as fr, fr is error generated from adjusted params
        if fr<fv(2) then
// if the error fr < the error due to a change in the first parameter
                if fr<fv(n+1) then
// if the error fr < the error due to a change in
// all the parameters then new approach
                        ve=Gamma*vr + (1-Gamma)*vbar;
// ve= 4 times vr plus (minus 3 times vbar)
                        Params(:)=ve;
```

```
                    [Cct_Branch]=update(Params,CBtype);
// This just puts the parameters and cct branch type
// back into 1 matrix i.e. Cct_Branch for use later
// on in the program (see next line)
        fe=Error2(Cct_Branch,Magnitude,Envelope,Frequency,cb,cnt,maxcnt);
// error is calculated with changed params
                    cnt=cnt+1;
                    if fe<fv(n+1) then
                            vk=ve;
                            fk=fe;
                    end;
                end;
        else
// if the error fr > the error due to a change in the first parameter
                vt=v(:,n+1);
                ft=fv(n+1);
                if fr<ft then
                        vt=vr;
                        ft=fr;
                end;
                vc=beta*vt + (1-beta)*vbar;
                Params(:)=vc;
                [Cct_Branch]=update(Params,CBtype);
        fc=Error2(Cct_Branch,Magnitude,Envelope,Frequency,cb,cnt,maxcnt);
                cnt=cnt+1
                if fc<fv(2) then
                        vk=vc;
                        fk=fc;
                else
                        for j=2:n
```

```
                    v(:,j)=(v(:,n+1)+v(:,j))/2;
                    Params(:)=v(:,j);
                    [Cct_Branch]=update(Params,CBtype);
        fv(j)=Error2(Cct_Branch,Magnitude,Envelope,Frequency,cb,cnt,maxcnt);
                end;
                cnt=cnt+n-1;
                vk=(v(:,2)+v(:,n+1))/2;
                Params(:)=vk;
                [Cct_Branch]=update(Params,CBtype);
        fk=Error2(Cct_Branch,Magnitude,Envelope,Frequency,cb,cnt,maxcnt);
                cnt=cnt+1;
            end;
        end;
        v(:,1)=vk;
        fv(1)=fk;
        [fv,j]=sort(fv);
        v=v(:,j);
end; // "end" of "while cnt<maxcnt"
Params(:)=v(:,n+1);
if cnt==maxcnt then
        disp('Warning: Maximum number of iterations exceeded');
end;
[Cct_Branch]=update(Params,CBtype);
```

Update

```
// Reconstructs Cct_Branch from Params and CBtype that have been changed by
simplex4
//
// copyright Brian Cregan
//
// 5/3/03
```

```
function [Cct_Branch]=update(Params,CBtype,cb);
for m=1:cb
// cb being the number of circuit branches added
        Params=Params';
// Params is a 6 X 1 Matrix and is tranposed to give a 1 X 6 Matrix
        Cct_Branch=[CBtype Params];
        Params=Params';
end;
errcatch(5,"continue")
if iserror(5)==1 then
        disp('count = ',cnt)
        abort
end;
```